AQRP Project 14-026

Quantifying Ozone Production from Light Alkenes Using Novel Measurements of Hydroxynitrate Reaction Products in Houston during the NASA SEAC[4]RS Project

Draft Final Report

Prepared for:

Gary McGaughey
Project Manager
Texas Air Quality Research Program

Chris Kite
TCEQ Project Liaison

Prepared by:

Greg Yarwood, Prakash Karamchandani and Lynsey Parker
Ramboll Environ, 773 San Marin Drive, Novato, CA 94998

David Parrish
David.D.Parrish, LLC, 4555 13th St. #2E, Boulder CO 80304

Thomas Ryerson
NOAA/ESRL/CSD, 325 Broadway R/CSD7, Boulder, CO 80305

Revised 30 November 2015

QA Requirements: Audits of Data Quality: 10% Required

ACKNOWLEDGEMENT

TABLE OF CONTENTS

APPENDIX

Appendix A: Simplified Chemistry Scheme for β-hydroxynitrate Formation during Alkene
             Oxidation

TABLES

FIGURES

iv

LIST OF ACRONYMS AND ABBREVIATIONS

βHN	β-hydroxynitrates
CAMS	Continuous Air Monitoring Station
CB6r2	Carbon Bond 6 revision 2
CH_2O	Formaldehyde
CH_3CHO	Acetaldehyde
CIMS	Chemical Ionization Mass Spectrometer
CMAQ	Community Multi-scale Air Quality model
CMAQ-APT	CMAQ with Advanced Plume Treatment
CO	Carbon monoxide
EPA	Environmental Protection Agency
HCHO	Formaldehyde
HGB	Houston-Galveston-Brazoria Area
HNO_3	Nitric acid
HO_2	Hydroperoxy radical
hr	Hour
HRVOC	Highly reactive volatile organic compound
HSC	Houston Ship Channel
HYSPLIT	Hybrid Single Particle Lagrangian Integrated Trajectory Model
MEGAN	Model of Emissions of Gases and Aerosols from Nature
NAA	Non-Attainment Area (for the ozone NAAQS)
NAAQS	National Ambient Air Quality Standard
NASA	National Aeronautics and Space Administration
NO	Nitric oxide
NO_2	Nitrogen dioxide
NOx	Oxides of nitrogen
NOy	Total reactive nitrogen oxides
NOz	Total oxidation products of NOx; operationally defined as NOy - NOx
O_3	Ozone
OH	Hydroxyl radical
OPE	Ozone Production Efficiency
Ox	Sum of O_3 plus NO_2
PAN	Peroxyacetyl nitrate
ppb	Parts per billion
ppt	Parts per trillion
QA/QC	Quality assurance and quality control
SCICHEM	Second-Order Closure Integrated puff model with CHEMistry
SEAC^{4}RS	Studies of Emissions and Atmospheric Composition, Clouds and Climate Coupling by Regional Surveys
SIP	State Implementation Plan (for the ozone NAAQS)

SO$_2$	Sulfur dioxide
SOF	Solar Occultation Flux
TCEQ	Texas Commission on Environmental Quality
ton	English short ton (2000 pounds)
tpd	Tons per day
VOC	Volatile organic compound
WAS	Whole-air-sample
yr	Year

EXECUTIVE SUMMARY

The objective of this study was to improve and quantify our understanding of ozone (O_3) and formaldehyde (HCHO) production from industrial emissions of Highly Reactive Volatile Organic Compounds (HRVOC) in the Houston area. The study took advantage of unique aircraft measurements during the National Aeronautics and Space Administration (NASA) Studies of Emissions and Atmospheric Composition, Clouds and Climate Coupling by Regional Surveys (SEAC[4]RS) project in the fall of 2013. The aircraft encountered plumes with enhanced O_3 downwind of petrochemical facilities in Houston. HRVOC, namely ethene, propene, butenes and 1,3-butadiene, cause these types of O_3 plumes but quantifying the relative contributions of individual HRVOC to O_3 formation has been difficult. Chemical compounds, called β-hydroxynitrates (βHNs), are formed when HRVOC react in the atmosphere in the presence of nitrogen oxides (NOx). Measurements of the C_2-C_5 hydroxynitrates aboard the DC-8 provide a novel means to link observed enhancements of O_3 and HCHO to reactions of specific HRVOC and isoprene.

The study objectives were accomplished by a combination of data analysis and reactive plume modeling using the SCICHEM Lagrangian puff model. QA/QC'd data (provided by Caltech) taken aboard the NASA DC-8 research aircraft during the 2013 SEAC[4]RS project in Houston were used in the analysis. The observational analysis was conducted for 20 plumes that were encountered on 11 flights in the Houston area from August 12 to September 23, 2013. The plume modeling focused on the September 18, 2013 flight which intercepted the Houston Ship Channel (HSC) plume at downwind distances of 40, 80 and 100 km. An HRVOC tracer mechanism was developed to describe first-generation formation of β-hydroxynitrates, aldehydes and O_3 from alkenes. This mechanism was used in both the observational analysis and the plume modeling to quantify the direct contributions of HRVOC oxidation to O_3 and aldehyde formation in the intercepted plumes. Direct contribution refers to O_3 and aldehyde produced immediately following OH reacting with the HRVOC.

In the observational analysis, the direct contributions were quantified from the measured βHN concentrations. O_3 enhancements in the plume intercepts ranged from 4 to 54 ppb. The fraction of these enhancements directly attributable to HRVOC and isoprene emissions (as indicated by the O_3/βHN ratios) ranged from 6% to 24%. Isoprene contributed, on average, 35% (range of 9% to 56%) of the directly attributable O_3 enhancement. This average contribution of isoprene is approximately equal to that of ethene, the most important HRVOC from the observational analysis. The direct contributions of individual HRVOC to the anthropogenic O_3 enhancement (i.e., excluding the isoprene contribution) on average ranked in this order: ethene (49%), propene (32%), butenes (13%) and butadiene (6%). However there were wide variations in these relative contributions: ethene (24% to 72%), propene (14% to 66%), butenes (8% to 24%) and butadiene (2% to 13%). Some of these variations represent

systematic changes in contributions with downwind distance as emissions were photochemically processed, with the more rapidly reacting HRVOC contributing a larger fraction early and the contribution from the more slowly reacting ethene gradually increasing.

The base case plume modeling for the September 18, 2013 flight considered the HSC as a single large source with an initial plume width of 6 km. HRVOC emissions from the HSC were based on SOF measurements conducted in Houston in 2011. Predicted profiles of O_3, NOy, NOz, HCHO and CH_3CHO concentrations for each downwind plume intercept were compared with corresponding DC-8 measurements. The model predicted peak O_3 increments in the HSC plume accurately, but the NOz and aldehyde results showed that chemistry proceeded more slowly in the model plume than indicated from the measurements during the early stages of the plume. Much better agreement for aldehydes and NOz was obtained in a sensitivity study in which 6 smaller sources along the Ship Channel were used to model the HSC emissions. The overall effect of using multiple narrower source plumes was that the chemistry proceeded more rapidly and model performance was improved at 40 km downwind.

The modeled direct contributions of HRVOC to downwind O_3 were generally consistent with the results from the observational analysis. The base case results showed that direct formation of O_3 from the HSC HRVOC emissions explained only 12 to 22% of the O_3 increments in the plume on September 18, 2013. The sensitivity study with 6 sources attributed 23 to 25% of the O_3 enhancements directly to HRVOC. Representing the HSC emissions by multiple, narrower source plumes accelerated plume chemistry and improved model performance. Another sensitivity study showed that plume chemistry is sensitive to whether HRVOC and NOx are released together or segregated in separate plumes that interact as they disperse and overlap each other.

The observational analysis and plume modeling of HSC plume intercepts during the SEAC[4]RS project represent a significant advance in our understanding of the role of HRVOC emissions from the HSC on O_3 concentrations in the Houston region. The results indicate the need for additional studies, discussed below.

Key Findings from Observational Analysis

- O_3 levels during the days when the aircraft sampled the HSC plume indicate that most of these days represent typical, moderate O_3 days in Houston without unusually large HRVOC emission events.
- The fraction of O_3 formation in the HSC plumes that is directly attributable to HRVOC and isoprene emissions (as indicated by the $O_3/\beta HN$ enhancement ratios) is surprisingly small, averaging only ~13% with a range from 6% to 24%.
- Isoprene contributed, on average, 35% (range of 9% to 56%) of the directly attributable O_3 enhancement, making this species' average contribution approximately equal to that of ethene, the most important HRVOC.

- The direct contributions of individual HRVOCs to the anthropogenic O_3 enhancement (i.e., excluding the isoprene contribution) on average ranked in this order: ethene (49%), propene (32%), butenes (13%) and butadiene (6%).
- The total O_3 formed downwind of HRVOC sources is larger than the sum of the direct contributions of the individual HRVOCs and isoprene derived from $O_3/\beta HN$ enhancement ratios.
- The observational analysis presented here has limitations that must be fully appreciated.

Key Findings from Plume Modeling of HSC Emissions

- Modeled ozone increments in the HSC plume on September 18, 2013 are in good agreement with aircraft measurements; noting that the HSC emissions were based on ambient measurements.
- Using several sources instead of a single source to represent the HSC emissions results in a better simulation of plume reactivity and formation of products such as NOz, HCHO, and CH_3CHO.
- Direct formation of O_3 from HRVOC emissions contributes 12 to 22% of the O_3 increments in the HSC plume on September 18, 2013 with a single source versus 23 to 25% for multiple sources.
- O_3 increments in the modeled plume are not sensitive to the source configuration (single source versus 6 sources) indicating that higher direct O_3 production from HRVOC emissions with 6 sources was offset by lower indirect O_3 production.
- O_3 increments in the modeled plume are sensitive to whether VOC and NOx are co-emitted or segregated.
- Butenes and propene are the largest HRVOC contributors to O_3 formation near the HSC. Ethene contributions become more important at larger downwind distances.
- More than 50% of the HCHO increments in the HSC plume are directly attributable to HRVOC emissions, with the highest contribution being about 80% at the nearest downwind distance of 40 km.
- Direct contributions of HSC HRVOC emissions to CH_3CHO concentration increments in the plume vary from 46% at the furthest downwind distance (100 km) to 100% at the nearest downwind distance (40 km).

Recommendations

The observational analysis suggests that there may be a loss mechanism(s) for βHNs in the gas phase. If this is indeed the case, then this may have implications for the availability of NOx in the gas-phase as the plume ages, because the βHNs are formed from many VOC and represent a substantial fraction of organic nitrates. Thus, additional studies of the fate of βHNs are warranted.

The modeling and observational analysis also indicate that a substantial fraction of the O_3 in the HSC plume is formed indirectly by the interaction of HRVOC emissions with other VOCs. For example, the observational analysis showed a large contribution of (biogenic) isoprene to O_3 in the HSC plume. More studies are required to understand direct versus

indirect O_3 formation in HSC plumes and to identify and quantify the various sources (including isoprene) of indirect contributions.

The plume modeling provided a unique opportunity to study the fine-scale photochemical interaction of plumes from nearby sources and initial segregation of NOx and VOC emissions. The current study provides a first look at these effects. Future studies can use more recent measurements of HSC emissions (e.g., from AQRP Project 14-007) and investigate further how initial plume width and emissions segregation influence O_3 production from industrial sources. Results from plume model and plume-in-grid model studies can show what resolution should be used in grid models. SCICHEM is well-suited to conducting these studies because it has full chemistry and allows overlapping plumes to interact photochemically. SCICHEM is also the underlying plume model in the recent EPA release of the plume-in-grid version of CMAQ 5.0.2, referred to as CMAQ-APT (where APT stands for Advanced Plume Treatment).

1. INTRODUCTION

1.1   BACKGROUND

Industrial emissions of highly reactive volatile organic compounds (HRVOC) contribute to localized ozone (O_3) production in Houston [*Ryerson et al.*, 2003]. Several aircraft flights conducted during the National Aeronautics and Space Administration (NASA) Studies of Emissions and Atmospheric Composition, Clouds and Climate Coupling by Regional Surveys (SEAC[4]RS) project encountered plumes with enhanced O_3 downwind of petrochemical facilities in Houston. One flight (18 September 2013) devoted an hour of flight repeatedly sampling the plume transported downwind from the Houston Ship Channel (HSC) area. Historically, direct emissions of highly reactive volatile organic compounds, referred to as HRVOC (specifically ethene, propene, butenes, and 1,3-butadiene), and formaldehyde (HCHO) have been implicated in these types of high O_3 events, but quantifying the relative contributions of different precursors to O_3 formation has been difficult.

This report describes a data analysis and plume modeling study to obtain further insight into the photochemical oxidation of HRVOC. The study uses new airborne data, taken aboard the NASA DC-8 research aircraft during the 2013 SEAC[4]RS project in Houston, TX. Information contained in Chemical Ionization Mass Spectrometer (CIMS) measurements of C_2-C_5 β-hydroxynitrates during the flights provides a novel means to link observed O_3 and HCHO enhancements to emissions of specific alkenes.

1.2   APPROACH

The approach consists of data analysis and reactive plume modeling using the highly spatially resolved airborne data collected aboard the DC-8. The data includes hydroxynitrate measurements and measurements of nitrogen oxides (NOx), HCHO, and other chemical tracers. Data from HSC plume encounters during DC-8 landing approaches into Ellington Field on multiple flights in August and September 2013 show clear enhancements in the C_2-C_5 β-hydroxynitrates. Analysis of this data, combined with known β-hydroxynitrate yields, permits a robust first-order attribution of observed O_3 and HCHO enhancements to the oxidation of individual HRVOC and isoprene. A systematic survey capturing plumes from the W.A. Parish power plant, the Houston urban area, and the HSC by the DC-8 aircraft on 18 September 2013 provides further data from which atmospheric reaction rates and yields can be determined.

Reactive plume modeling of the HSC plume is conducted using the SCICHEM 3.0 model and revision 2 of the Carbon Bond 6 (CB6r2) chemical mechanism with reactions added for individual HRVOC. The modeling evaluates current chemical mechanisms against in-situ data and tests how plume dilution influences chemical processing and therefore how grid

model resolution can influence modeled impacts of HRVOC sources. The analyses and modeling, enabled by the novel β-hydroxynitrate data, better link industrial alkene emissions to their reaction products O_3 and HCHO, and permit a more quantitative assessment of HRVOC sources and their impacts on the Houston atmosphere.

Section 2 of this report presents the data analysis for selected days when the HSC plumes were measured during the SEAC[4]RS experiment. Section 2 also describes how β-hydroxynitrates are formed from HRVOC and the simplified chemistry scheme for β-hydroxynitrate production used in both the data analysis and the modeling. Section 3 describes the reactive plume modeling conducted with SCICHEM for 18 September 2013. Section 4 presents our conclusions and recommendations.

2. OBSERVATIONAL ANALYSIS

During the SEAC[4]RS flights over Houston, the Caltech instrument detected the presence of β-hydroxynitrates (βHN) produced in the gas-phase oxidation of alkenes, including those produced from the oxidation of ethene, propene, butenes, 1,3-butadiene, and isoprene. While these small β-hydroxy nitrates have been previously observed in the laboratory, this is the first systematic detection of their presence in ambient air. β-hydroxynitrates produced from these five alkenes were all present and detected with excellent signal-to-noise ratios.

The quality assured and quality controlled (QA/QC'd) βHN data for all SEAC[4]RS flights over Texas were obtained. These data were provided to the AQRP study team by Caltech who QA/QC'd the data with support from NASA. While Caltech did not directly participate in this AQRP study, issues and questions that arose during the data analysis were resolved through collaboration with Caltech. The data were reviewed and the flights of most interest for analysis and modeling in this project were identified. The major focus was on a systematic survey capturing plumes from the W.A. Parish power plant, the Houston urban area, and the HSC by the DC-8 aircraft on 18 September 2013. However, one drawback of this flight is that prevailing winds transported the plume over the Houston urban area, introducing urban emissions into the HSC plume and complicating the observational analysis and modeling. Two flights (19 August and 4 September) intercepted plumes from the HSC area over regions other than the Houston urban area; data from these two flights will be the second focus of future potential modeling. Eight additional flights also intercepted plumes from the HSC area; they have all been examined in the observational analysis. In all, measurements from twenty plume intercepts were analyzed. The observational analysis described here provides measurement-based estimates of plume initial conditions, background concentrations, and dispersion as constraints for the plume modeling described in Section 3, as well as providing the basis for assessing the chemical evolution in the HSC plumes.

The observational analysis discussed in this section examined βHN data in conjunction with observations of NOx (NO + NO$_2$), hydrocarbon, peroxyacetyl nitrate (PAN), nitric acid (HNO$_3$), total reactive nitrogen oxides (NOy), O$_3$, formaldehyde (CH$_2$O or HCHO), acetaldehyde (CH$_3$CHO), and other chemical and meteorological parameters measured aboard the NASA DC-8. The goals were to determine the relationships between the ambient concentrations of photochemical products (particularly the βHN, O$_3$ and aldehydes) and precursor species and to elucidate net O$_3$ and aldehyde production rates and yields. As alkenes are oxidized, CH$_2$O and CH$_3$CHO are formed along with the βHN. Thus, we expect strong correlations between these species. However, analysis indicates that loss processes for some of these species are rapid, leading to the loss of this correlation as the plume moves downwind, and that other VOCs may have played a dominant role in fueling the photochemistry in many of the plumes. The photochemical modeling described in Section 3

is a necessary complement to this analysis to provide a complete picture of the photochemical oxidation of HRVOC downwind of the HSC.

In the discussion below, the observational analyses are first exemplified by results from four of the SEAC[4]RS flights: 18 September, 19 August, 4 September and 23 September, and then aspects of all of the plume analyses are discussed.

2.1 PLUME TRAJECTORY ANALYSIS

Enhanced concentrations of the β-hydroxynitrates were observed not only downwind of the HSC, but also in wildfire plumes. Trajectory analysis was conducted for plumes suspected to have originated in the HSC area to confirm their origin and to provide a semi-quantitative indication of the plume transport history. Back trajectories were calculated from the DC-8 flight track for specific plume transects, with the origin generally taken as the location where the highest βHN concentrations were observed. The NOAA/ESRL/PSD trajectory tool (http://www.esrl.noaa.gov/psd/programs/2013/texaqs/traj/) was used to perform the trajectory calculations. The wind profiler network deployed in the Houston area during the SEAC[4]RS field campaign provided the wind data on which the trajectories are based.

Figure 2.1 shows this trajectory analysis for the four example flights. A variety of transport conditions are shown, from relatively rapid direct transport on 18 September and 19 August to evidence for recirculating airflow on 4 September.

2.2 EMISSION RATIOS OF ALKENES OVER THE HSC REGION

The rates at which different alkenes are emitted from the HSC petrochemical facilities determine the initial concentrations of the alkenes that are processed to form photochemical products. Ambient concentrations of hydrocarbons over the HSC region can provide information regarding these initial concentrations. During the 18 September flight the DC-8 circled over the HSC region (see flight path in Figure 2.1) while 14 whole air samples were collected. Post-flight analysis of the alkene concentrations provides the basis for estimating the relative initial concentrations of the alkenes. Figure 2.2 shows the correlations of propene, butenes (sum of the four isomers) and 1,3-butadiene with ethene; the slopes of these correlations (annotated in the figure panels) provide the estimated relative initial concentrations. All three correlations indicate positive ethene intercepts, which is interpreted to indicate ethene emissions from sources other than the industrial facilities in the HSC, e.g. vehicle tailpipe emissions.

Figure 2.2 indicates that there is a great deal of variability in the relative alkene emissions implied by the 14 samples. As a consequence, there is a substantial uncertainty in estimating the relative initial concentrations at the time of this particular aircraft flight. There may be even greater variability during the SEAC[4]RS study period since emissions from the petrochemical facilities are believed to vary on time scales from hours to years.
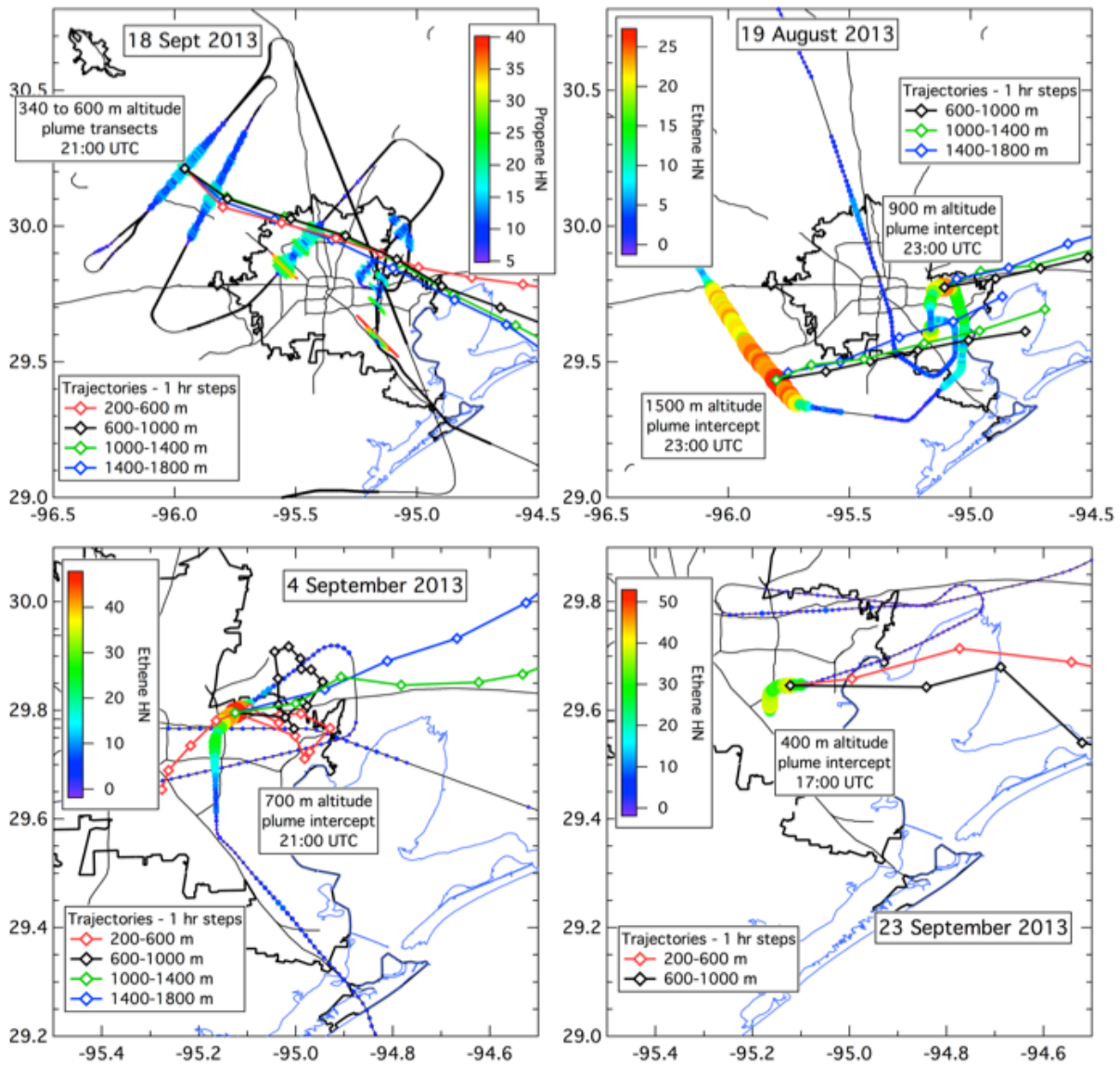
Figure 2.1. Trajectory analysis for four of the SEAC4RS flights. Trajectories calculated from winds averaged over four altitude bins were calculated, although some are not shown for clarity. Each symbol along a trajectory represents one hour of transport time. The flight tracks of the DC-8 are color-coded according to a measured β-hydroxynitrate as indicated by the color scale. The time and altitude of the plume intercept are indicated. On 18 September (upper left pane), the DC-8 sampled HSC emissions over the HSC and at three downwind distances, referred to below as T40, T80 and T100 where the numbers indicate the approximate downwind distances.
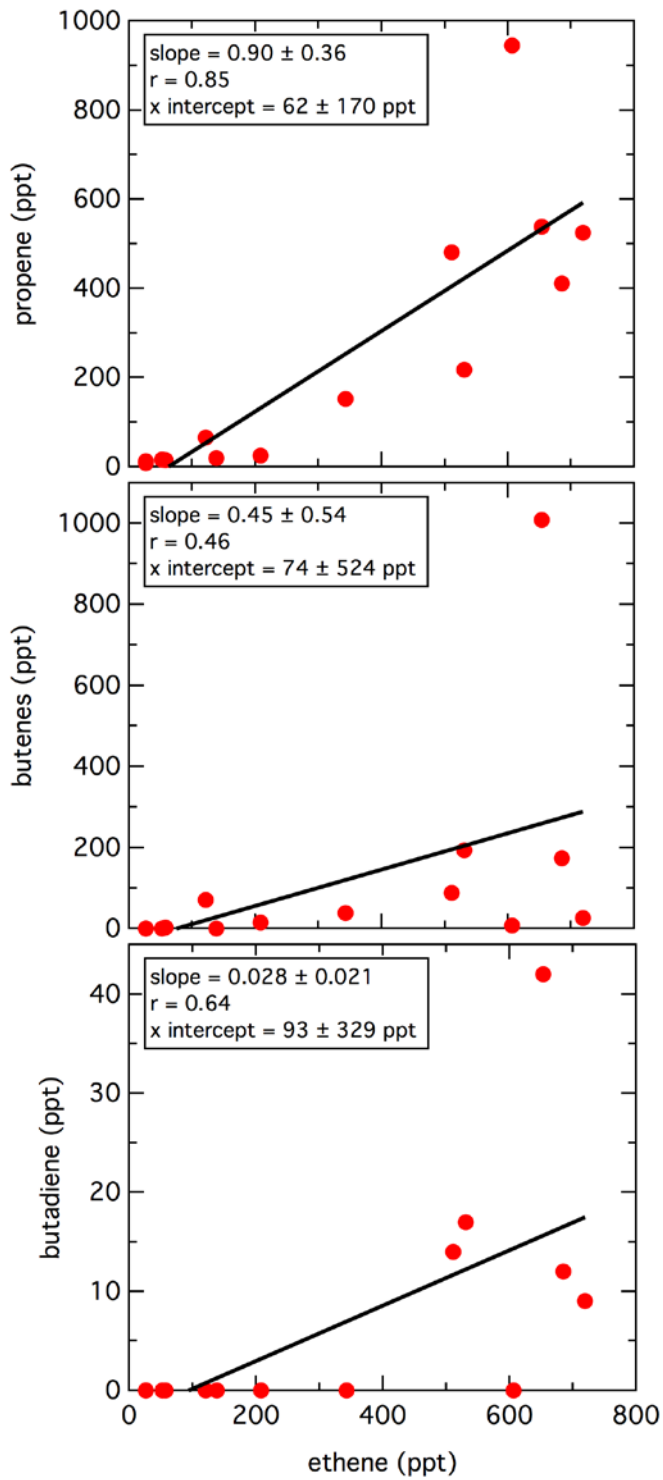
Figure 2.2. Relationships between alkene concentrations measured during the 18 September SEAC4RS flight. These data are from analysis of 14 whole air samples collected over the HSC area (flight track in Figure 2.1). Standard linear regression fits are shown with the slopes and intercepts with 95% confidence limits annotated. Data reported as below detection limit are included here as zero.

Table 2.1 compares the relative emissions rates derived from Figure 2.2 with values reported from other studies. The propene to ethene ratio agrees within the 95% confidence limits with the ratio of the emissions from HSC measured by *Johansson et al.* (2014a) in 2011. The modeling presented in this work used the measured 2011 emissions of *Johansson et al.* (2014a), and the emissions of the butenes and butadiene required to match the ratios derived from the correlations in Figure 2.2. All of these emission ratios are in approximate agreement with the ratios of the average ambient concentrations measured by *Gilman et al.,* 2009 in the Houston and Galveston Bay area (Table 2.1).

Table 2.1. Ratios of alkenes to ethene for the HSC.

Alkene ratio	Fig. 2.2	*Johansson et al.,* 2014a	*Gilman et al.,* 2009
Propene/Ethene	0.90 ± 0.36	0.61	0.57
Butenes/Ethene	0.45 ± 0.54	---	0.27
Butadiene/Ethene	0.03 ± 0.02	---	0.03

2.3   EVOLUTION OF β-HYDROXYNITRATES FROM PARENT ALKENE OXIDATION AND THEIR RELATIONSHIP TO EACH OTHER

In the HSC plumes sampled during SEAC[4]RS, the measured βHN concentrations in many cases correlated well with each other; Figure 2.3 shows correlations between two of the βHNs in two example plume transects. The slopes of the linear regressions shown in Figure 2.3 are taken as the best measure of the ratio of respective βHNs produced in the plumes. In other plumes the correlations were much poorer; thus the precision of the determination of the βHN ratios varied widely. Here we investigate what the ratios tell us about the evolution of the βHNs from their parent alkenes. In total, the ratios of βHNs from propene, the butenes, and butadiene to ethene hydroxynitate were calculated for 19 separate plumes in the manner illustrated in Figure 2.3.

Under simplifying approximations, the ratios of βHN concentrations can be formulated as a function of the initial emission ratios of the parent alkenes and kinetic parameters. These assumptions are

1. the initial alkene concentration ratios are equal to those derived from Figure 2.2 and included in Table 2.1,
2. the βHN are not removed from the atmosphere - they simply accumulate in the air parcels as the plume is transported downwind, and
3. the HSC is the only important source of the parent alkenes.
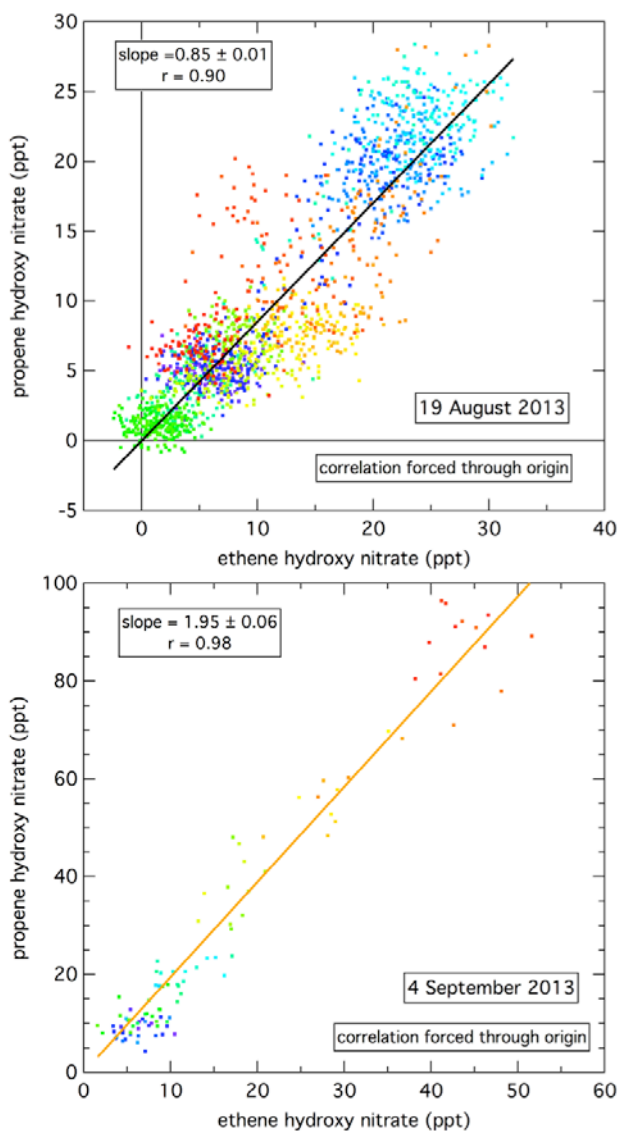
Figure 2.3. Correlations between concentrations of two □HNs measured during HSC plume transits from two SEAC4RS flights. Standard linear regression fits with intercepts forced to zero are shown with the slopes and 95% confidence limits annotated. Data points are measured 1-sec average mixing ratios, and are color-coded in order of measurement time during the plume transit.

Finally we assume that dispersion can be considered to be dilution by clean air, i.e. with zero concentrations of βHN and parent alkenes; in the following we deal only with concentration ratios, so dispersion can then be ignored. The evolution with time, t, of the concentrations of a given βHN and its parent alkene, A, are then given as

$$[A] = [A]_0 \exp(-k[OH]t) \qquad (2.1)$$

and

$$[\beta HN] = [A]_0 (1 - \exp(-k[OH]t)) f_a \alpha \qquad (2.2)$$

where $[A]_0$ is the initial alkene concentration, the symbols f_a and α are reaction branching ratios defined in Appendix A, and k is the rate constant for the reaction of the alkene with OH. Table 2.2 gives the kinetic parameters utilized in this analysis.

The ratio of two βHNs can be analytically evaluated in two limits. First, early in the evolution (i.e., in fresh plumes) the exponential in Equation 2.2 can be approximated as 1-k[OH]t so that $[\beta HN] \sim [A]_0 k[OH]t \cdot f_a \alpha$ The ratio of two βHNs is then

$$\frac{[\beta HN_2]}{[\beta HN_1]} = \frac{[A_2]_0 k_2 \cdot f_{a_2} \alpha_2}{[A_1]_0 k_1 \cdot f_{a_1} \alpha_1}. \qquad (2.3)$$

Second, when plumes are completely aged all of the alkenes have reacted, and the exponential in Equation 2.2 goes to zero, so

$$\frac{[\beta HN_2]}{[\beta HN_1]} = \frac{[A_2]_0 \cdot f_{a_2} \alpha_2}{[A_1]_0 \cdot f_{a_1} \alpha_1}. \qquad (2.4)$$

Table 2.2. Parameters used in calculating β-hydroxynitrates, aldehyde and O_3 enhancements from alkene oxidation. Values for butene are weighted averages over the four isomers.

Alkene	k (10^{-12} cm^{3}s^{-1})	f_a	α	γ	δ	O_3 yield
Ethene	0.852	1.00	0.023	1.6	0	1.95
Propene	2.630	0.97	0.053	1.0	1	1.87
Butene	4.400	0.95	0.106	1.0	1	1.76
Butadiene	6.660	0.97	0.104	1.0	0	1.77
Isoprene	10.000	0.92	0.120	1.0	0	1.69

In Figure 2.4, the solid curve indicates the evolution of two βHN ratios between the two limits. Equation 2.3 gives the ratios early in the oxidation process (upper right endpoint, solid circle). The ratios decrease as the original alkene mixture photochemically ages, and when all the alkenes have reacted, reach the lower limits (lower left endpoint, open symbol). Numerical evaluation of Equation 2.2 for the concentrations of two βHN gives the solid curve connecting the endpoints.

9
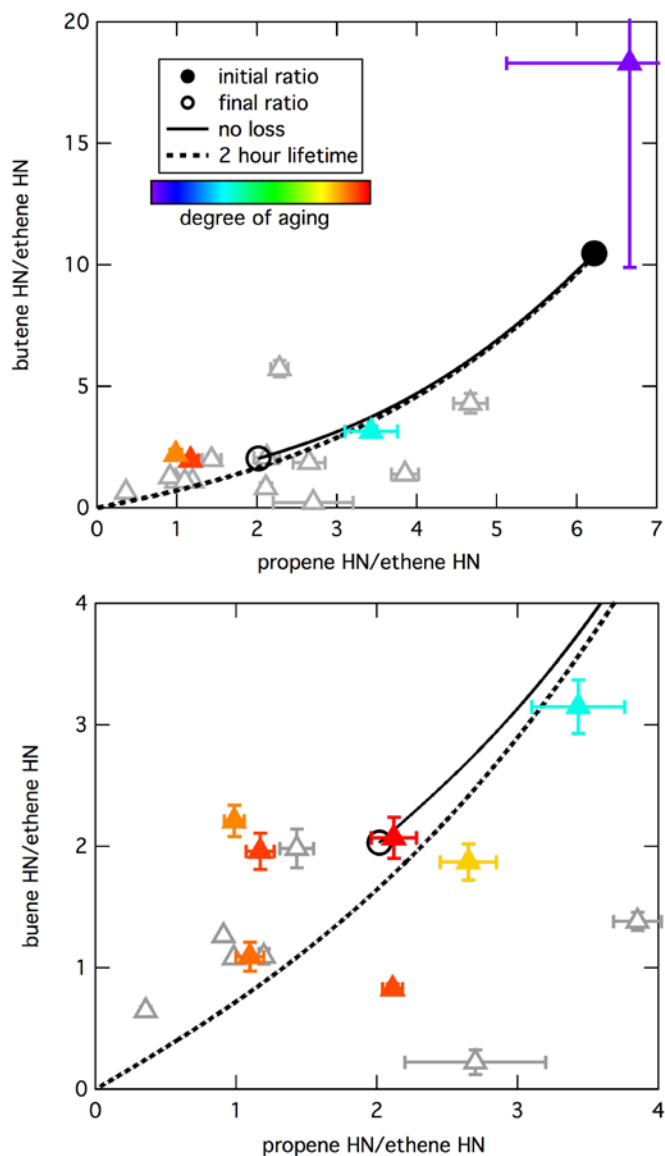
Figure 2.4. Relationship between two β-hydroxynitrate ratios. Symbols show measured ratios in HSC plumes during all SEAC4RS flights; error bars give 95% confidence limits derived from linear regressions as illustrated in Figure 2.3. As discussed in the text, lines give the evolution expected for a plume with initial alkene concentration ratios indicated in Table 2.1 and loss of βHN of zero (solid lines) or a 2-hour e-folding lifetime (dotted lines). The initial and final ratios given by Equations 2.3 and 2.4 are indicated by solid and open circles, respectively. The points are color-coded by degree of photochemical aging as indicated by the NOx/NOy ratio, which varied from 0.92 in the freshest plume to 0.17 in the most aged. In the top panel, only the points from the four plume intercepts on the 18 September flight are color-coded. In the bottom panel with expanded axes, all of the plumes with NOy data available are color-coded.

In the upper panel of Figure 2.4, the evolution of the βHN ratios in the 18 September flight (colored points) approximately follows the simplified analysis of Equations 2.1-2.4. The data from over the HSC (violet points) are poorly correlated, and therefore give uncertain ratios, but within the confidence limits there is reasonable agreement with the expected initial ratio (closed circle). The initial butene to ethene ratio is also quite uncertain (Table 2.1); a smaller assumed emission ratio would improve the agreement. The T40 point (blue, see Figure 2.1 caption for labeling of plume transects) closely fits the solid line, as do the T80 and T100 points (orange and red, respectively), except that the propene HN/ethene HN ratios are smaller than the expected final ratio (open circle).

The lower panel of Figure 2.4 indicates that it is common for ratios in aged plumes to be less than the expected lower limit for both the propene HN/ethene HN and butene HN/ethene HN ratios. Removal of the βHNs during plume photochemical evolution and transport is one explanation for this feature. The dotted lines in Figure 2.4 show the integration of Equation 2.2 with the inclusion of removal of all βHNs with a common 2-hour e-folding lifetime. Due to its smaller rate constant, ethene is oxidized more slowly so that, on average, ethene HN is produced later in the photochemical evolution. Thus, the removal process has a smaller effect on its concentration than the concentrations of the more reactive βHNs, which then decreases the ratios since the ethene HN concentration is in the denominator. The dotted line indicates that the ratios approach zero as the photochemical evolution is completed, and thus can explain the smaller than expected ratios. Figure 2.5 shows similar behavior for the butadiene HN/ethene HN ratio.

The large scatter of the data points in Figures 2.4 and 2.5 likely indicates the influence of variable alkene emission rates. The systematic underprediction of the butadiene-HN/ethene-HN ratio in Figure 2.5 may indicate that the butadiene to ethene emission ratio is systematically underestimated in Table 2.1.

It should be mentioned that one plume analyzed from the 23 September flight gave a propene HN/ethene HN ratio that is much larger (10.7) than seen in any other plume, and larger than consistent with the assumed ethene to propene emission ratio. This plume also contained the largest propene HN concentrations (~ 500 ppt) observed in any of the HSC plumes. Large emissions very rich in propene relative to ethene are evidently responsible for this plume, which may represent an exceptional event in the HSC.
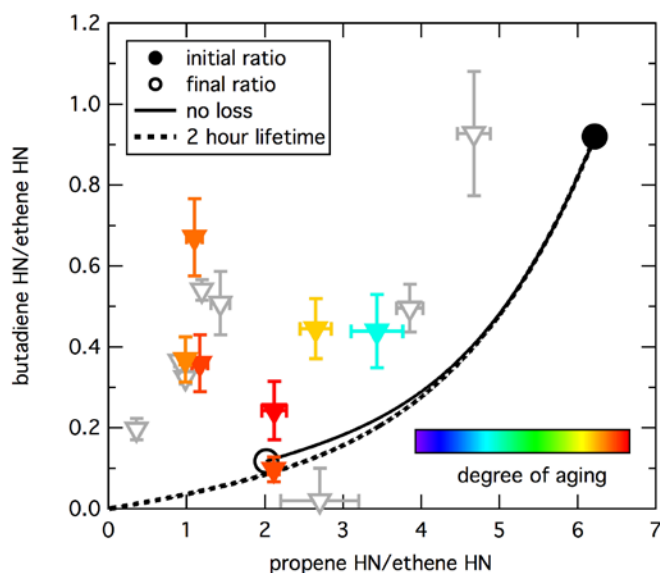
Figure 2.5. Relationship between two β-hydroxynitrate ratios in generally the same format as Figure 2.4.

2.4   RELATIONSHIP OF ALDEHYDES TO β-HYDROXYNITRATES

As alkenes are oxidized, formaldehyde and acetaldehyde are formed along with the βHN. Thus, we expect strong correlations between these species in the sampled HSC plumes. *Teng et al.* [2015] show such strong correlations (their Figure 8) for the 18 September flight. Our goal here is to investigate the quantitative relationships, which can be directly related to branching ratios of the alkene oxidation reactions.

A simplified chemistry scheme for β-hydroxynitrate formation during alkene oxidation was developed to investigate these relationships and to underpin the observational analysis and modeling. The scheme is described in detail in Appendix A. This scheme utilizes the known βHN yields following OH-initiated reactions of their parent alkenes [*Teng et al.*, 2015], and permits a first-order attribution of the O_3 and aldehydes formed as a result of emissions of each specific alkene. Section 3 describes reactive plume modeling that explicitly treats losses of photochemical products and formation of 2nd-generation reaction products, which augments this simple observation-based analysis. Alkene emissions inferred from hydroxynitrate observations are compared to the DC-8 whole-air-sample (WAS) data on ethene, propene, butene, and butadiene in these plumes, and linked to the original emission ratio for individual plumes by the observed NOx/ethene ratio, which is preserved during transport from the source [*Ryerson et al.,* 2003].

Based on the simplified chemistry scheme described in Appendix A, the quantitative relationships between aldehydes and the β-hydroxynitrates can be expressed as:

$$\Delta[CH_2O] = \sum_i \frac{\gamma_i(1-\alpha_i)}{\alpha_i} \times [\beta HN]_i \qquad (2.5)$$

and $\qquad \Delta[CH_3CHO] = \sum_i \frac{\delta_i(1-\alpha_i)}{\alpha_i} \times [\beta HN]_i \qquad (2.6)$

where the summations are over all important alkenes. The parameters in Equations (2.5) and (2.6) are defined in the kinetics scheme described in Appendix A. Table 2.2 gives the parameters selected for this analysis. Figure 2.6 compares the results of the formaldehyde concentrations calculated from Equation (2.5) with those measured during four example SEAC[4]RS flights downwind from the HSC area. Excellent correlations (correlation coefficients are all ~0.9) are found for CH_2O measured by two separate instruments in all plume intercepts. Figure 2.7 shows similar results for CH_3CHO concentrations calculated from Equation (2.6) with those measured by a third instrument. Excellent correlations (correlation coefficients are all ~0.9) are also found for CH_3CHO.

Despite the good correlations observed in Figures 2.6 and 2.7, the slopes of the correlations are generally significantly less than unity. This difference suggests that other factors (e.g., contributions to aldehyde production from VOCs other than the alkenes or different rates of removal of the aldehydes and the β-HNs) affect these slopes. This issue will be discussed further in the next section.

Figures 2.8 and 2.9 compare time series of calculated and measured aldehyde concentrations for the 18 September flight; the calculated β-HN concentrations are increased by a factor of 2 in these comparisons. This factor approximately corrects the systematic difference between the calculated and measured concentrations indicated by the slopes in Figures 2.5 and 2.6, which are all near 0.5 for this flight. These figures show remarkable agreement between the calculations and measurements, which emphasizes the good correlations shown in Figures 2.5 and 2.6. The measured aldehyde concentrations are also offset by the approximate concentrations measured outside the plumes.
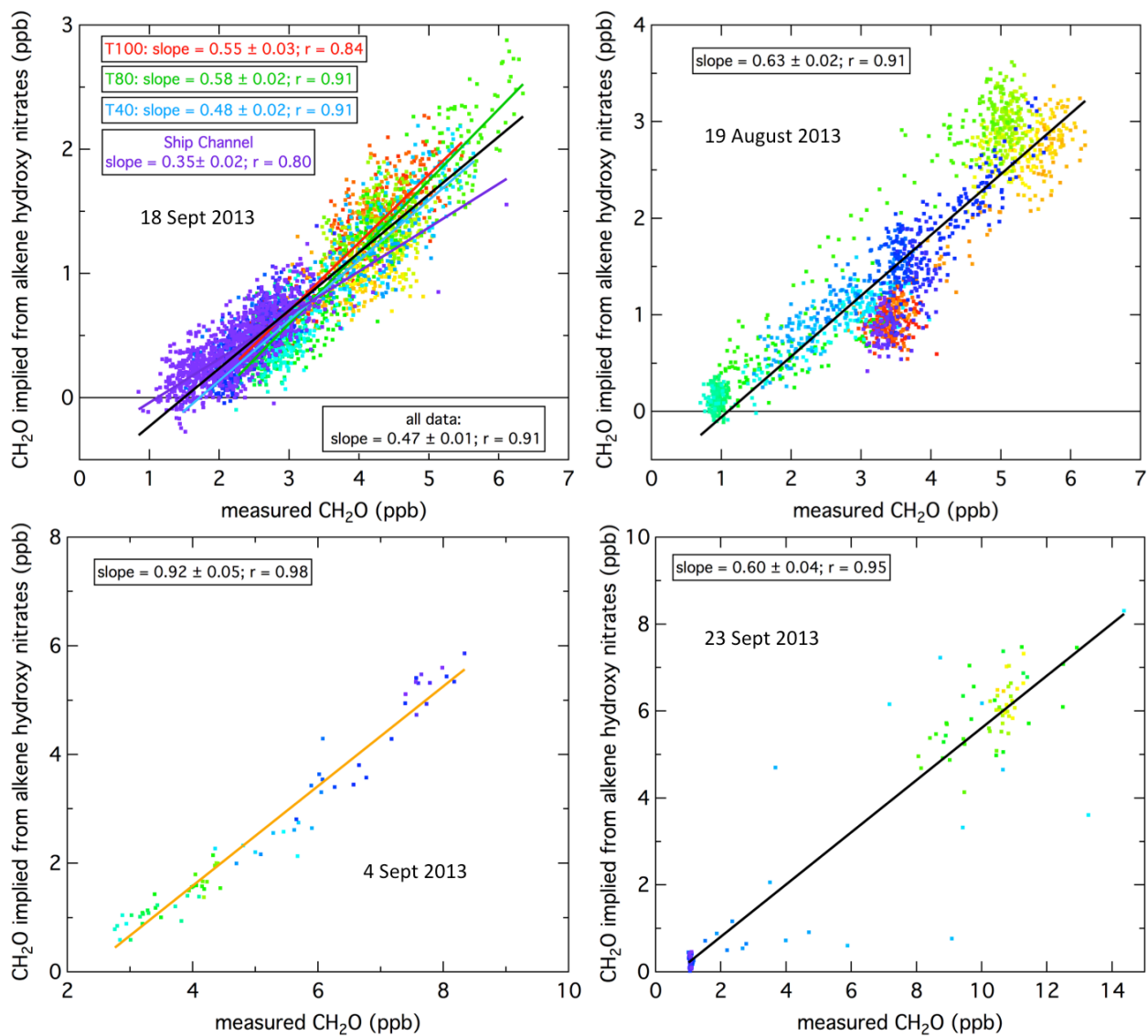
Figure 2.6. Correlation between CH_2O concentrations calculated from the oxidation of five alkenes from Equation (2.5) versus CH_2O measured for four of the SEAC[4]RS flights. Data points are color-coded from early in the plume (warm colors) to late in the plume (cool colors). The slopes with 95% confidence limits and correlations for the standard linear regressions (lines) are annotated. The 18 September flight includes the four plume intercepts shown in Figures 2.1 and 2.8.
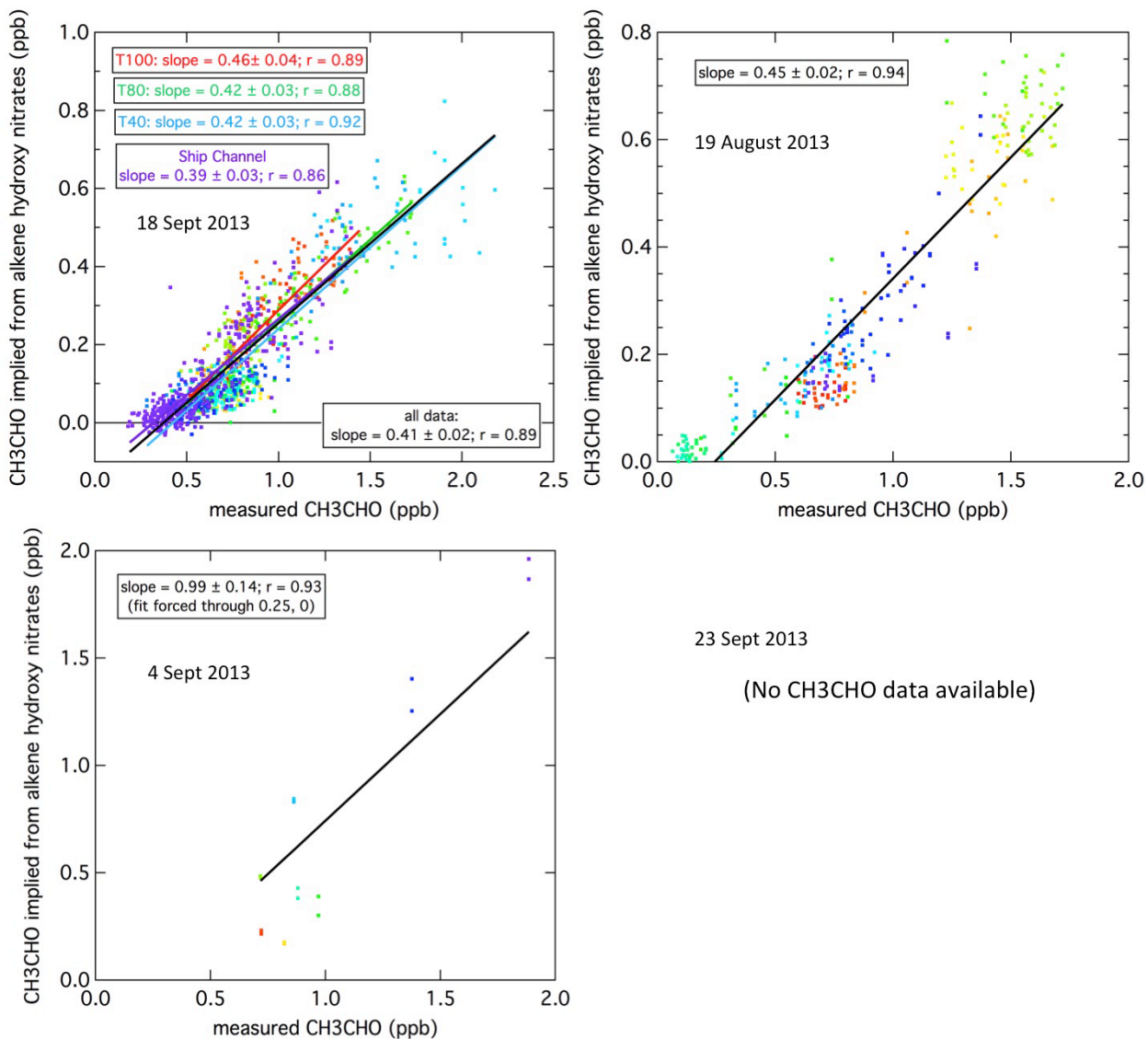
Figure 2.7. Correlation between CH$_3$CHO concentrations calculated from the oxidation of five alkenes from Equation (2.6) versus CH$_3$CHO measured for four of the SEAC^{4}RS flights in the same format as Figure 2.6. The data from the 4 September flight were sparse and scattered; the x-intercept of the fit was forced to be 0.25 ppb to be approximately consistent with the other three flights.
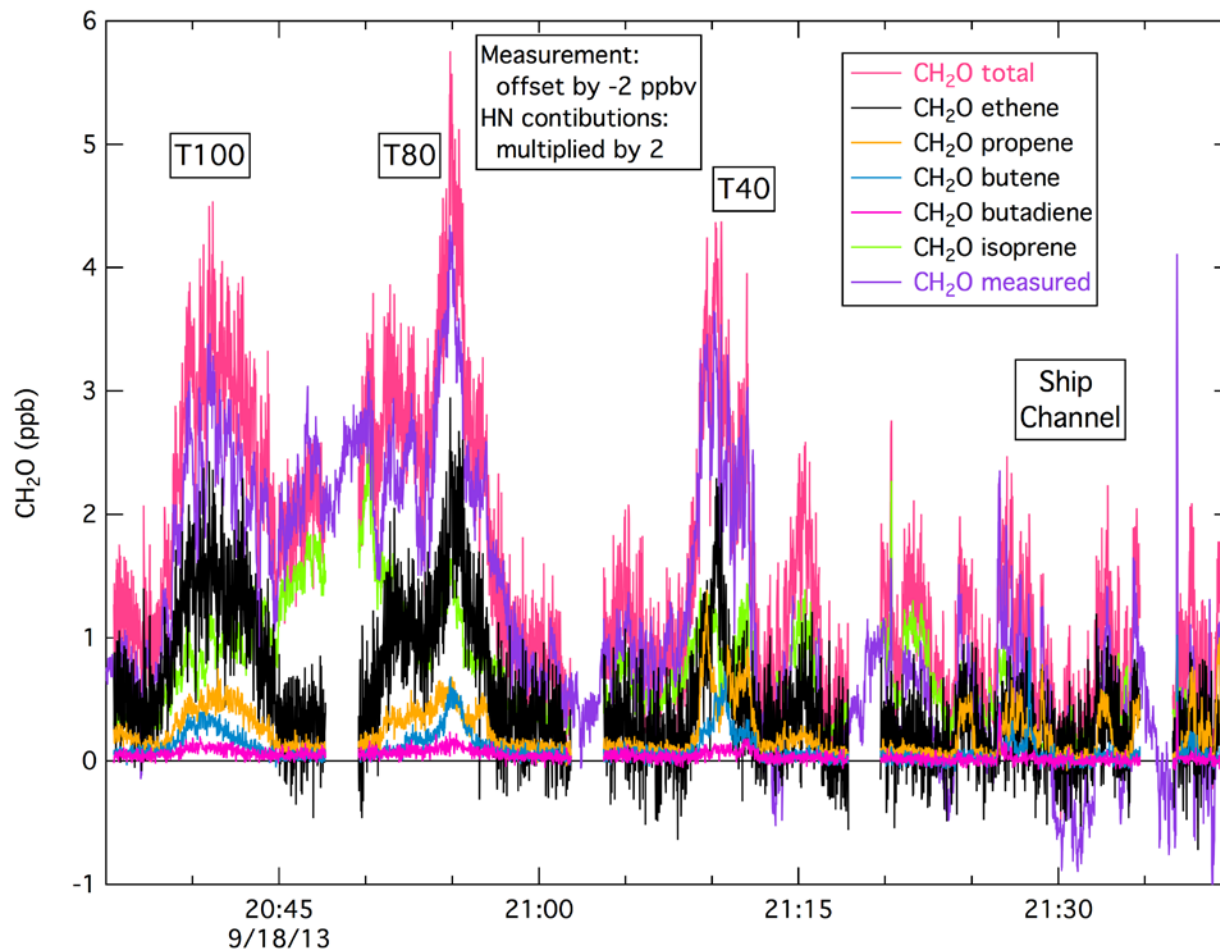
Figure 2.8. Comparison of time series of CH_2O concentrations calculated from the oxidation of five alkenes with those measured on the 18 September 2013 flight. The calculated contributions from five alkenes are shown separately, along with their total; these have all been multiplied by a factor of 2 (see discussion in text). An offset of 2 ppb has been subtracted from the measurements (see discussion in text). All curves are color-coded according to the annotation. The color scale at the top indicates the time color-coding of the data points in the data from this flight in Figures 2.6, 2.7 and 2.10. The three downwind plumes are marked with approximate downwind distances. Data collected over the HSC are also indicated.

16
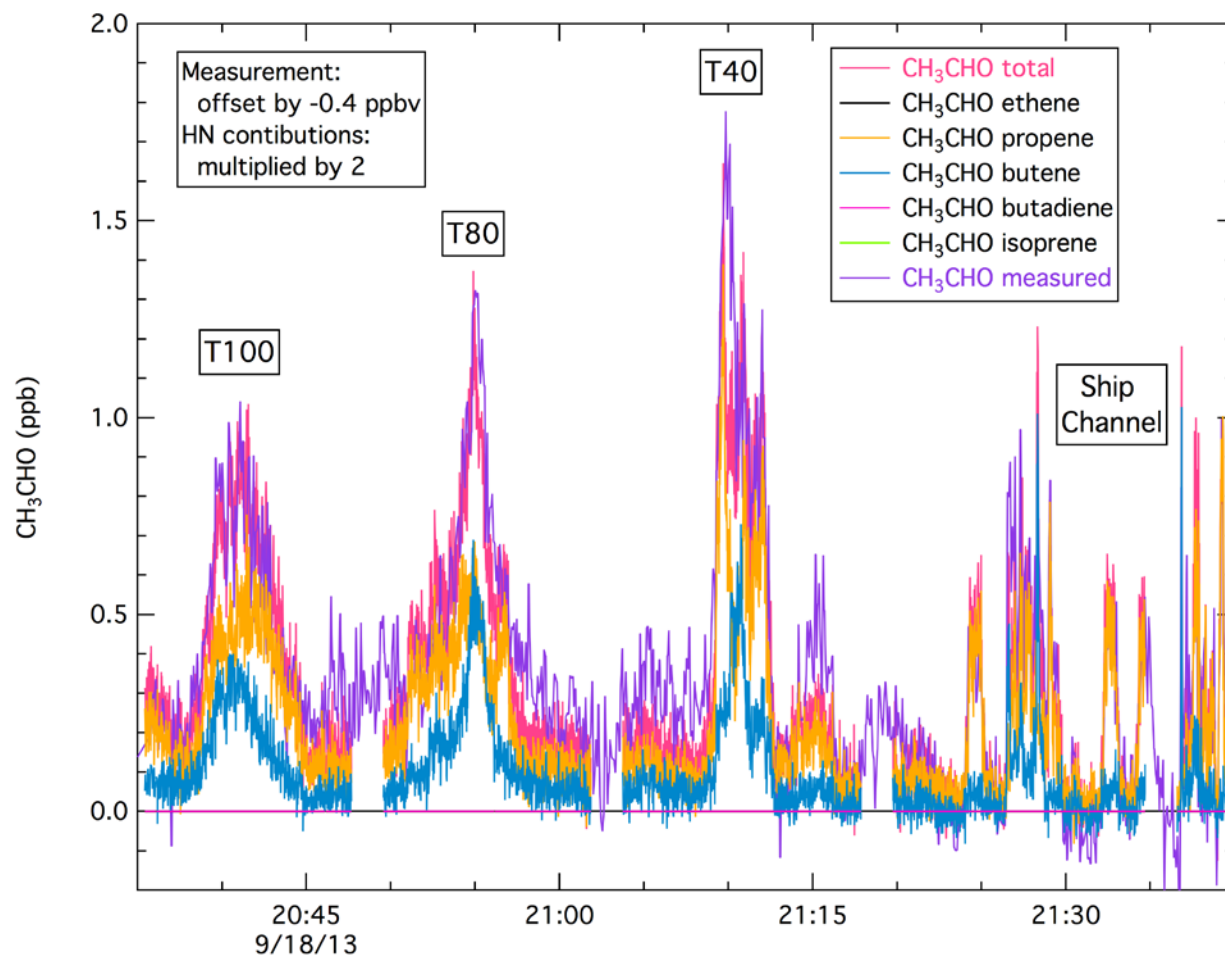
Figure 2.9. Comparison of time series of CH₃CHO concentrations calculated from the oxidation of five alkenes with those measured on the 18 September 2013 flight in the same format as Figure 2.8. The calculated contributions from five alkenes are shown separately (although 3 of the 5 are zero), along with their total; these have all been multiplied by a factor of 2 (see discussion in text). An offset of 0.4 ppb has been subtracted from the measurements (see discussion in text). All curves are color-coded according to the annotation.

2.5 RELATIONSHIP OF OZONE TO β-HYDROXYNITRATES AND SPECIES LIFETIMES

As alkenes are oxidized, O_3 is also formed along with the βHN and aldehydes. Thus, we also expect strong correlations between βHN and O_3 with a relationship that can be directly related to branching ratios of the oxidation reactions. This relationship is:

$$\Delta[O_3] = \sum_i \frac{O_3 yield_i}{f_{ai}\alpha_i} \times [\beta HN]_i \qquad (2.7)$$

where the summation is over all important alkenes.

17

Figure 2.10 compares the results of the O_3 concentrations calculated from Equation (2.7) with those measured during the four example SEAC[4]RS flights downwind from the HSC area. The parameters for this analysis are in Table 2.2. Correlations are again strong (correlation coefficients are all ~0.7-0.99) in all individual plume intercepts. However, the slopes of the correlations are not only less than unity, but are also significantly smaller than found in the aldehyde correlations (except perhaps for the 23 September flight). Figure 2.11 compares time series of calculated and measured O_3 concentrations ($Ox = O_3 + NO_2$ is plotted for the measurements to avoid distortion of the relationship due to O_3 titration by fresh NO emissions); the factor of 2 increase in the β-hydroxynitrate concentrations has been included in the comparisons in this figure. It is clear that the calculation from the β-hydroxynitrates greatly underestimates the observed O_3 concentrations.

Dominance of photochemical O_3 production by VOCs other than alkenes is perhaps the simplest explanation for the small slopes observed in Figure 2.10. Taken at face value, these slopes indicate that oxidation of these five alkenes generally account for no more than 25% of the O_3 production in the plumes downwind of the HSC. There are some exceptions where the alkenes account for a greater fraction. Lines with a slope of 0.5 (dashed brown lines in Figure 2.10) provide good fits to the data over the HSC on 18 September and a section of the data from 19 August. Finally, the plume encountered on 23 September gives the highest observed slope (0.58) of all plumes encountered, but as discussed above, this plume is characterized by a very large propene to ethene ratio and may represent an unusual emission release over the HSC.

Rapid removal of the βHNs is another explanation for the failure of Equation 2.7 to accurately reproduce O_3 in the downwind transects. This can explain the systematic decrease in the slopes in Figure 2.10 for the 18 September flight with downwind distance, with the larger slope directly over the HSC where a smaller fraction of the βHNs have been lost. This rapid removal is consistent with the good correlations shown in Figures 2.6 through 2.9, since the aldehydes are themselves lost rapidly from the atmosphere. If the βHNs were not removed at a similar rate, then the correlations would be expected to degrade in downwind transects. Evidently, the lifetimes of CH_2O, CH_3CHO and the βHNs are of the same order, thereby providing the good correlations seen in Figures 2.6 through 2.9.

The back trajectory calculations shown in Figure 2.1 indicate that, on 18 September, the plume traveled about 5 hours from emission to the furthest downwind transect. In that time, the NOx/NOy ratio decreased from unity to ~0.2. Assuming that the primary loss mechanism of NOx is the $NO_2 + OH$ reaction, this NOx to NOy conversion rate implies an average OH concentration of 8×10^6 cm^{-3} (assuming that $OH + NO_2$ is the dominant conversion process, and that the PAN contribution can be ignored). This OH concentration (along with photolysis of CH_2O) would imply lifetimes of 1.9 and 2.2 hours for CH_2O and CH_3CHO, respectively.
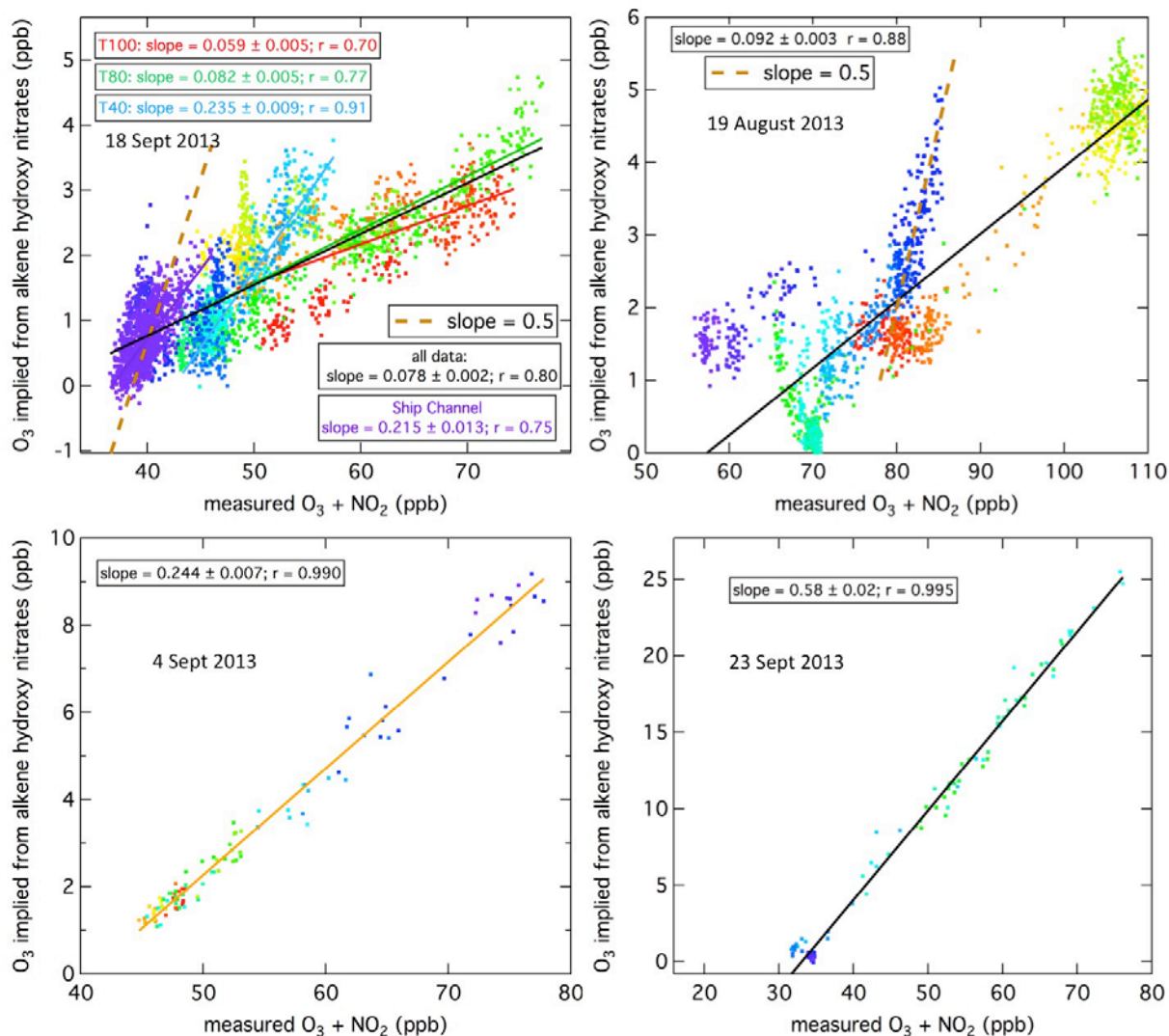
Figure 2.10. Correlation between O_3 concentrations calculated from the oxidation of five alkenes versus that measured for four of the SEAC[4]RS flights in the same format as Figure 2.6. For the HSC plume on18 September and a short period of the plume on 19 August, lines with a steeper slope = 0.5 are indicated by the brown dashed lines.

The above argument implies that the lifetime for the βHNs must have been of the order of ~2 hours as well. Photolysis and reaction with OH for the βHNs are much too slow to account for such a short lifetime. However, the βHNs are very soluble, so take up by aerosol may be an important loss process. Figures 2.6 and 2.7 suggest that on each flight, good correlations are found for the aldehydes with the βHNs, but that the slopes differ between plumes intercepted on different flights. This difference may indicate varying OH concentrations, photolysis rates, and aerosol loading between flights, which affect the loss rates of CH_2O, CH_3CHO, and the βHNs to varying extents. Analysis of additional plumes intercepted on other SEAC[4]RS flights may enlighten us regarding these differences.

19
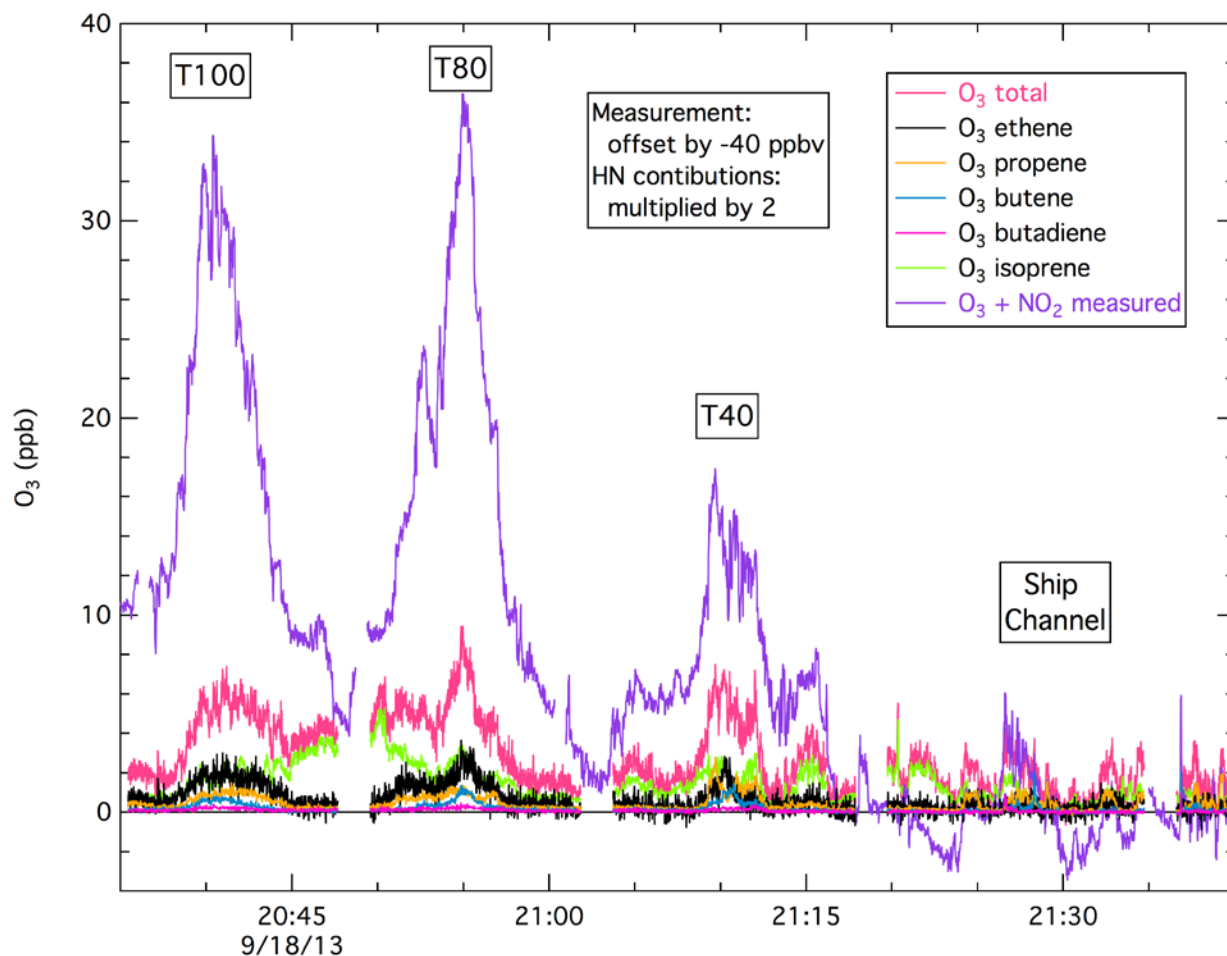
Figure 2.11. Time series of O_3 concentrations calculated from the oxidation of five alkenes and measured on the 18 September 2013 flight in the same format as Figure 2.8. The calculated contributions from five alkenes are shown separately, along with their total; these have all been multiplied by a factor of 2 (see discussion in text). An offset of 40 ppb has been subtracted from the measurements (see discussion in text). All curves are color-coded according to the annotation.

.

(A side note: In the above lifetime discussion, the role of PAN in the NOx, NOy system is ignored. From the HSC to T100 the PAN contribution to NOy increases from near zero to 0.25. This PAN contribution would lead to both an overestimate and an underestimate in the approximate OH concentration. The overestimate arises since no account was made for the amount of NO_2 converted to PAN instead of to nitric acid. The underestimate arises since no account was made for the amount of NO_2 sequestered as PAN, and hence unavailable to react with OH. Hence, the OH concentration estimate likely does not suffer from large errors.)

2.6 RELATIONSHIP OF SECONDARY PHOTOCHEMICAL PRODUCTS TO β-HYDROXYNITRATES IN ALL HSC PLUMES

A total of twenty plumes from the HSC suitable for analysis were intercepted on eleven SEAC[4]RS flights. Figure 2.12 compares some relationships between photochemical products for all of these plume intercepts. This comparison indicates that the 18 September flight, which is the primary focus of the analysis, is not atypical of all of the plume intercepts.

Points to note in this figure:

- In no case is the concentration of either aldehyde or O_3 implied by the measured βHNs higher than that measured (i.e., all ratios are less than 1), which indicates that the βHNs are removed from all of the plumes at least as fast as either aldehyde or O_3, assuming that the alkenes are the major precursors of all of these photochemical products.

- Most of the ratios are considerably less than unity, which indicates either that the βHNs are removed from all of the plumes considerably faster than either aldehyde and especially O_3, or that other VOCs are the primary precursors of O_3 and quite significant precursors of the aldehydes.

- In both graphs, the slopes of the linear regression fits to the points from all plumes (solid lines) are less than unity. This indicates that formaldehyde is removed, on average, more rapidly than acetaldehyde, and much more rapidly than O_3.

The $(O_3 + NO_2)$ to $(NO_y – NO_x)$ ratio in the HSC plumes provides a measure of the ozone production efficiency (OPE). Figure 2.13a indicates this efficiency has not changed substantially from TexAQS 2006 (see Figure 9 of *Neuman et al.,* 2009). Figure 2.13b shows an alternative representation of the OPE as the ratio of O_3 to NO_y in the plume.
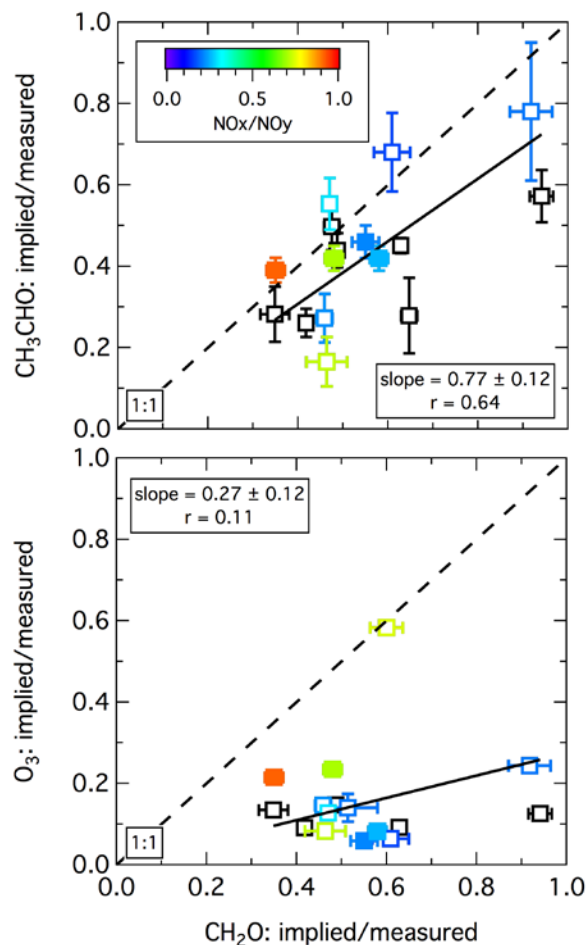
Figure 2.12. Comparison between the ratios of the secondary photochemical products implied by the measured β-hydroxynitrates and that measured directly. Each data point was derived from a correlation slope similar to those illustrated in Figures 2.5, 2.6 and 2.9. The points are color-coded according to the degree of photochemical processing as indicated by the NOx/NOy ratio (ratio = 1 in fresh plumes and decreases with aging). For several plumes, NOy data are not available; those are the black symbols. The filled symbols are the four plumes from the 18 September flight. The solid lines indicate the result of standard linear regressions with the intercepts forced to zero, and the dashed lines indicate the 1:1 relationship.
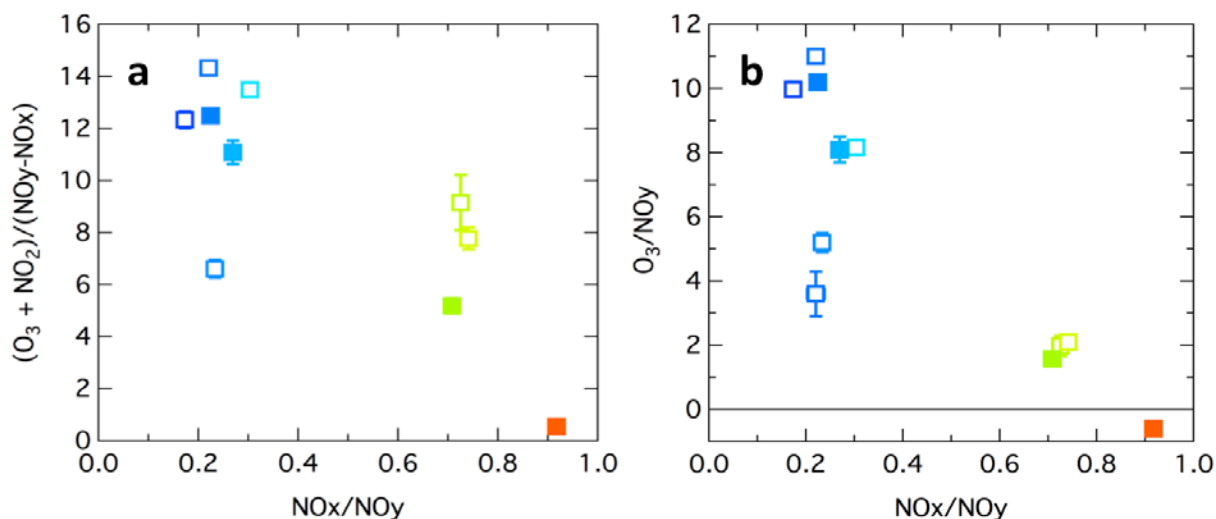
Figure 2.13. Relationship between **a)** the (O_3 + NO_2) to (NOy - NOx) ratio and **b)** the O_3 to NOy ratio versus the NOx to NOy ratio in the sampled plumes. The color-coding is the same as in Figure 2.12.

2.7 EVOLUTION OF β-HYDROXYNITRATE TO NOy RATIOS IN 18 SEPTEMBER FLIGHT

The 18 September flight provides the only data collected during multiple transects of a plume transported downwind from the HSC over a period of several hours (see trajectory calculations in Figure 2.1). Here we investigate how the ratios of the βHNs to NOy vary with progressive photochemical aging through the four plume transects. Our implicit assumptions here are that if we consider only concentration ratios, then we can ignore dispersion, and that NOy can be considered to be a conserved tracer over the time scale of transport (approximately 4 to 5 hours) so that [NOy] = [NOy]$_0$. Analogous to Figure 2.13, we will use the [NOx]/[NOy] as an indicator of the degree of photochemical aging.

Following the same simplifying approximations and arguments discussed in Section 2.3, an equation for the evolution of the βHN to NOy concentration ratio can be formulated. Initially all NOy is in the form of NOx, whose evolution can be approximated as

$$[NOx] = [NOy]_0 \exp\left(-k_{NO_2}[OH]t\right),$$ (2.8)

where k is the effective rate constant for the conversion of NOx to more highly oxidized NOy species (i.e., primarily HNO_3 and PAN). We assume that k can be approximated by the rate constant for the OH + NO_2 reaction to yield HNO_3, which we take as 1.1 x 10^{-12} cm^3 s^{-1}. Solving for [OH]t in Equation 2.8 and substituting into Equation 2.2 and manipulating gives

23

$$\frac{[\beta HN]}{[NOy]} = \frac{[A]_0}{[NOy]_0} f_a \alpha \left(1 - \left(\frac{[NOx]}{[NOy]}\right)^b\right) \qquad (2.9)$$

where $[A]_0/[NOy]_0$ is the initial alkene to NOy emission ratio and $b = k_{HC}/k_{NO2}$ is the ratio of the rate constants for the reactions of the alkene and NOx with OH. Table 2.2 gives the kinetic parameters utilized in this analysis.

Figure 2.14 shows least-squares regression fits of Equation 2.9 to the data collected on the 18 September flight, where the initial $[A]_0/[NOy]_0$ emission ratio is the variable determined in the regression. Table 2.3 compares the derived emission ratios to those assumed in the modeling described in Section 3. The modeling ratios are determined from the emissions of ethene (612 kg/hr), propene (563 kg/hr) and NOx (1830 kg/hr NO$_2$ and 396 kg/hr NO assuming that 75% of the NOx emissions are NO$_2$) measured in 2011 (*Johansson et al.*, 2014a), and the observed butene and butadiene to ethene ratios over the HSC (Table 2.1). Note that HSC emission rates for 2013 are now available from AQRP Project 14-007 but were not available at the time of this work. Figure 2.15 shows similar fits to data from all of the flights, and the corresponding derived emission ratios are included in Table 2.3.
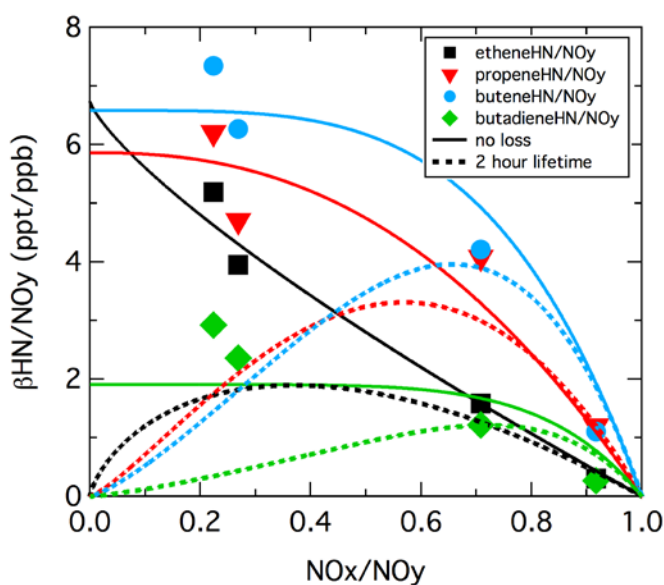
Figure 2.14. Relationship between the βHN to NOy ratios and the NOx to NOy ratio. The symbols show the measurements between the four 18 September HSC plume transects, with the progressively smaller NOx to NOy ratios at progressively further downwind distances. The solid lines give least square regression fits of these data to Equation 2.9. The dashed lines show how the solid lines would change if the βHNs were subject to removal with a two-hour lifetime.

Table 2.3. Comparison of alkene to NOx emission ratios for HSC on 18 September estimated from observed βHN to NOy concentration ratios and assumed in plume modeling

Alkene	Observations (18 Sept flight)	Observations (all flights)	Modeling
Ethene/NOy	0.293	0.182	0.410
Propene/NOy	0.114	0.102	0.250
Butene/NOy	0.065	0.053	0.190
Butadiene/NOy	0.019	0.015	0.013
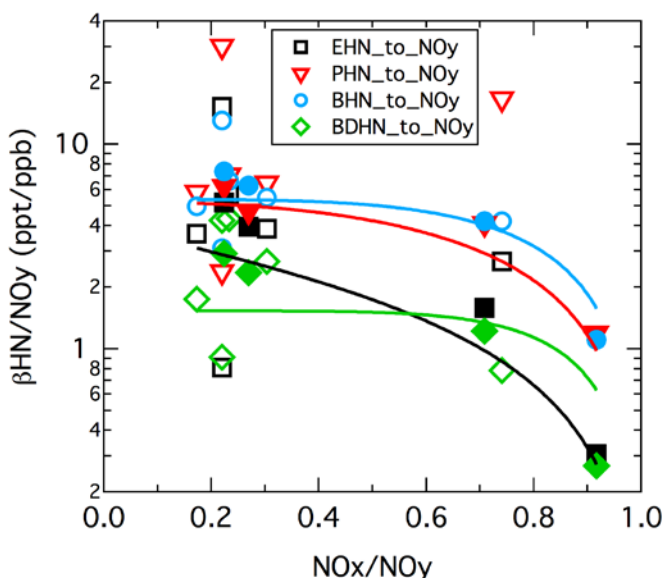
Figure 2.15. Relationship between the βHN to NOy ratios and the NOx to NOy ratio including measurements from all flights. The format is the same as Figure 2.14 except a log scale is used for the ordinate. The solid lines give least square regression fits of these data to Equation 2.9. The closed symbols show the measurements from the 18 September flight included in Figure 2.14.

The solid curves in Figures 2.14 and 2.15 are derived from Equation 2.9; they give reasonable qualitative descriptions of the observed ratios. However, the quantitative emission ratios derived from these fits are (except for butadiene) all lower than expected from the emissions used in the modeling by factors of 1.4 to 3.6), which would imply that the modeling alkene emissions are too high, or the NOx emissions too low, by these factors. Since the modeling emission ratios are primarily based on the measurements of *Johansson et al.* (2014a), such large errors in the emissions seem unlikely. Failure of some of the assumptions leading to Equation 2.9 must be considered. The influence of emissions from sources downwind of the HSC may be a likely contributor to this failure.

It is important to note that the dashed curves in Figure 2.14 give very poor fits to the observed ratios. Removal of the βHNs with a 2-hour e-folding time implies that the ratios to NOy of the βHNs produced from the more reactive alkenes would reach maxima by the T40 transect, but no such maxima are observed. Figure 2.15 indicates that the βHN to NOy ratios generally do not decrease as NOx is progressively oxidized to other NOy species. Previous sections suggested that rapid removal of βHNs offers a possible explanation for some observed features of the data; those suggestions are likely incorrect.

2.8 QUALITY ASSURANCE PROCEDURES

The analysis presented in Section 2 has been developed specifically for the interpretation of β-hydroxynitrate measurements. Since no such analysis has been presented previously, no routine quality assurance procedures are available. In lieu of such a routine approach, we have relied upon thoughtful evaluation of the analysis by the co-authors of this report, and by the Caltech scientists who made the measurements and uploaded the data to the SEAC[4]RS web site after a QA/QC process. Further quality assurance evaluation will come in the peer review process when this material is submitted for publication.

2.9 CONCLUSIONS FROM OBSERVATIONAL ANALYSIS

During eleven SEAC[4]RS flights, β-hydroxynitrates formed from the phototchemical oxidation of five alkenes were measured in twenty plumes that originated from HSC emissions. Trajectory analysis confirmed the HSC origin of these plumes. The major focus of the analysis is the 18 September flight when the aircraft sampled extensively directly over the HSC, and intercepted the transported plume at three downwind distances. The measurements over the HSC provide approximate quantification of the relative emissions from the HSC, background concentrations into which the HSC emissions were injected, and the meteorological parameters that controlled the plume transport.

In the transported plumes all of the measured photochemical products of alkene oxidation correlated well with each other. Of those products, the observational analysis focused on formaldehyde, acetaldehyde, O_3, NOy-NOx and the β-HNs. The observed correlations indicate that the β-HNs are useful tracers of the impact that photochemical oxidation of alkenes has on the Houston area troposphere. However, the interpretation of the measured concentrations of these tracers is complex. These measured concentrations indicate the amount of the respective alkenes that must have been oxidized in the transported plume. However, the measured O_3 concentrations are generally much higher, and the measured aldehyde concentrations are often higher, than expected from the alkene oxidation that formed the βHNs. It is suggested that photochemical oxidation of other VOCs also makes major contributions to the measured aldehyde and O_3 concentrations, and/or that the β-HNs are rapidly lost from the plumes. In the downwind plumes the O_3 enhancements that correspond to the measured β-HN concentrations cannot generally account for more than 25% of the

measured O_3 enhancements, emphasizing the importance of the dominant role of the photochemical oxidation of other VOCs in addition to the alkenes, and/or loss of β-HNs from the plumes. The overall conclusion is that measured β-HN concentrations cannot be simply interpreted; complementary plume modeling is necessary for a comprehensive understanding of the photochemical oxidation of VOCs from the HSC.

3. REACTIVE PLUME MODELING

In this section, we present the reactive plume modeling conducted with a Lagrangian puff model with chemistry for selected days of the SEAC[4]RS measurement period based on the analysis of the measurements described in Section 2. The puff dispersion component of the model is based on the Second-Order Closure Integrated PUFF (SCIPUFF) model (*Sykes et al.*, 1993; *Sykes and Henn*, 1995). SCIPUFF with chemistry is referred to as SCICHEM and includes chemistry modules, consistent with those used in photochemical grid models, such as CAMx and CMAQ, to represent chemical interactions between plume pollutants and the surrounding atmosphere. The model accounts for puff overlaps in the chemistry calculations. SCICHEM has previously been successfully evaluated using helicopter measurements of power plant plumes, including plume widths and plume chemistry (*Karamchandani et al.*, 2000). SCICHEM was also applied in AQRP Project 10-020 conducted by NOAA and Ramboll Environ to study NOx reactions and transport in nighttime plumes and their impacts on next-day O_3.

3.1 MODEL CHEMISTRY

The publicly available version of SCICHEM uses the CB05 gas-phase chemistry mechanism. For this study, the mechanism was updated to the latest version of the Carbon Bond mechanism (CB6r2), which was developed in AQRP Project 12-012 and is implemented as the base mechanism in CAMx version 6.20 (ENVIRON, 2015). In addition to the CB6r2 updates, explicit alkene species and their reactions and reaction products were incorporated in the model as described below to represent hydroxynitrate production from individual HRVOC as described in Appendix A.

The HRVOC tracer mechanism was implemented using the following approach:

1. Introduce species corresponding to each individual alkene and their reaction products. The individual alkenes were ethene (ET), propene (PR), 1-butene (1B), 2-methyl propene (MP), cis-2-butene (C2B), trans-2-butene (T2B), 1,3-butadiene (13B), and isoprene (ISO). Note that ethene and isoprene are also explicitly treated in the CB6r2 mechanism as ETH and ISOP, respectively.

2. The reactions of these alkenes and their products with base mechanism species such as OH, NO and HO_2 were formulated to conserve the base mechanism species.

3. Tracers were introduced for formaldehyde (HCHO tracer) and acetaldehyde (CCHO tracer) to track the evolution of these species from the hydroxynitrate chemistry separately from the corresponding CB6r2 species (FORM and ALD2, respectively). These aldehyde tracers were allowed to decay by reaction with OH at the same rate as the corresponding CB6r2 species.

4. Tracers were introduced to count NO to NO_2 conversions (NONO2 tracer) and to accumulate direct O_3 production (XO3 tracer) from NO to NO_2 conversions.

3.2   MODEL SETUP

The September 18, 2013 flight was the focus of the reactive plume modeling with SCICHEM. As described in Section 2, the DC-8 aircraft sampled multiple downwind transects of the HSC plume and also conducted measurements over the HSC region. The sampling over the HSC region provides a basis for initial concentrations in the HSC plume and thus a basis for specifying HSC emissions for some species based on the initial concentration ratios.

On September 18, 2013, the HSC plume was transported to the WNW over the Houston urban area at a bearing of 287 to 295 degrees from the HSC. The DC-8 aircraft sampled downwind transects of the plume between 20:30 to 21:00 UTC at three downwind distances: 97 km (Transect T100), 79 km (Transect T80), and 41 km (Transect T40). The aircraft also sampled the HSC region as noted above.

The following sections describe the setup of SCICHEM inputs for modeling the September 18, 2013 flight.

3.2.1 Meteorology

The modeling was conducted for a 24-hour period starting at midnight on September 18, 2013. In addition to the meteorological measurements conducted by the aircraft during the sampling period, standard surface and upper air meteorological measurements from stations in the region were used in the modeling. These included surface data from the William P. Hobby Airport (KHOU) and the George Bush Intercontinental Airport (KIAH), and upper air data from Corpus Christi International Airport (KCRP). The SCICHEM package includes a meteorological pre-processor, referred to as METSCI, which reformats standard surface and upper air data to create input meteorological files for the model. The aircraft meteorological data during the sampling period were processed with a Python script and integrated into the METSCI output to supplement the routine observations. Note that METSCI is just a reformattor and does not perform any additional processing of the observed meteorological data.

3.2.2 HSC Emissions

The HSC emissions were based on a combination of recent flux measurements of VOCs (alkanes and alkenes), SO_2 and NO_2 emissions using the Solar Occultation Flux (SOF) method *(Johansson et al.,* 2014a) and concentrations measured by the DC-8 aircraft over the HSC during the September 18, 2013 flight. 2011 HSC emissions for ethene, propene, alkanes, SO_2 and NO_2 were obtained from Table 4 in *Johansson et al.* (2014a). (As noted previously, SOF-based HSC emission rates for 2013 are now available from AQRP Project 14-007 but were not available at the time of this work.) Emissions for other alkenes (butenes and 1,3-

butadiene) were estimated using the ratios of these alkenes to ethene in the aircraft measurements over the HSC (see Table 2.1). Formaldehyde emissions from the HSC were estimated as 25% of ethene emissions on a mass basis based on Table 7 of *Johansson et al.* (2014b). Primary acetaldehyde emissions from the HSC were assumed to be negligible. Emissions for the CB6 alkane and aromatic species were estimated using the HSC VOC composition in Table 1 of *Johansson et al*. (2014a). For the base case study, the HSC emissions were specified as a single source at the center of the Sam Houston Tollway Ship Channel Bridge with a release height of approximately 600 m (corresponding to the average height of the aircraft measurements near the HSC). The initial HSC plume spreads were specified as $\sigma_y = 1.5$ km and $\sigma_z = 200$ m. The aircraft measurements over the HSC suggest an initial plume width of 6 to 10 km. Figure 3.1 shows the location of the HSC source and Table 3.1 provides the emission rates used in the plume modeling.

Table 3.1. HSC emission rates for plume modeling.

Species	Emission Rate (kg/hour)	Source
NO_2	1830	*Johansson et al., 2014a*
Ethene	612	*Johansson et al., 2014a*
Propene	563	*Johansson et al., 2014a*
Alkanes	11569	*Johansson et al., 2014a*
HCHO	150	*Johansson et al., 2014b*
1,3-Butadiene	36	*Based on aircraft ratio to ethene*
Butenes	706	*Based on aircraft ratio to ethene*

3.2.3 Background Chemistry and Emissions

Background concentrations are an important input in SCICHEM modeling applications since plume chemistry is affected by these concentrations as the plume is transported downwind. These concentrations can be specified as fixed values, or diurnally varying regional averages, or as three-dimensional diurnally varying fields based on photochemical grid model outputs. In this study, we avoided the uncertainties associated with specifying background concentrations by simultaneously simulating the transport and chemistry of regionally averaged (60 km by 60 km boxes) surface background emissions to the west (urban), south (suburban with lower biogenic emissions), and northeast (high biogenic emissions) of the HSC. This allows a more accurate interaction of the regional background with the HSC plume. The background emission rates were obtained from the CAMx modeling inventory for the Houston-Galveston-Brazoria 4 km resolution modeling domain as average emission rates over each box. Figure 3.2 shows an emissions map of the CAMx modeling domain and the three background emission boxes (marked in red).
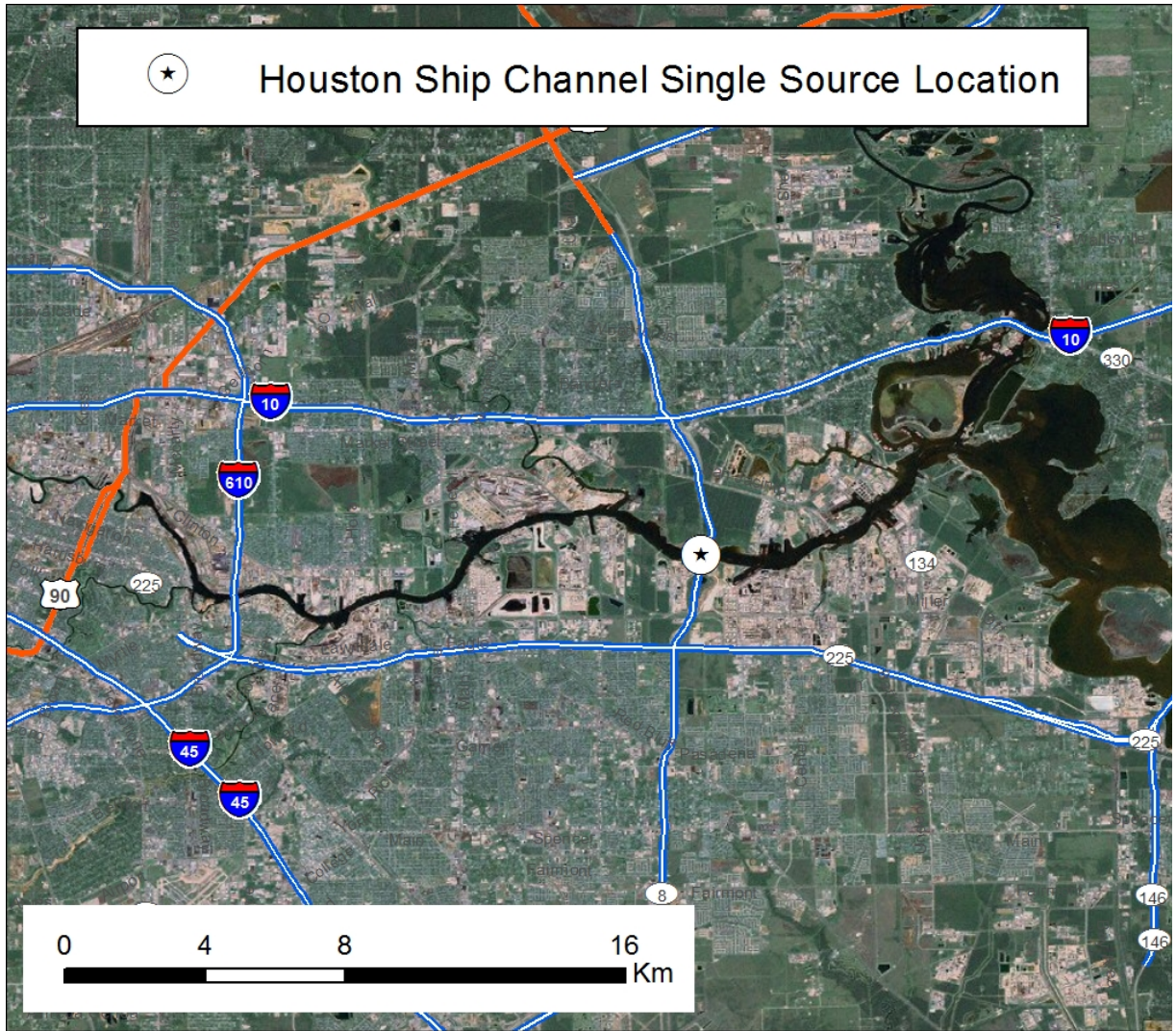
Figure 3.1. Location of single HSC source for the 18 September 2013 base case simulation.
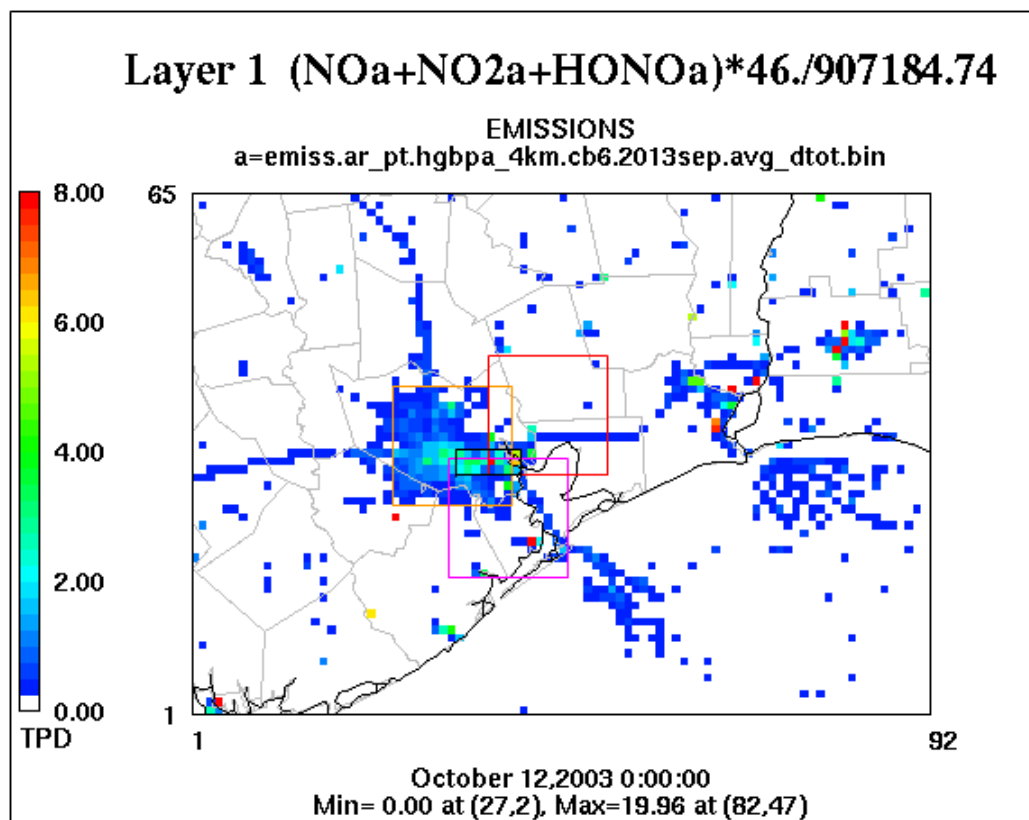
Figure 3.2. Background emission regions (red boxes) for the plume simulations.

3.2.4 Receptor Locations

The modeled plume centerlines at the same downwind distances and heights as the aircraft transects were determined as the locations of the maximum SCICHEM tracer (TRAC) concentration along an arc with a radius equal to the downwind distance for each transect. Figure 3.3 shows the modeled plume (TRAC concentrations) at 21:00 UTC at a height of 600 m. Note that the modeled plume is being transported to the WNW similar to the observed plume, as shown in Figure 3.4. However, there is some displacement of the modeled plume centerline and the observed plume centerline due to differences in wind direction. The modeled plume is transported at a bearing of 291 to 302 degrees from the HSC. The deviations between the modeled and observed plume directions range from 4.5 degrees to 14.5 degrees for the three downwind transects. To account for this displacement, the modeled and observed plumes were aligned by using receptors along virtual transects at the same downwind distance as the aircraft transects and at the same crosswind distances from the plume centerline as the aircraft measurements. The heights of the samplers matched the measurement heights and ranged from 340 m for T80 to 600 m for T100. Figure 3.5 shows the actual aircraft transects and the receptor locations used in the modeling.

3.2.5 Quality Assurance Procedures

The SCICHEM input files for the base case were reviewed by someone who did not create the files and any problems were corrected before finalizing the model setup. The SCICHEM model configuration files for each simulation were independently reviewed by someone who was not involved in setting up simulations and any issues or questions were resolved before finalizing the results of that simulation.
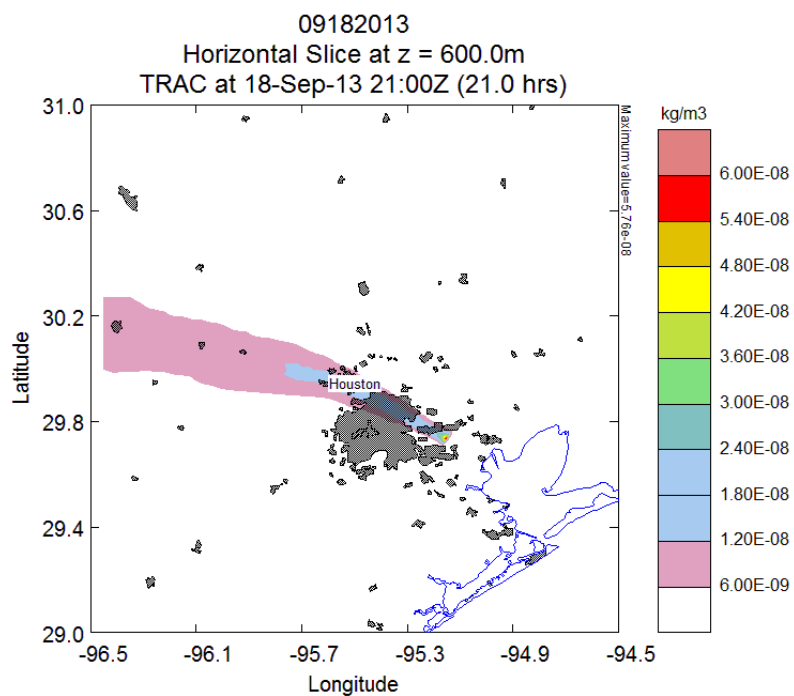
Figure 3.3. Modeled transport of HSC plume on 18 September 2013.
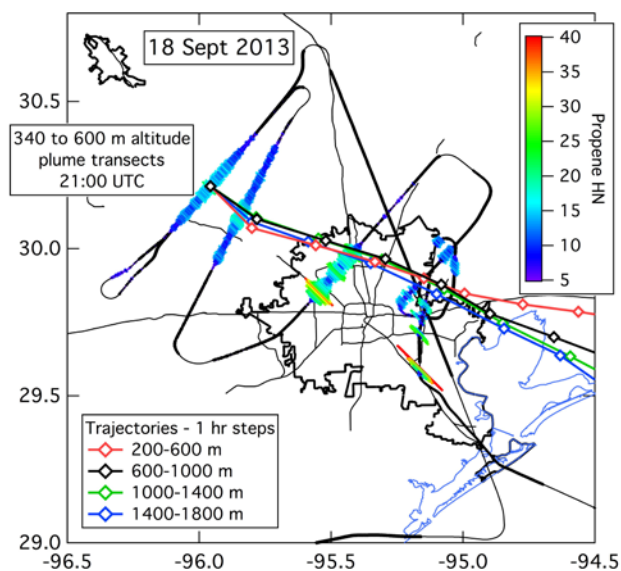
Figure 3.4. Aircraft transects of HSC plume on 18 September 2013 (from Figure 2.1).
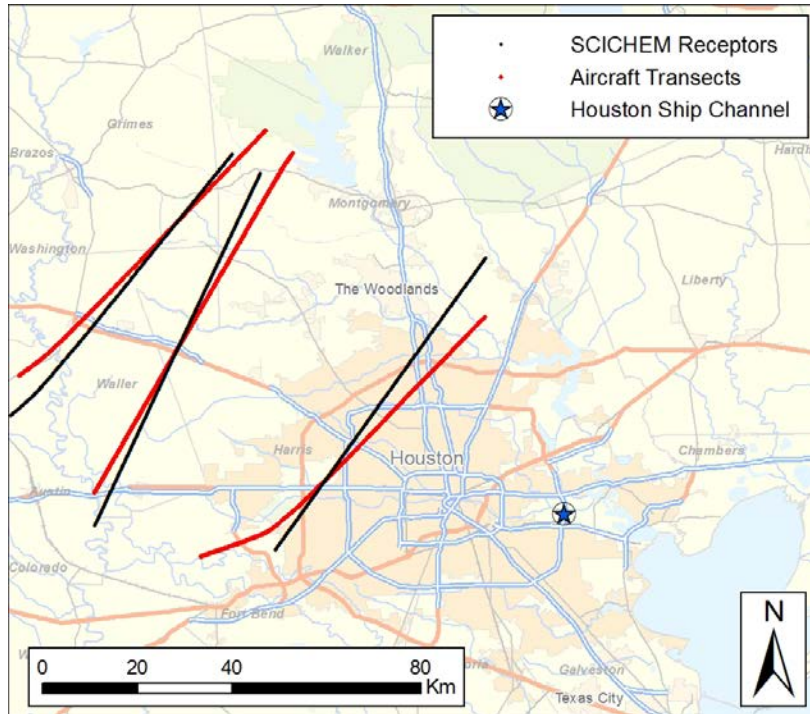
Figure 3.5. Aircraft and model transects at 3 downwind distances (40 km, 80 km, and 100 km) from the HSC.

3.3   MODEL RESULTS

3.3.1 Comparisons with Observations

Figure 3.6 compares the profiles of modeled and measured O_3 concentrations for the three downwind transects (T100 at 97 km downwind of the HSC; T80 at 79 km downwind; and T40 at 41 km downwind). T100 measurements were conducted from 20:37 to 20:45 UTC at an average altitude of about 600 m, while T80 was sampled from 20:49 to 20:59 UTC at an average altitude of 340 m, and T40 was sampled from 21:05 to 21:14 UTC at an average altitude of 518 m. Model results were calculated at 15 minute intervals, and the modeled values shown in Figure 3.6 are at 20:30 UTC for T100, 20:45 UTC for T80, and 21:00 UTC for T40 at the same altitudes as the measurements.
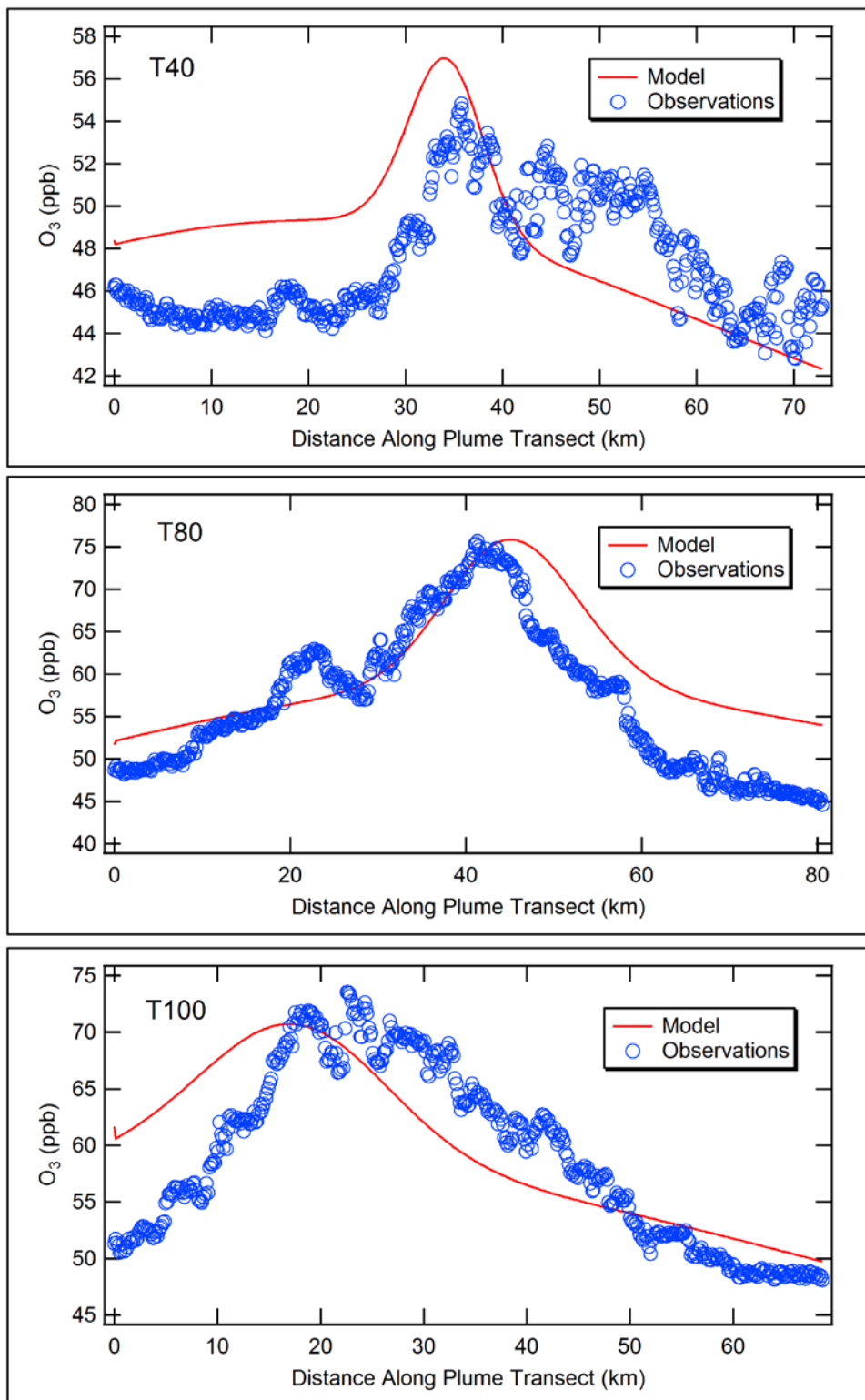
Figure 3.6. Modeled (single HSC source) and measured O_3 concentrations in the September 18, 2013 HSC plume at the three downwind transects.

At all three downwind transects, the crosswind profiles of measured and modeled O_3 concentrations are in good agreement. At the nearest downwind transect to the HSC (T40), the peak modeled value differs by about 2 ppb from the peak measured value. The background levels in the model and measurements also differ by about 2 ppb at the left edge of the plume, so the peak incremental measured and modeled O_3 values are quite comparable. The measurements show some O_3 wings at the edges of the plume transect that are not reproduced by the model. Previous studies (e.g., *Chowdhury et al.*, 2015) have shown that such edge effects in the early stages of the plume can be simulated to some extent by using a higher puff resolution in the model.

Figures 3.7 and 3.8 compare the measured and modeled downwind transect profiles for NOy and NOz in the HSC plume, respectively. As in the case of O_3, the measured and modeled NOy profiles at the three downwind transects are in good agreement. At the two downwind transects nearest to the HSC (T40 and T80), the modeled peak NOy plume increments (levels above the background) are in very good agreement with the observed plume increments. At the furthest downwind transect at 97 km, the modeled peak NOy increment is lower than the observed increment by about 0.5 to 1 ppb. The results for NOz are somewhat different, showing an under-prediction of NOz formation near the HSC for the downwind traverse at 40 km. The modeled NOz results at 80 km and 100 km downwind are in better agreement with the observations.

Figures 3.9 and 3.10 show the plume transect comparisons of modeled formaldehyde and acetaldehyde against aircraft measurements, respectively. The model under-predicts both the formaldehyde and acetaldehyde concentrations by 50% or more. For the nearest downwind transect, acetaldehyde concentrations are under-predicted by more than a factor of 2. The acetaldehyde under-estimates are generally larger than the formaldehyde estimates. As mentioned in Section 3.2.1, the primary acetaldehyde emissions for the HSC are set to zero, while the formaldehyde emissions are set to about 25% of the ethene emissions.

The under-estimation of aldehyde results and the NOz results for T40 suggest that the modeled HSC plume is less reactive than the actual plume near the HSC. Possible explanations for this could be under-estimates in the reactivity of the background (represented by background emissions) or the configuration of the HSC source as a single large diluted source. To determine the role of source configuration and plume dilution on the model results, we conducted a sensitivity study in which the HSC was represented with 6 smaller sources. Figure 3.11 shows the source configuration used for the sensitivity study. One of the six sources (source C) is at the same location as the large HSC source used in the base case simulation, while 2 sources (A and B) are downwind and 3 sources (D, E and F) are upwind. The spacing between each source pair varies from 1.5 km to 2 km. The HSC emissions are equally divided among the 6 sources, and each source has an initial plume width of 100 m.
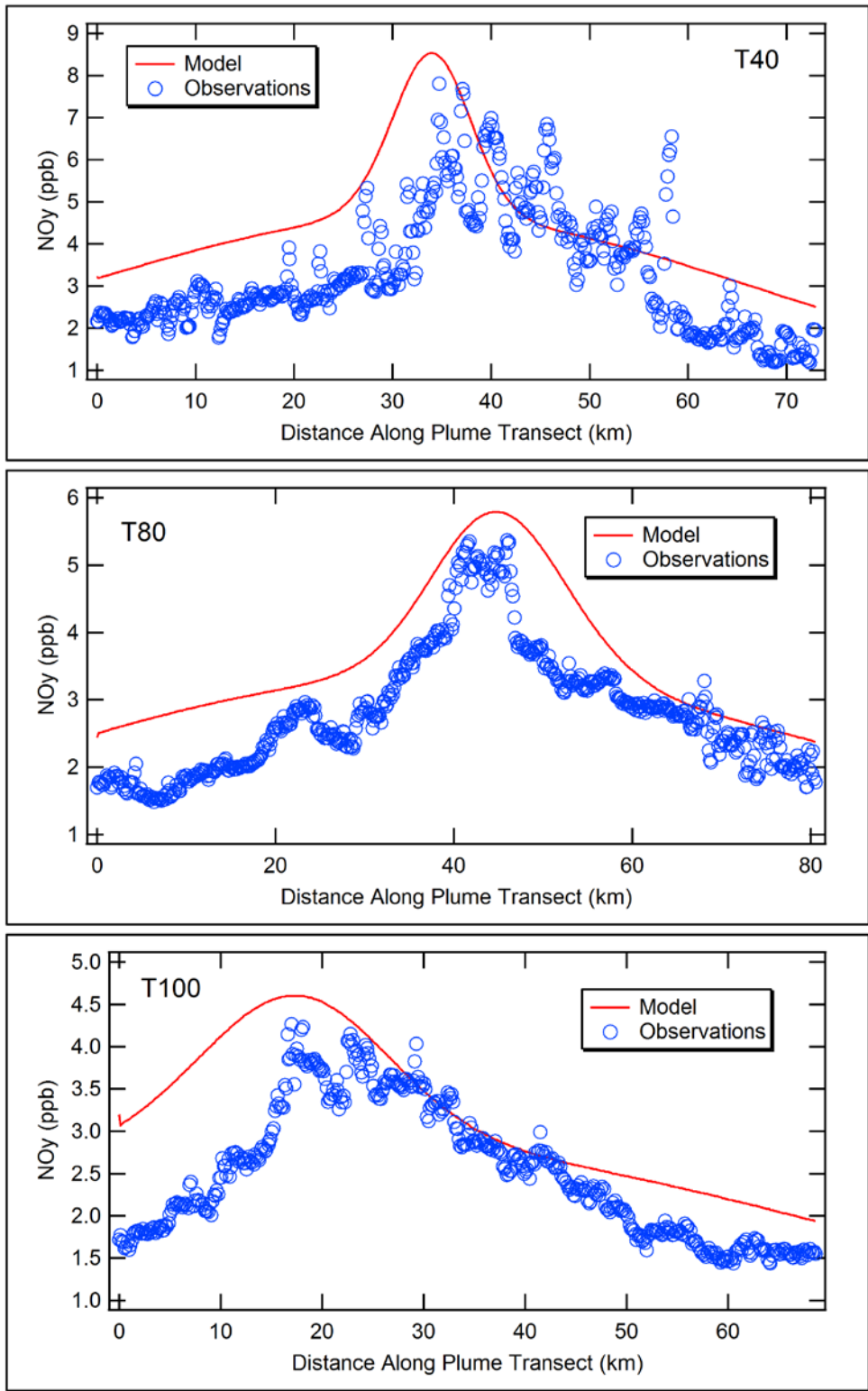
Figure 3.7. Modeled (single HSC source) and measured NOy concentrations in the September 18, 2013 HSC plume at the three downwind transects.
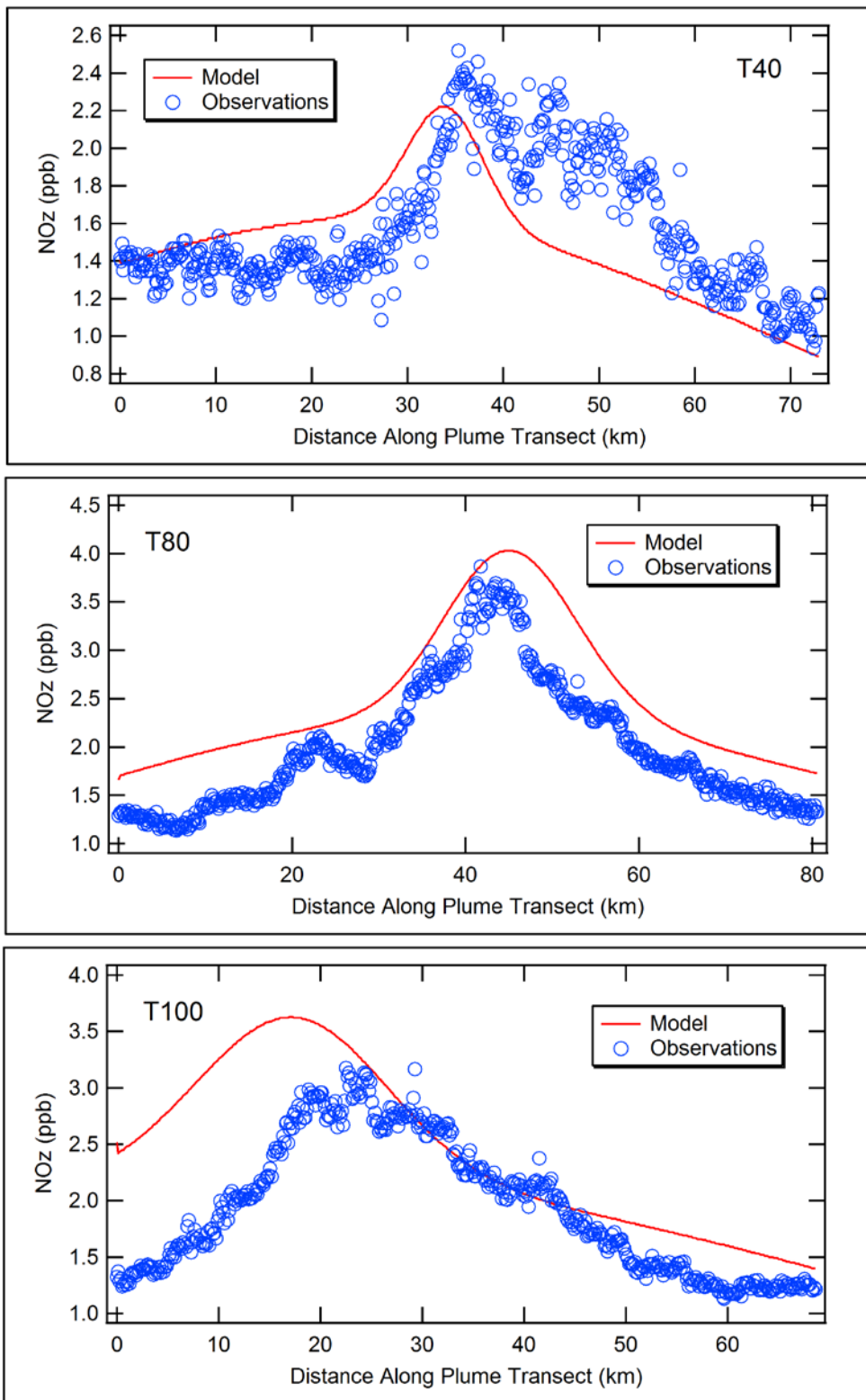
Figure 3.8. Modeled (single HSC source) and measured NOz concentrations in the September 18, 2013 HSC plume at the three downwind transects.
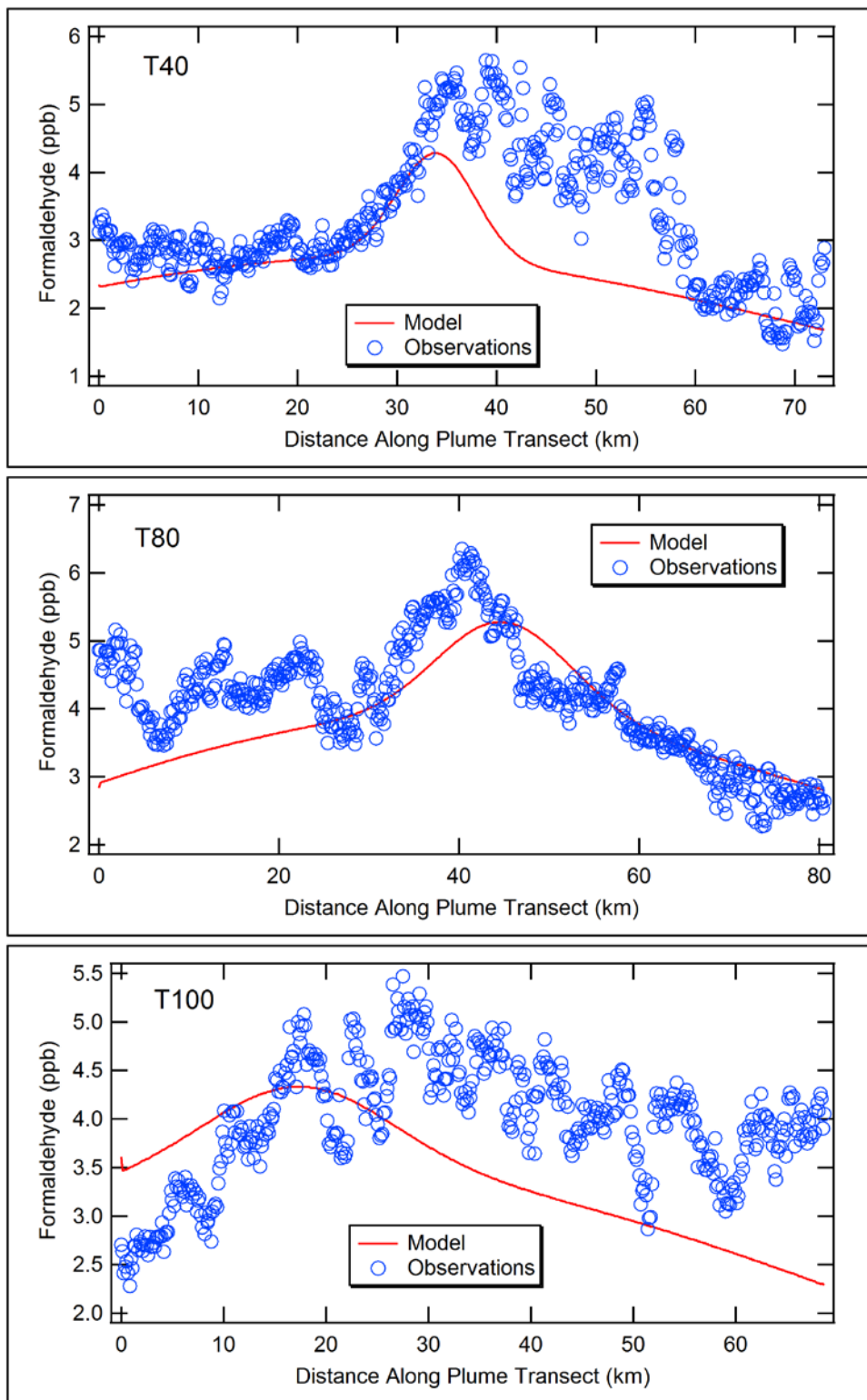
Figure 3.9. Modeled (single HSC source) and measured formaldehyde concentrations in the September 18, 2013 HSC plume at the three downwind transects.
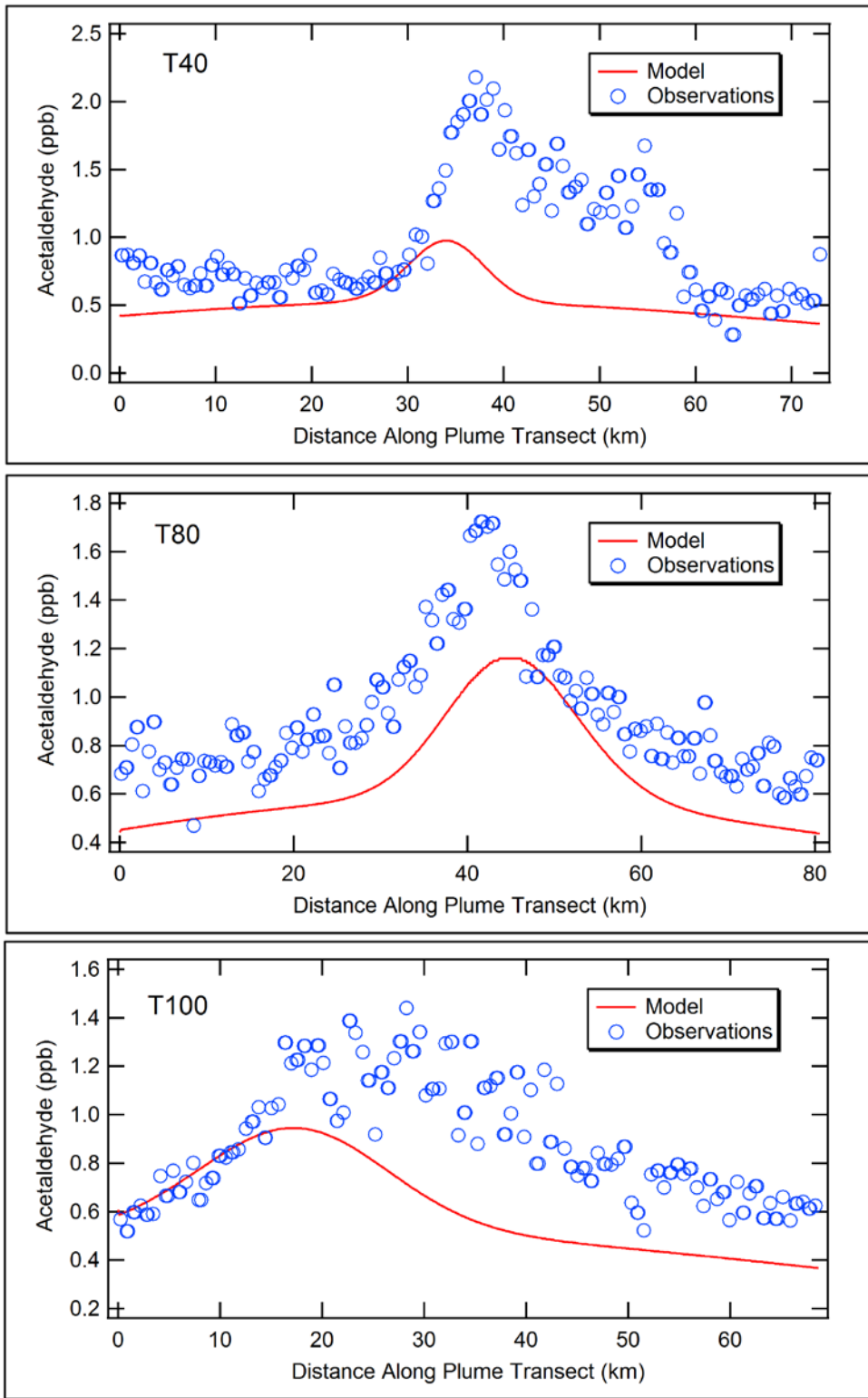
Figure 3.10. Modeled (single HSC source) and measured acetaldehyde concentrations in the September 18, 2013 HSC plume at the three downwind transects.
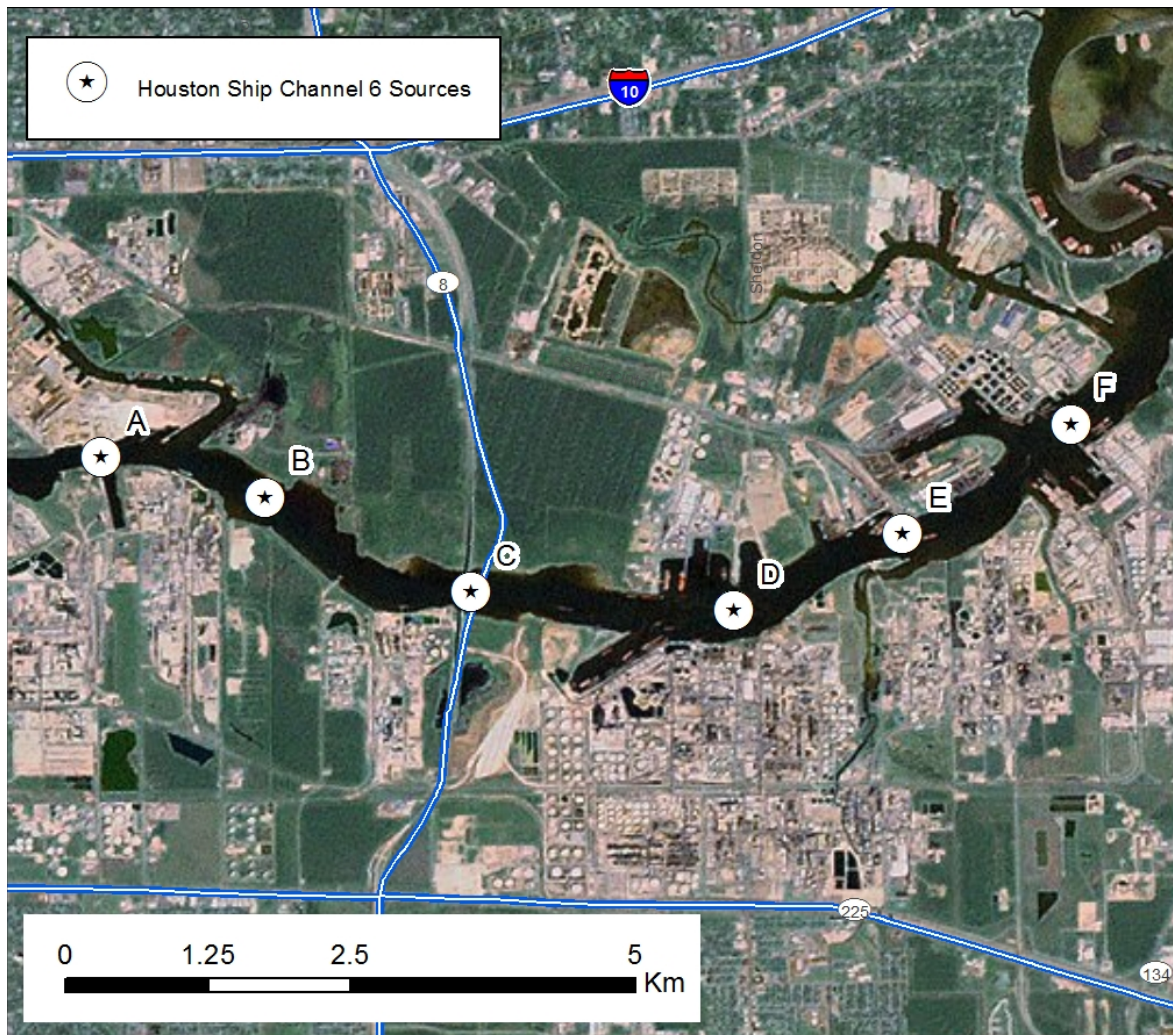
Figure 3.11. Location of 6 sources representing the HSC emissions for the 18 September 2013 sensitivity simulation.

Figure 3.12 compares measured O_3 plume profiles with modeled values using the modified source configuration for the three downwind transects. A comparison with the corresponding figure (Figure 3.6) for the base case simulation results shows that using multiple sources to represent the HSC emissions provides a better performance for O_3 concentrations and slightly narrower plumes at the three downwind transects.

The multiple source sensitivity study results for NOy and NOz are shown in Figures 3.13 and 3.14, respectively. These results also show the slightly narrower modeled plumes with the multiple HSC source configuration. While the peak predicted NOy levels are higher than the measured levels, this is partly due to the higher background NOy levels. When the incremental peaks are compared, the peak modeled NOy increment is about half a ppb higher than the observed peak increment for the nearest transect (T40) and the furthest transect (T100). For the intermediate transect at 80 km downwind (T80), the modeled NOy peak increment is slightly more than 1 ppb than the observed increment. The results for NOz at the 40 km downwind transect (top panel in Figure 3.14) show a marked improvement when 6 smaller sources are used to represent the HSC emissions than a single large source (compare with the base case results shown in Figure 3.8). However, NOz is formed more rapidly in the modeled plume at 80 km and 100 km downwind than in the observed plume.

Simulating the HSC emissions as 6 smaller sources instead of one large source also results in higher formaldehyde and acetaldehyde concentrations in the plume, as shown in Figures 3.15 and 3.16, respectively. The large under-predictions in HCHO and CH_3CHO concentrations noted in the base case simulation (compare with Figures 3.9 and 3.10) are reduced with the multiple source configuration. In particular, there is a marked improvement in model performance for acetaldehyde.

The results with the 6 source configuration indicate a more reactive HSC modeled plume with concentrations that are generally in better agreement with measured values. However, the higher NOy and NOz values in the modeled plume suggest that the HSC NOx emissions used in the simulations could be an over-estimate. A second sensitivity study was conducted with the 6 source configuration in which the HSC NOx emissions were reduced by about 30%. This sensitivity study was also conducted for the single source configuration, but only the results from the multiple source sensitivity study are shown here.
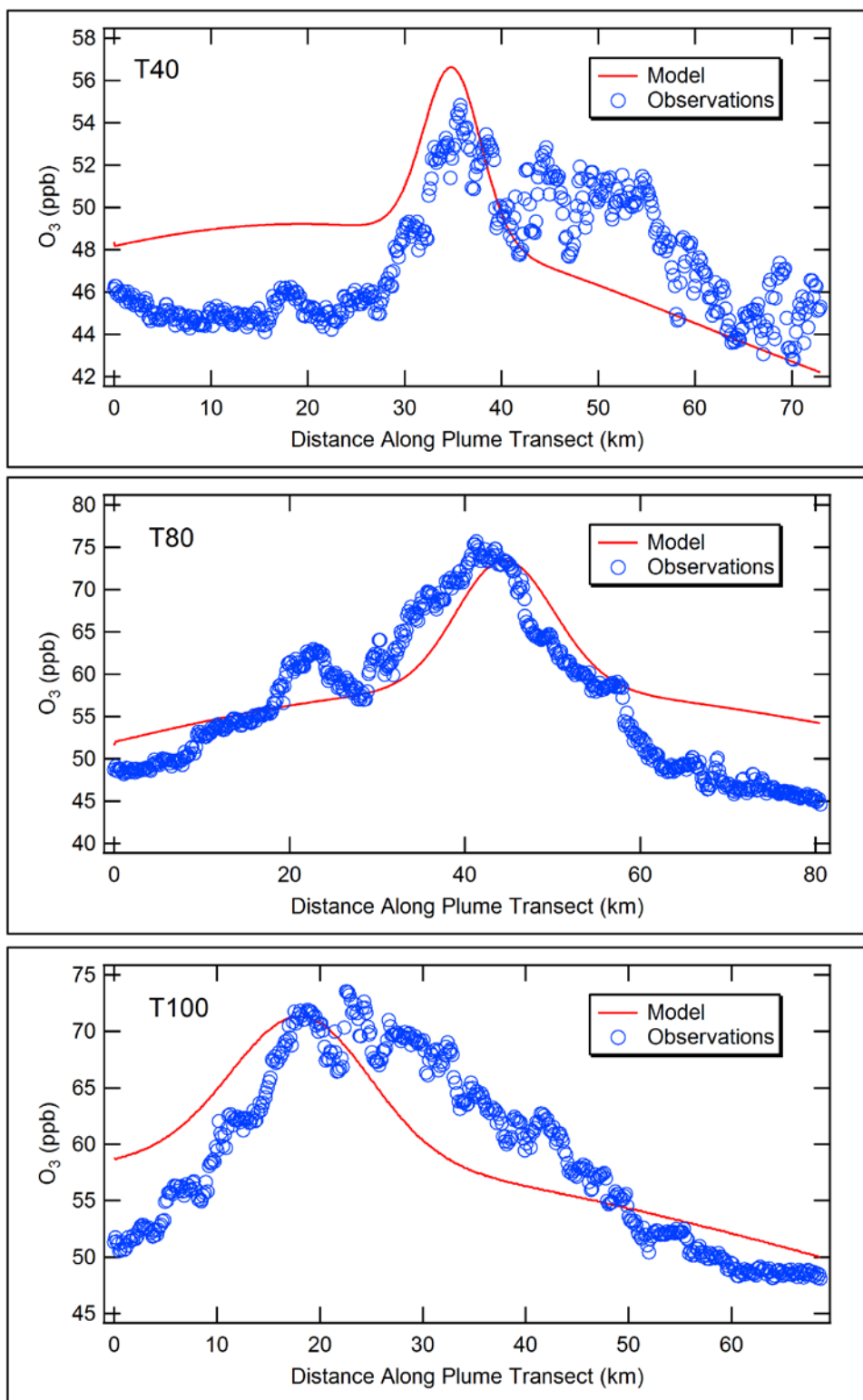
Figure 3.12. Modeled (multiple sources) and measured O_3 concentrations in the September 18, 2013 HSC plume at the three downwind transects.

44
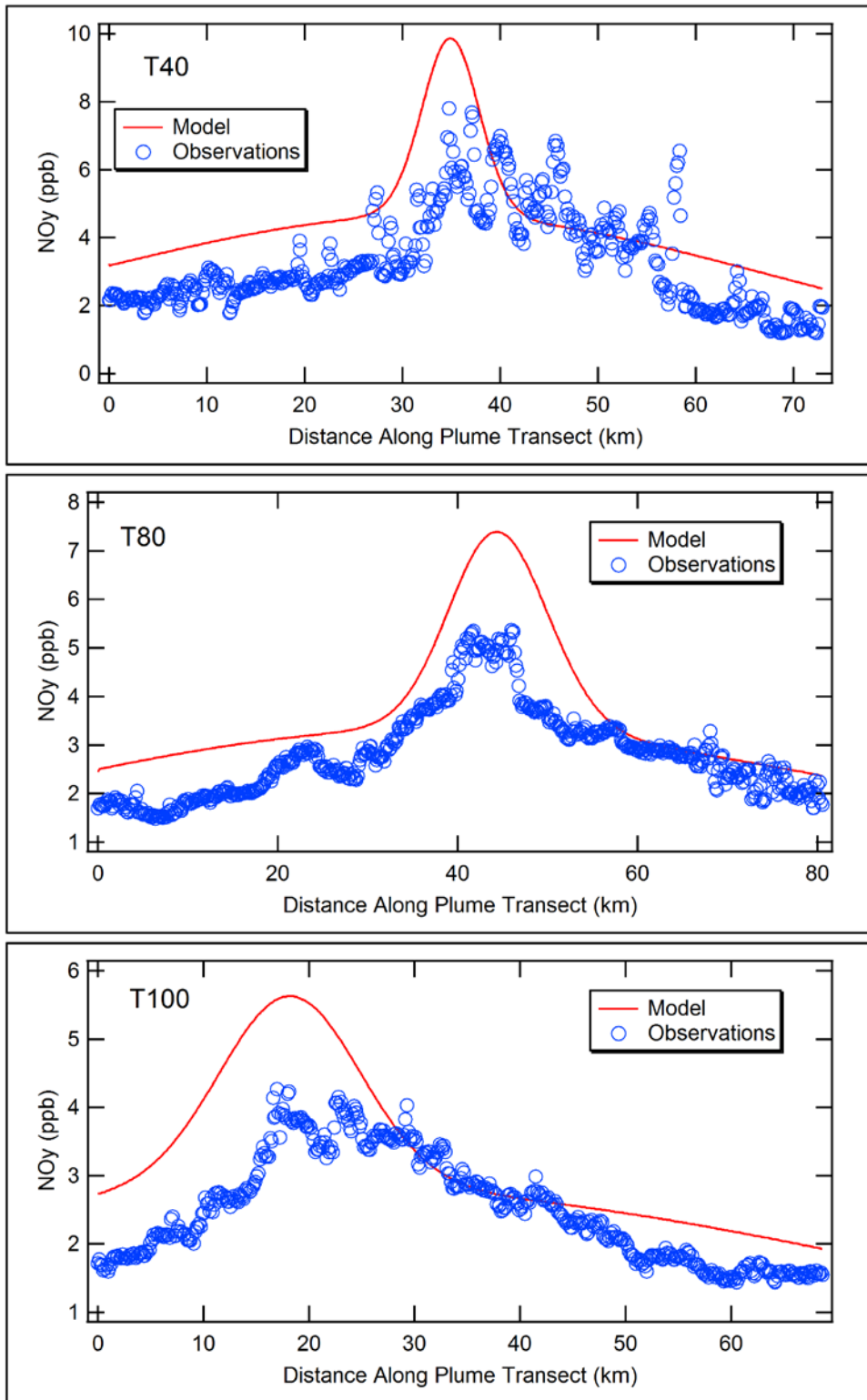
Figure 3.13. Modeled (multiple sources) and measured NOy concentrations in the September 18, 2013 HSC plume at the three downwind transects.
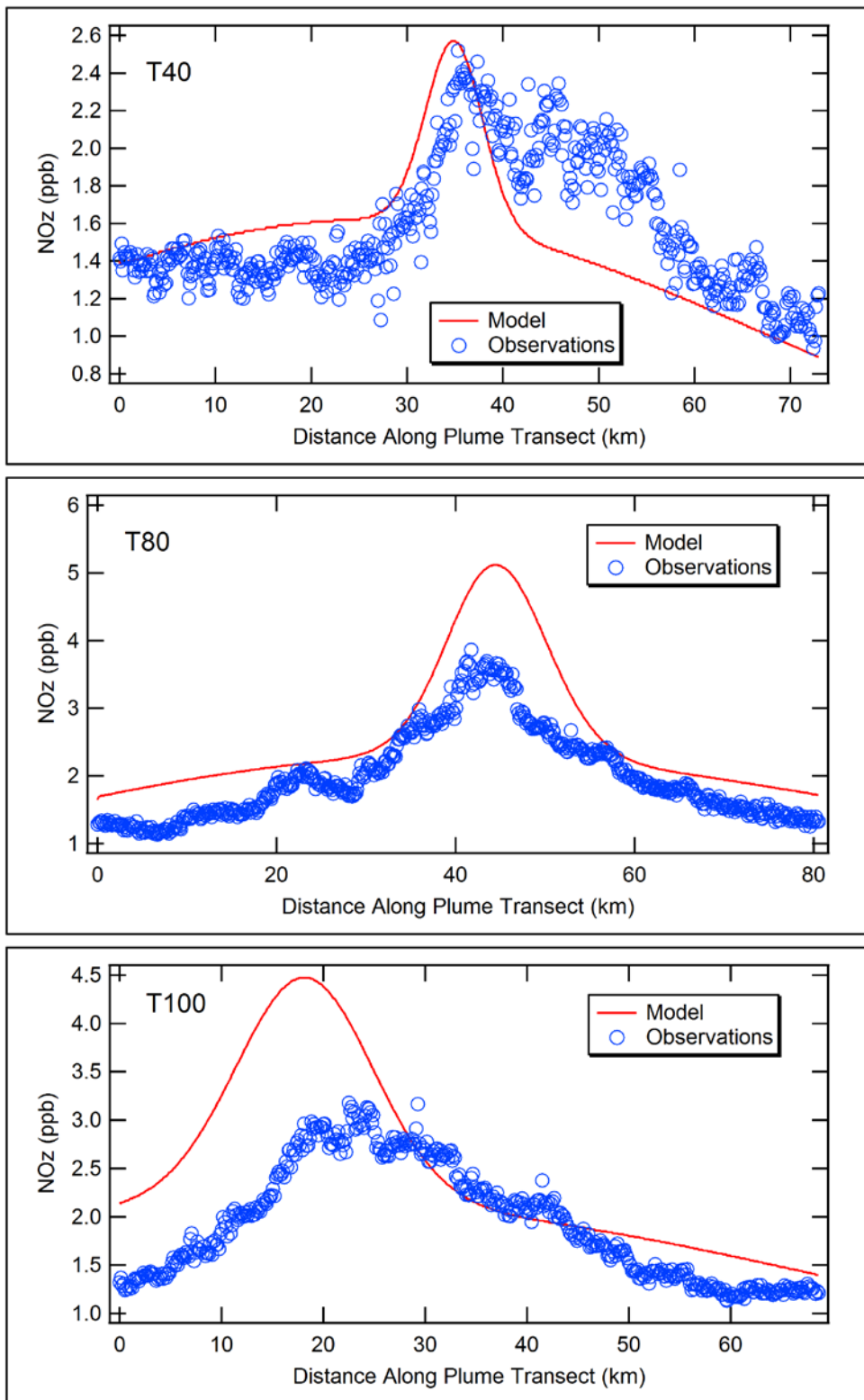
Figure 3.14. Modeled (multiple sources) and measured NOz concentrations in the September 18, 2013 HSC plume at the three downwind transects.
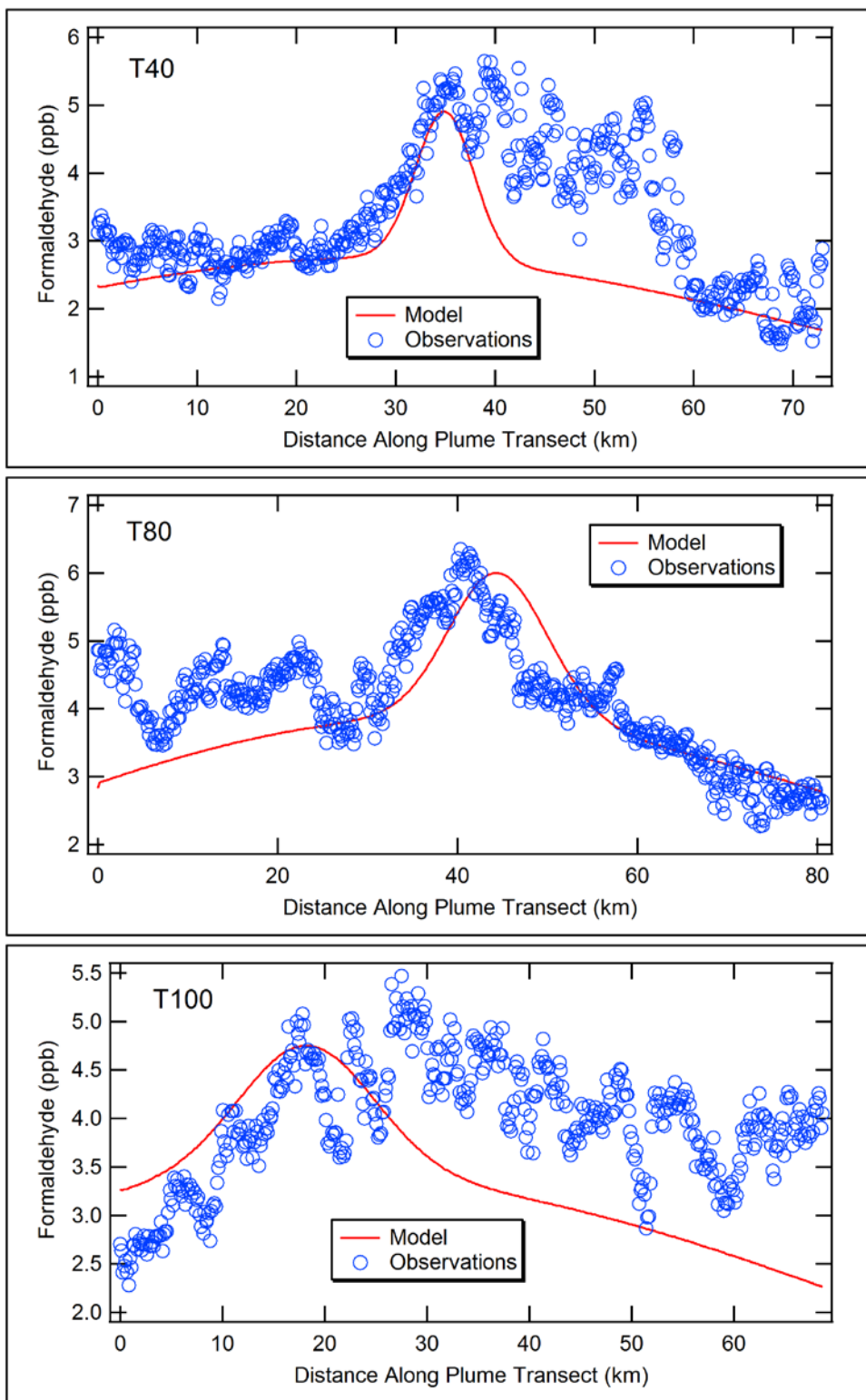
Figure 3.15. Modeled (multiple sources) and measured formaldehyde concentrations in the September 18, 2013 HSC plume at the three downwind transects.
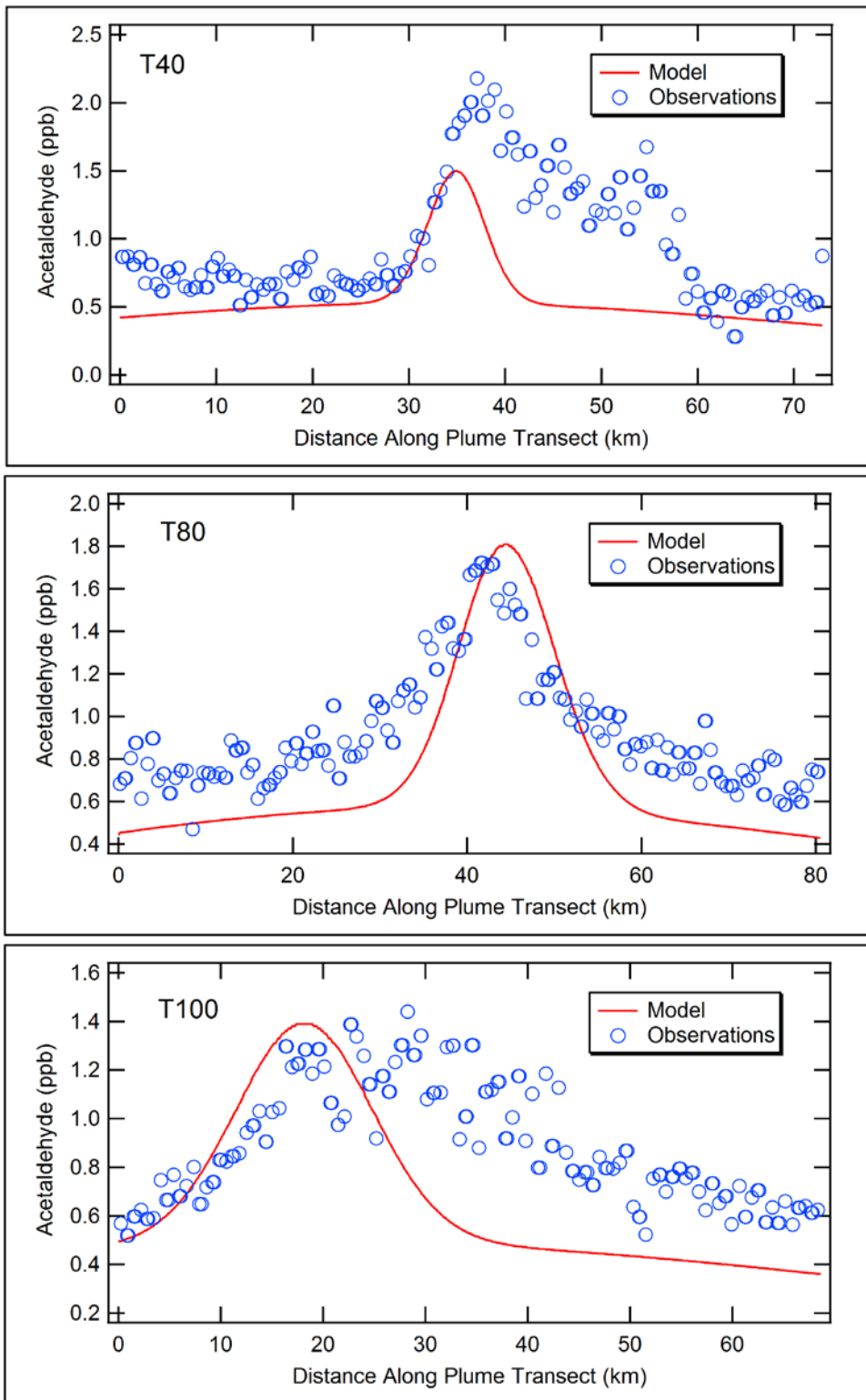
Figure 3.16. Modeled (multiple sources) and measured acetaldehyde concentrations in the September 18, 2013 HSC plume at the three downwind transects.

Figure 3.17 compares measured O_3 plume profiles with modeled values using the modified source configuration and lower NOx emissions for the three downwind transects. The reduction in HSC NOx emissions appears to have a negligible effect on the modeled O_3 values, as can be seen by comparing Figure 3.17 with 3.12. Similarly, Figures 3.18 and 3.19 show that the effects of the lower NOx emissions on predicted formaldehyde and acetaldehyde levels in the plume are also negligible (compare with corresponding results with base case NOx emissions in Figures 3.15 and 3.16). However, NOy and NOz levels in the modeled plume are now in better agreement with the measurements, as shown in Figures 3.20 and 3.21, respectively. Thus, the lower NOx emissions appear to have a negligible impact on the reactivity of the plume and the production of O_3 and aldehydes downwind, but yield NOy and NOz results that agree well with observed values.

The comparisons between model results and measurements indicate that the model does an adequate job of simulating the HSC plume. The best overall results are from the sensitivity study in which several smaller sources are used to represent the HSC emissions instead of a single large source, and the HSC NOx emissions are about 30% lower than those estimated by Johansson et al. (2014a).

In the following section, we discuss the relationships between modeled species following an approach similar to that used in the observational data analysis in Section 2.

3.3.2 Modeled Relationships

Figure 3.22 shows the O_3 tracer concentrations for the September 18, 2013 flight plotted against the modeled Ox ($O_3 + NO_2$) concentrations in the plume. The model results are for the base case simulation with a single source representing the HSC emissions. Recall that the O_3 tracer tracks the O_3 formed from the HRVOC hydroxynitrate chemistry in the HSC plume. Thus, Figure 3.22 is analogous to Figure 2.10 in the observational analysis section. As in Figure 2.10, the slope for the nearest downwind transect (T40) is higher than those for T80 and T100, indicating that relatively more O_3 is formed from the HSC alkene emissions near the source than further downwind. The modeled slopes for the three transects are generally similar to those inferred from the observational data analysis in Figure 2.10. The corresponding model results for the sensitivity study with 6 smaller HSC sources are shown in Figure 3.23. The selection of these sources and their locations was arbitrary since the intent was to evaluate the sensitivity of the model results to the source configuration. The higher reactivity of the HSC plume in this scenario is seen in the larger slopes for the O_3 tracer concentrations relative to the Ox concentrations. Even at the larger downwind distances, the slopes from the model results are greater than 20%, while Figure 2.10 shows that the slopes for both T80 and T100 are less than 10%.
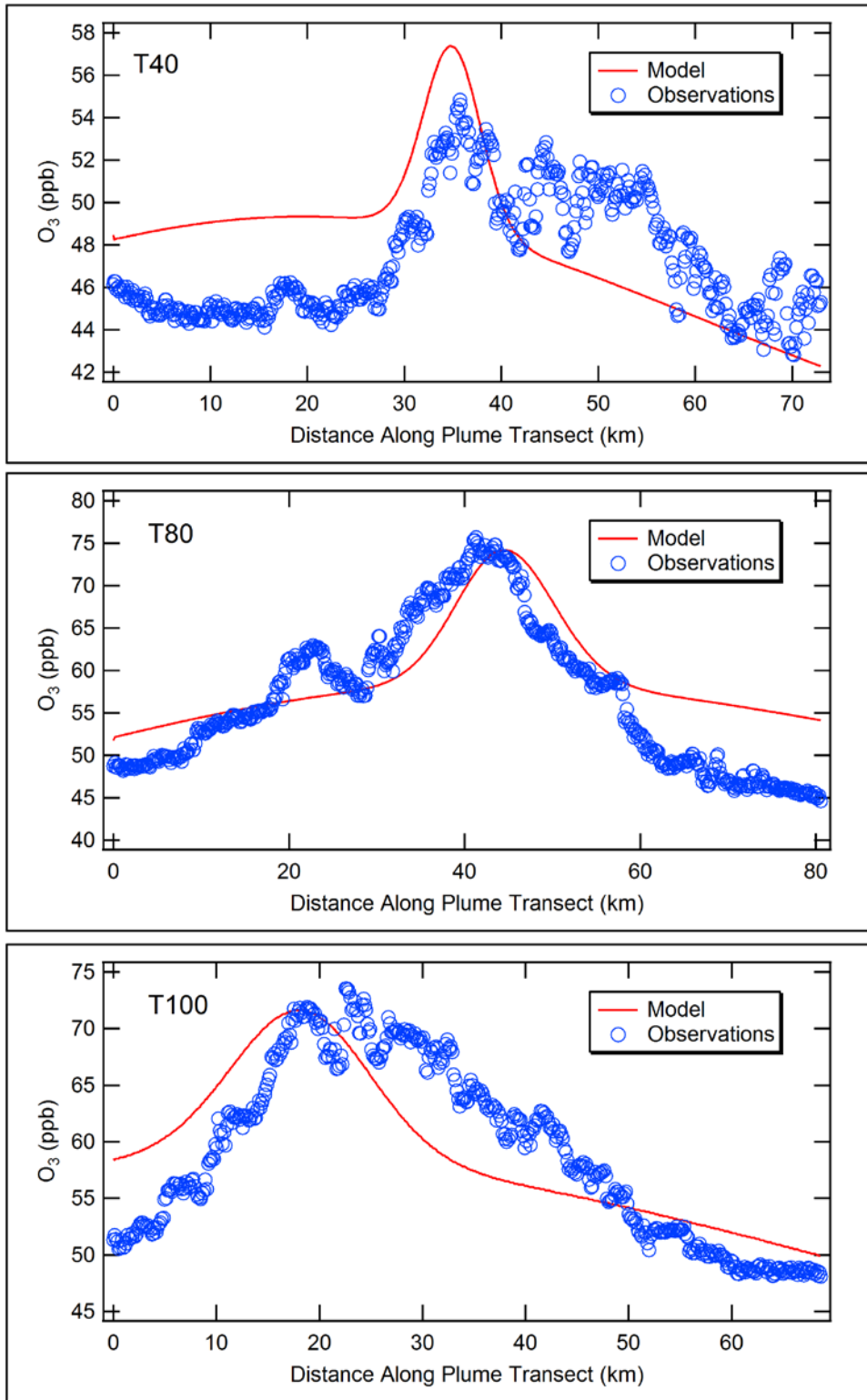
Figure 3.17. Modeled (multiple sources and lower NOx emissions) and measured O_3 concentrations in the September 18, 2013 HSC plume at the three downwind transects.
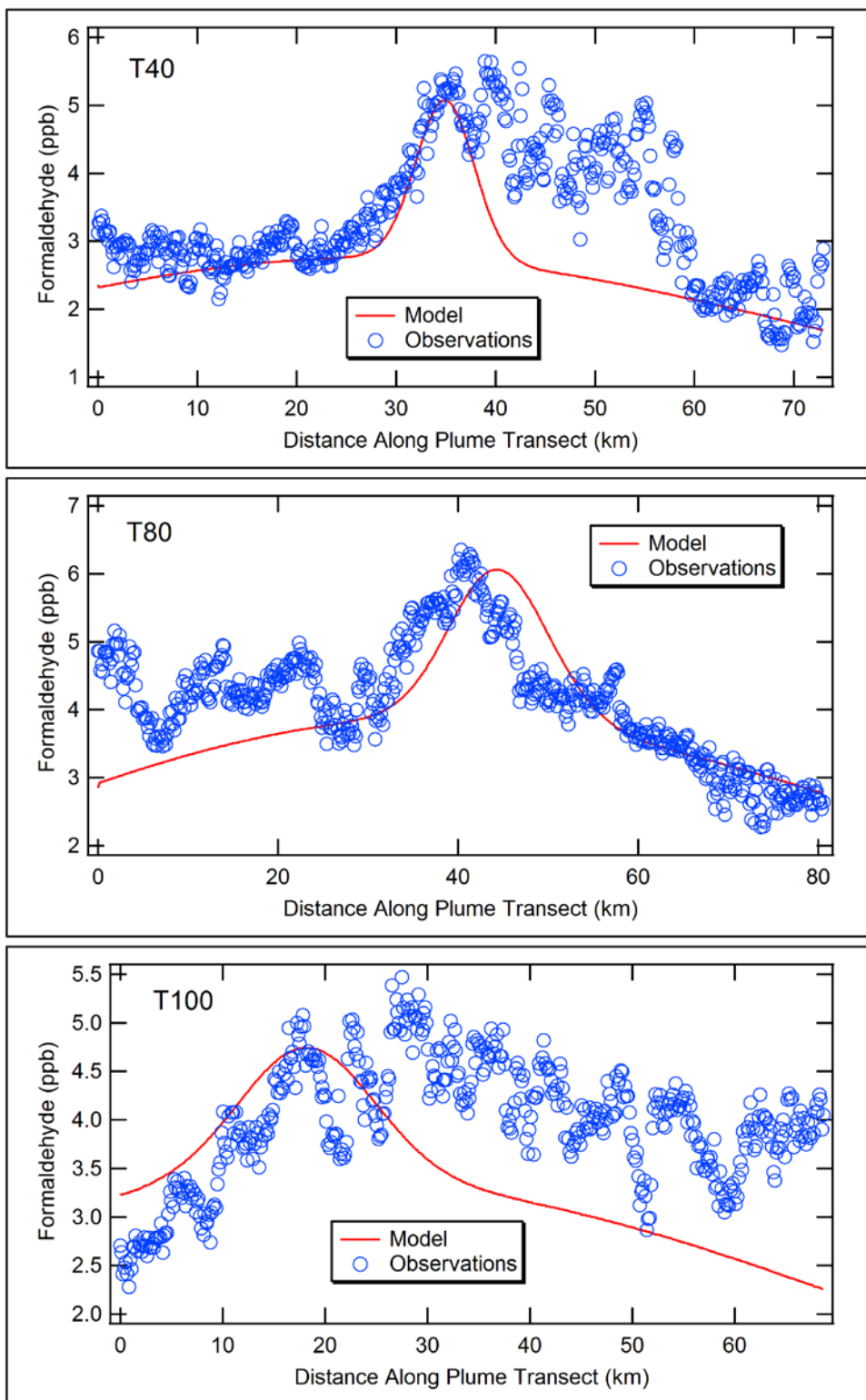
Figure 3.18. Modeled (multiple sources and lower NOx emissions) and measured formaldehyde concentrations in the September 18, 2013 HSC plume at the three downwind transects.
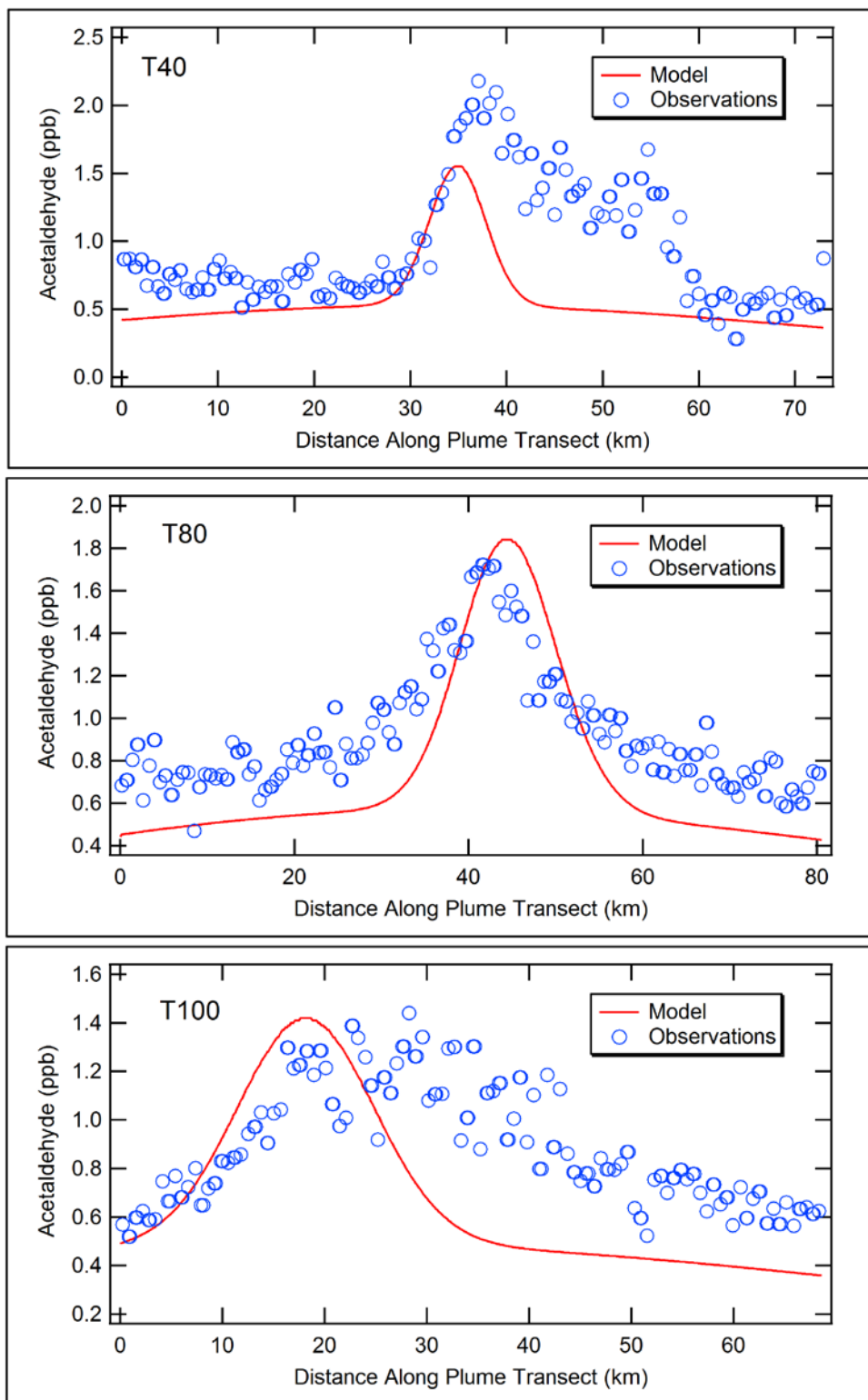
Figure 3.19. Modeled (multiple sources and lower NOx emissions) and measured acetaldehyde concentrations in the September 18, 2013 HSC plume at the three downwind transects.
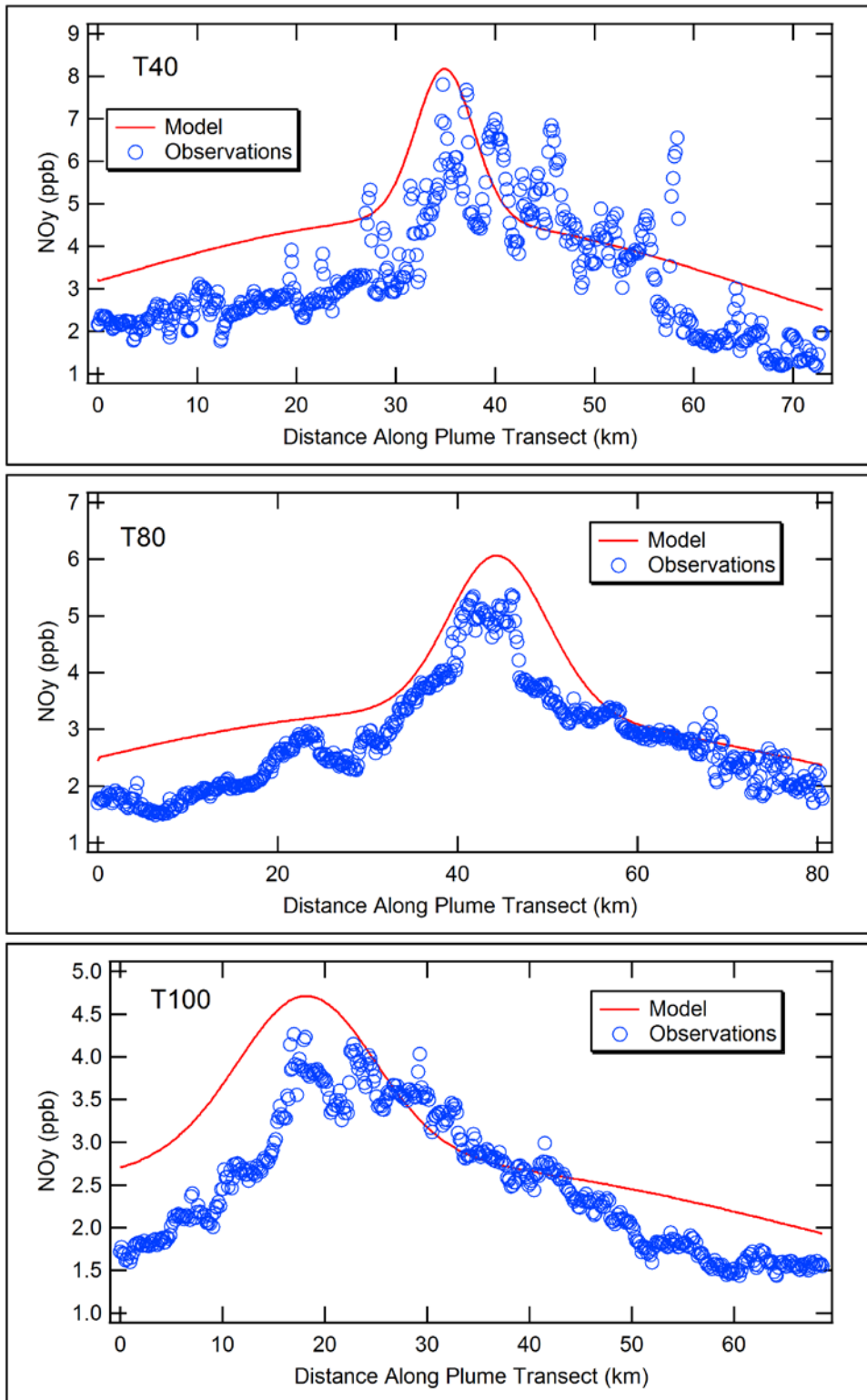
**Figure 3.20.** Modeled (multiple sources and lower NOx emissions) and measured NOy concentrations in the September 18, 2013 HSC plume at the three downwind transects.
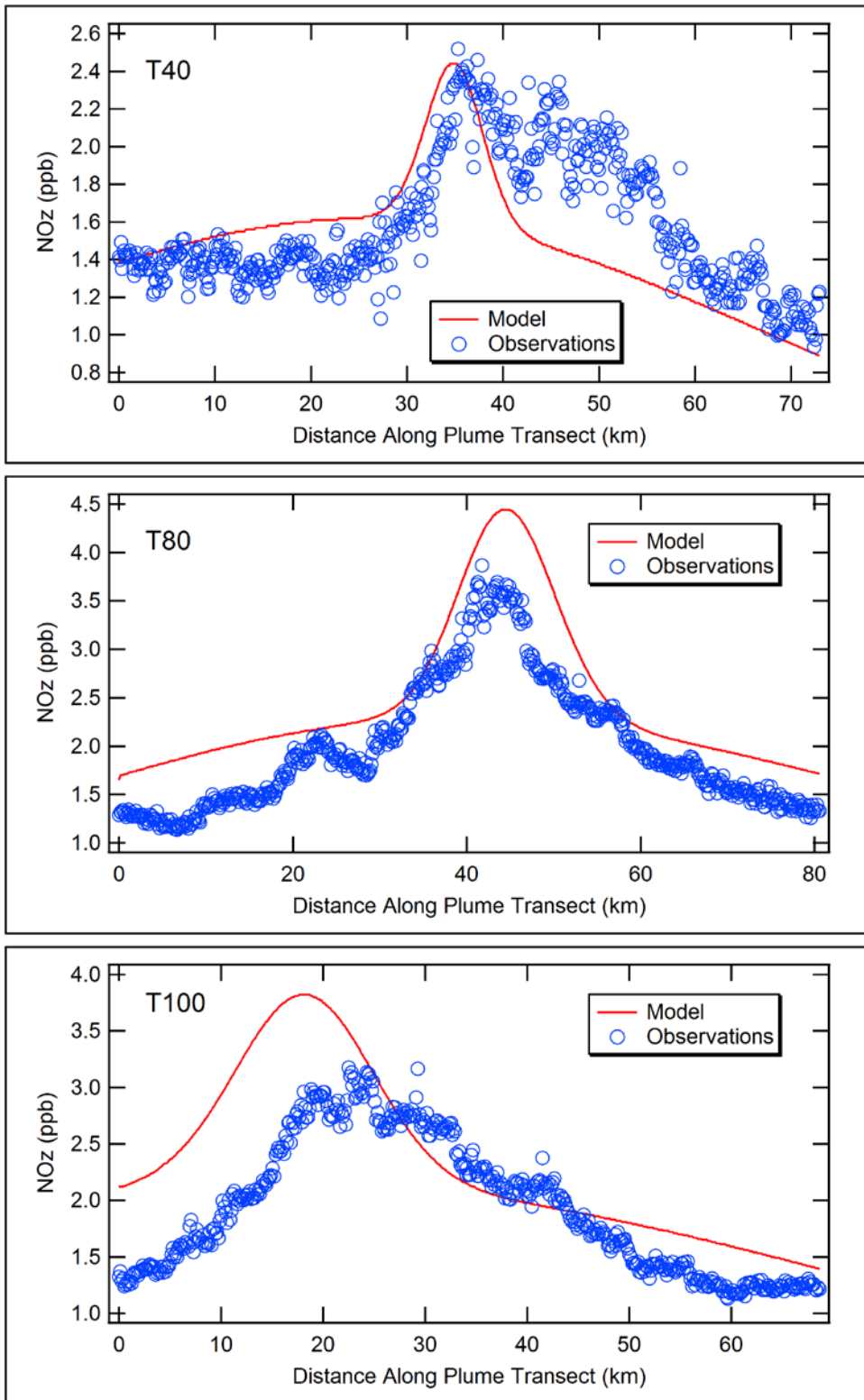
Figure 3.21. Modeled (multiple sources and lower NOx emissions) and measured NOz concentrations in the September 18, 2013 HSC plume at the three downwind transects.
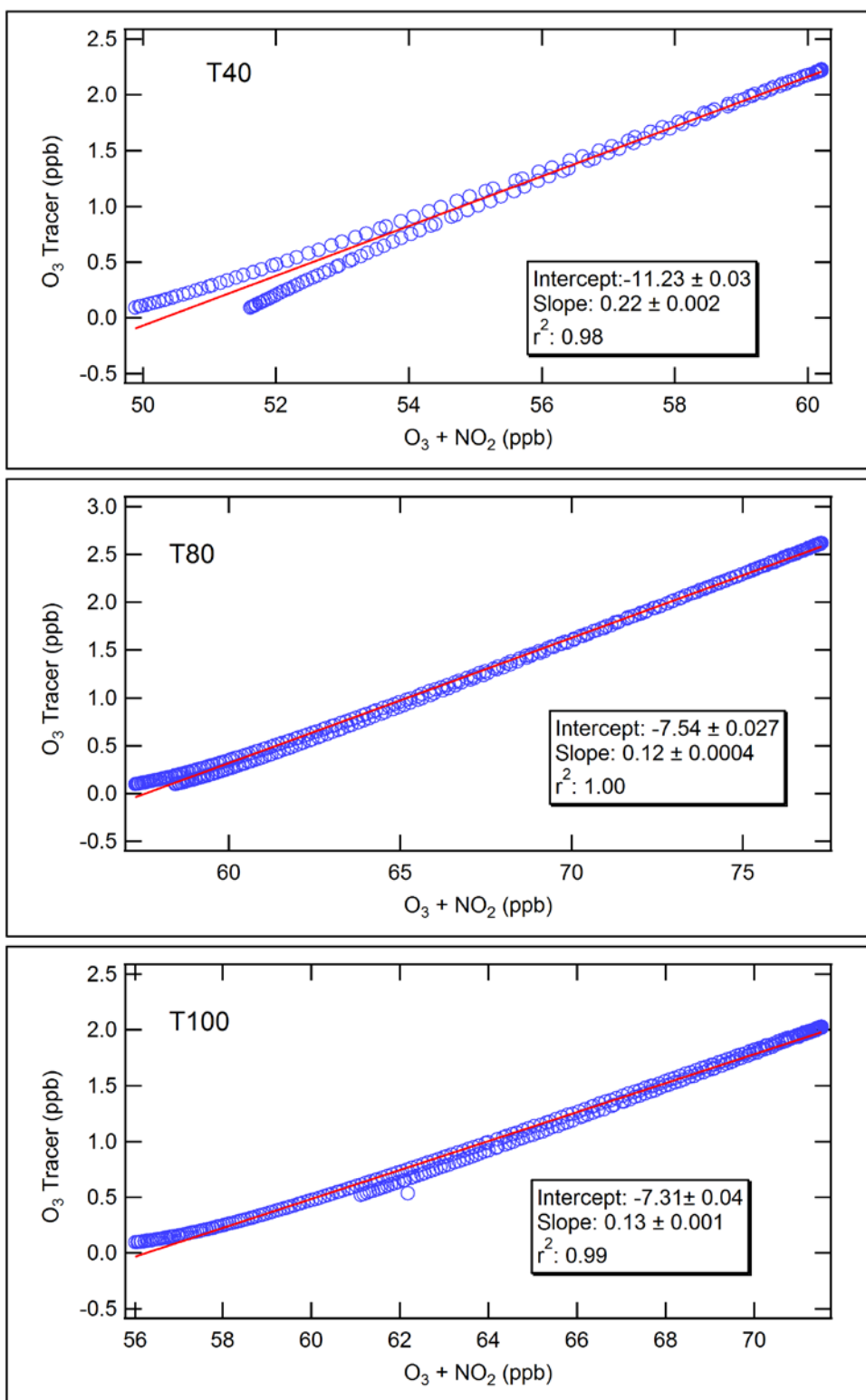
Figure 3.22. O_3 formed from alkene hydroxynitrate chemical mechanism versus Ox (O_3 + NO_2) in the September 18, 2013 HSC plume at the three downwind transects (compare with Figure 2.10). Model results are for the base case simulation with one large source representing the HSC emissions.
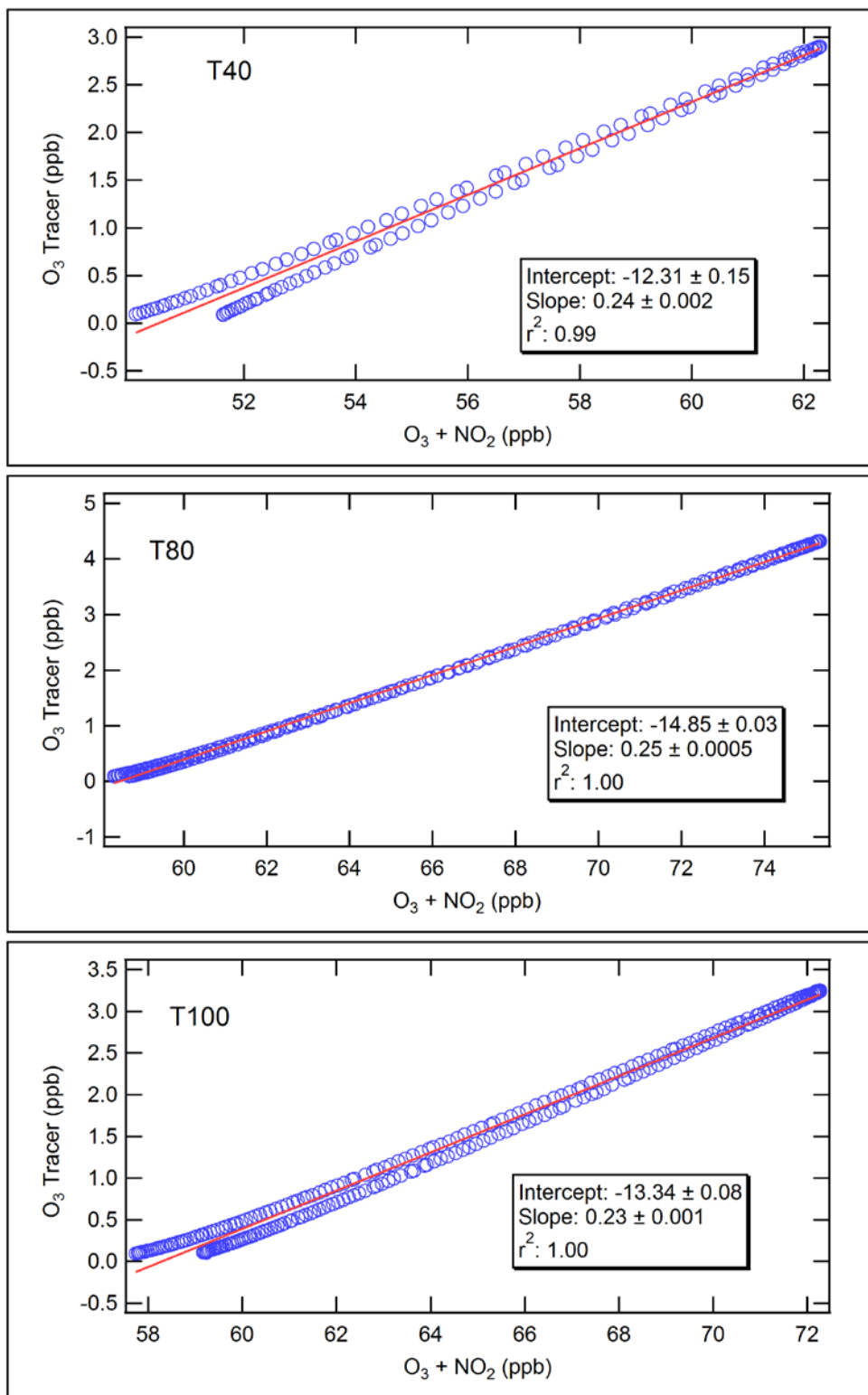
Figure 3.23.   O$_3$ formed from alkene hydroxynitrate chemical mechanism versus Ox (O$_3$ + NO$_2$) in the September 18, 2013 HSC plume at the three downwind transects (compare with Figure 2.10). Model results are for the sensitivity simulation with 6 sources representing the HSC emissions.

Figure 3.24 shows the HCHO tracer, representing formaldehyde (primary + formed from the HRVOC hydroxynitrate chemistry) from the HSC emissions, versus total formaldehyde. This figure is analogous to Figure 2.6 in the observation analysis section. The model results are from the base case simulation with one large HSC source. As shown in Figure 3.24, the majority (70% or more) of the HCHO formed in the HSC plume (i.e., HCHO levels above the background) can be attributed to direct formation from HRVOC oxidation. The largest slope of 82% is in the 40 km downwind traverse, indicating that HCHO formation near the HSC is dominated by the HRVOC emissions from the HSC. The corresponding results for the 6 source sensitivity study, shown in Figure 3.25, also show that HRVOC emissions dominate the formation of HCHO in the plume, although the trend is slightly different, with a 77% slope at 40 km downwind, increasing to 80% at 80 km downwind and 86% at 100 km downwind.

Figure 3.26 shows the base case (single HSC source) results for CH_3CHO tracer, representing acetaldehyde formed from the oxidation of the HSC alkene emissions, versus total acetaldehyde from all sources (compare with Figure 2.7 in the observational analysis section). At the closest downwind transect (T40), essentially all of the excess aldehyde in the plume comes from the oxidation of the HSC alkene emissions. As the plume travels further downwind, the contributions of HSC alkenes decrease, but are still relatively high (nearly 50% at 100 km downwind). For the sensitivity study with 6 smaller sources, the overall CH_3CHO trends are the same, but the slopes are lower than for the base case study with a single HSC source, as shown in Figure 3.27.

Figure 3.28 shows the ratios of the secondary photochemical products formed from the HSC alkene emissions to the total concentrations of these products, based on the base case study results. This figure is analogous to Figure 2.12 in the observational analysis section. The color coding is similar to that in Figure 2.12. The corresponding results for the sensitivity study with 6 HSC sources are shown in Figure 3.29. In contrast to the results from the base simulation, the trends in the HCHO, O_3 and CH_3CHO ratios as a function of downwind distance, i.e., as a function of plume aging, are more consistent for the multiple source case. These results, and the previous results comparing model performance with the single and multiple source cases, suggest an overall more consistent simulation by treating the HSC as a cluster of smaller sources rather than a single large source.
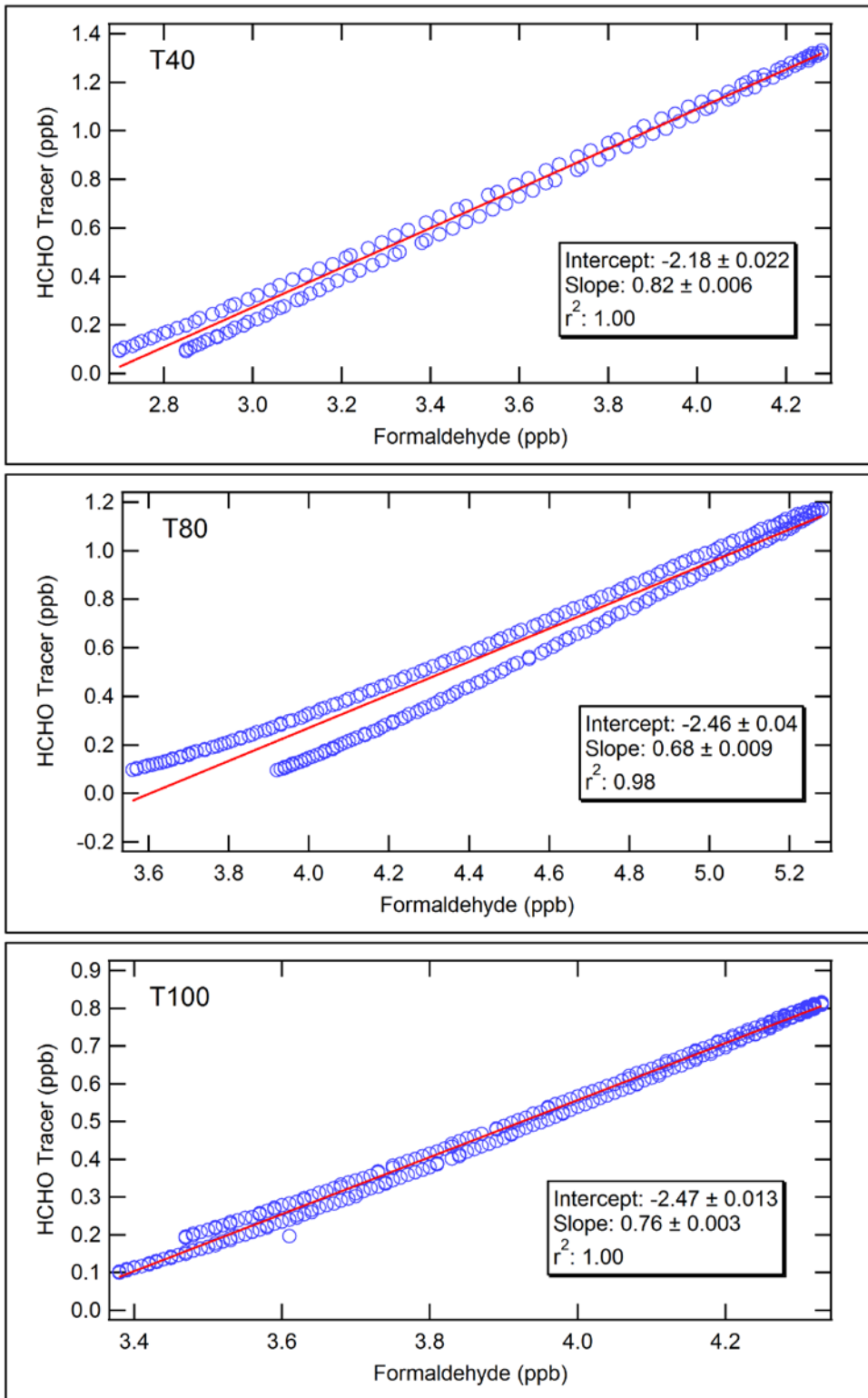
Figure 3.24. HSC HCHO tracer (primary + formed from alkene hydroxynitrate chemical mechanism) versus total HCHO in the September 18, 2013 HSC plume at the three downwind transects (compare with Figure 2.6). Model results are for the base case simulation with one large source representing the HSC emissions.

58
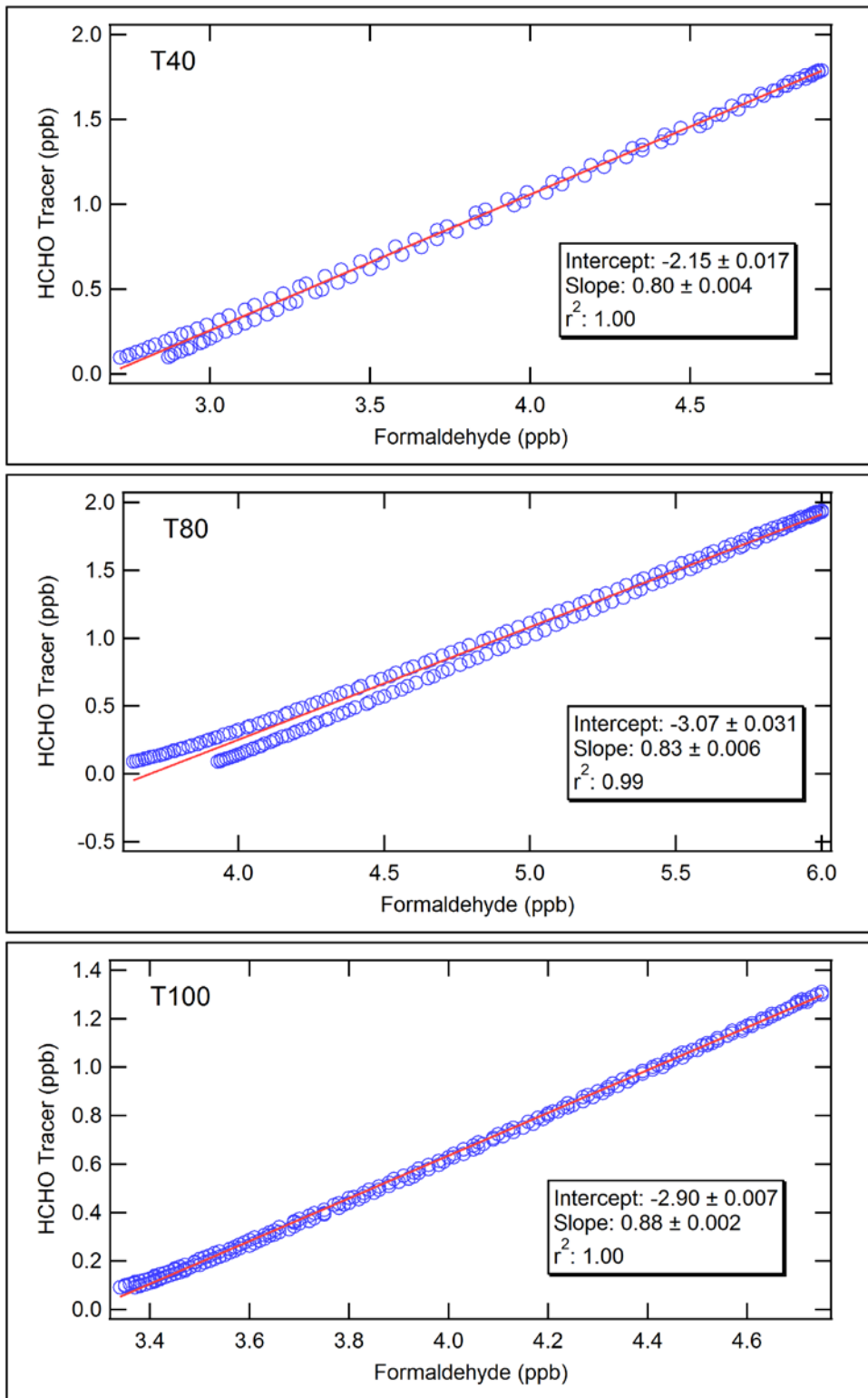
Figure 3.25.   HSC HCHO tracer (primary + formed from alkene hydroxynitrate chemical mechanism) versus total HCHO in the September 18, 2013 HSC plume at the three downwind transects (compare with Figure 2.6). Model results are for the sensitivity simulation with 6 sources representing the HSC emissions.
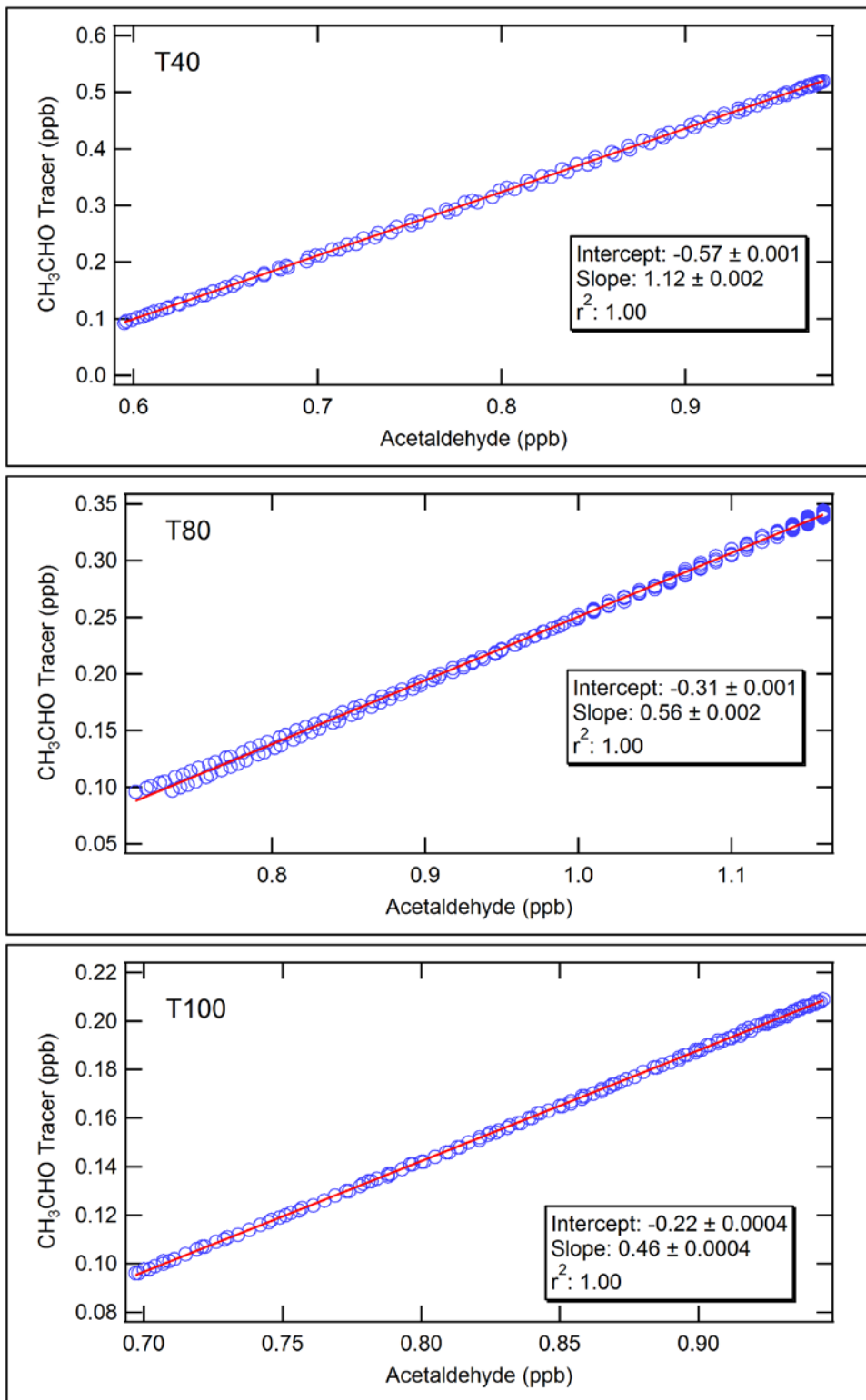
Figure 3.26. HSC CH$_3$CHO tracer (formed from alkene hydroxynitrate chemical mechanism) versus total CH$_3$CHO in the September 18, 2013 HSC plume at the three downwind transects (compare with Figure 2.8). Model results are for the base case simulation with one large source representing the HSC emissions.
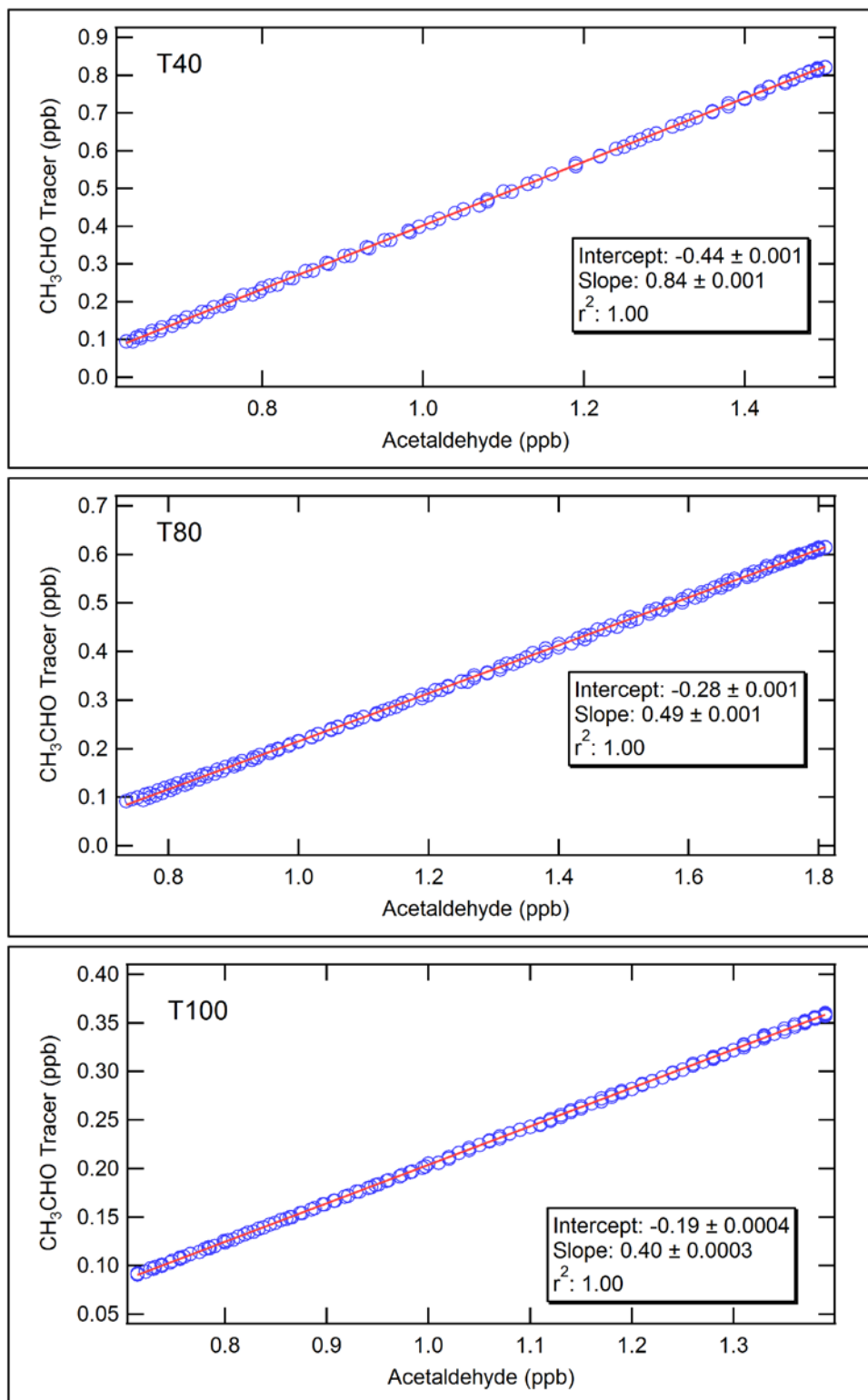
Figure 3.27. HSC CH₃CHO tracer (formed from alkene hydroxynitrate chemical mechanism) versus total CH₃CHO in the September 18, 2013 HSC plume at the three downwind transects (compare with Figure 2.8). Model results are for the sensitivity simulation with 6 sources representing the HSC emissions.
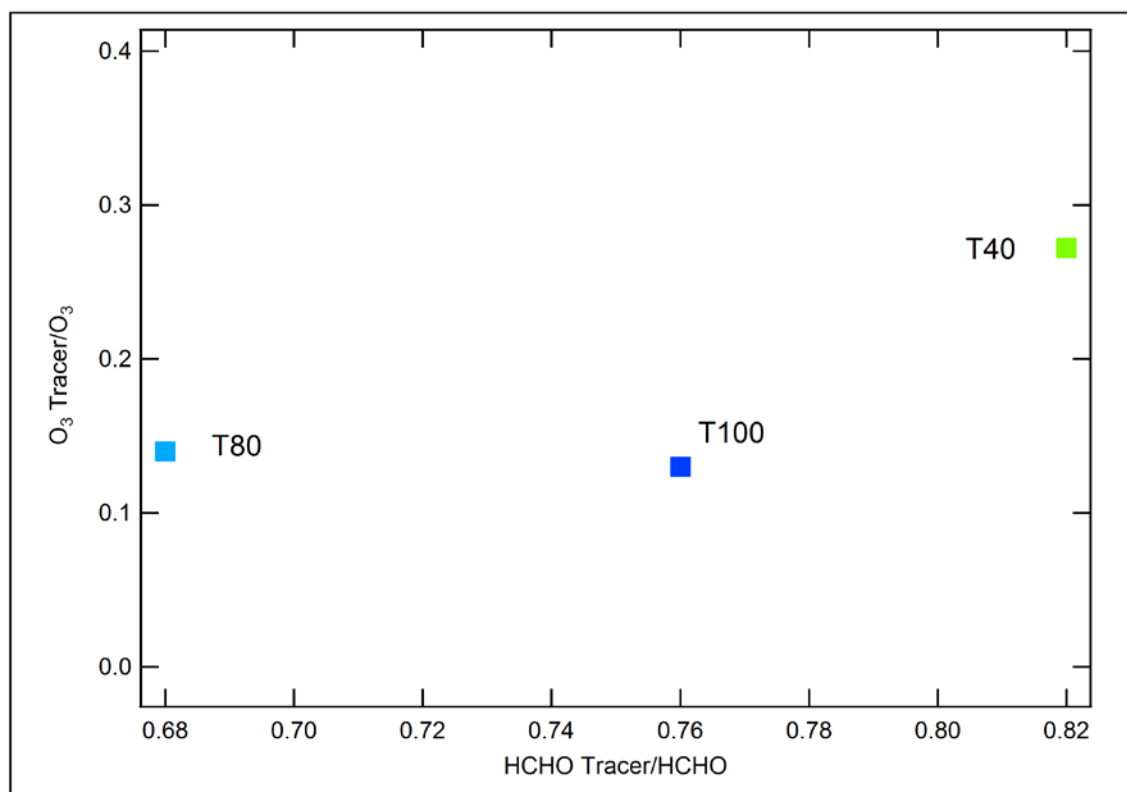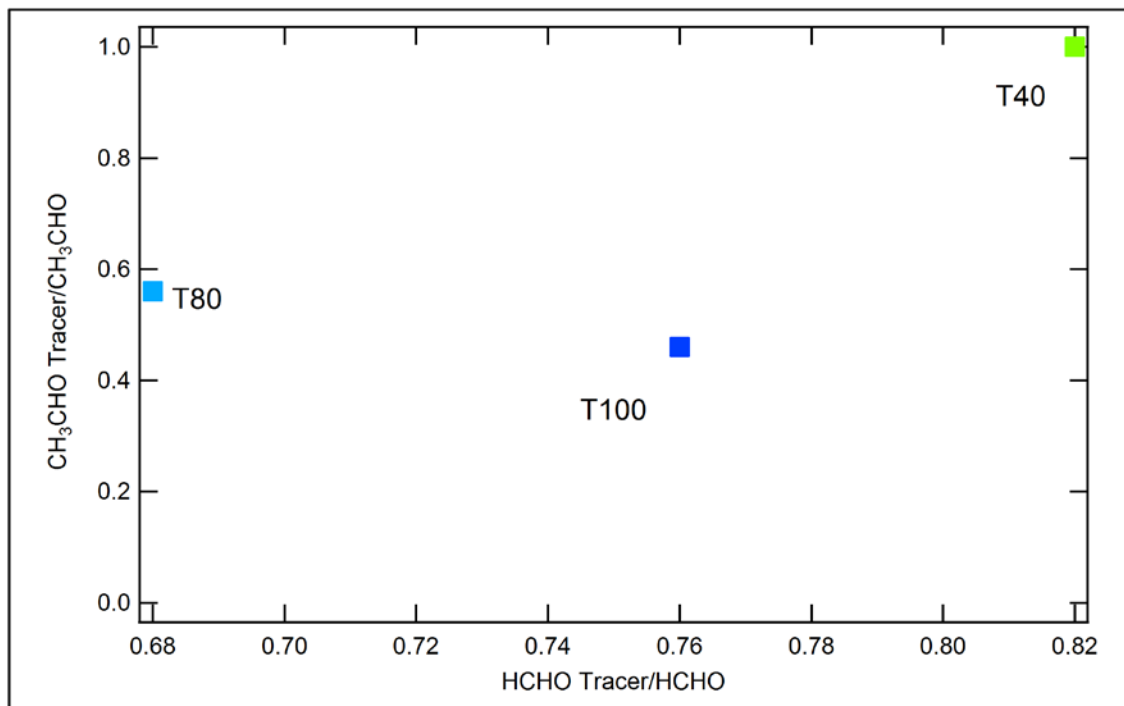
Figure 3.28. Comparison between the ratios of the secondary photochemical products (O₃, HCHO and CH₃CHO tracers) from HSC alkene emissions to total species concentrations at the three downwind transects. Model results are for the base case simulation with one large source representing the HSC emissions.
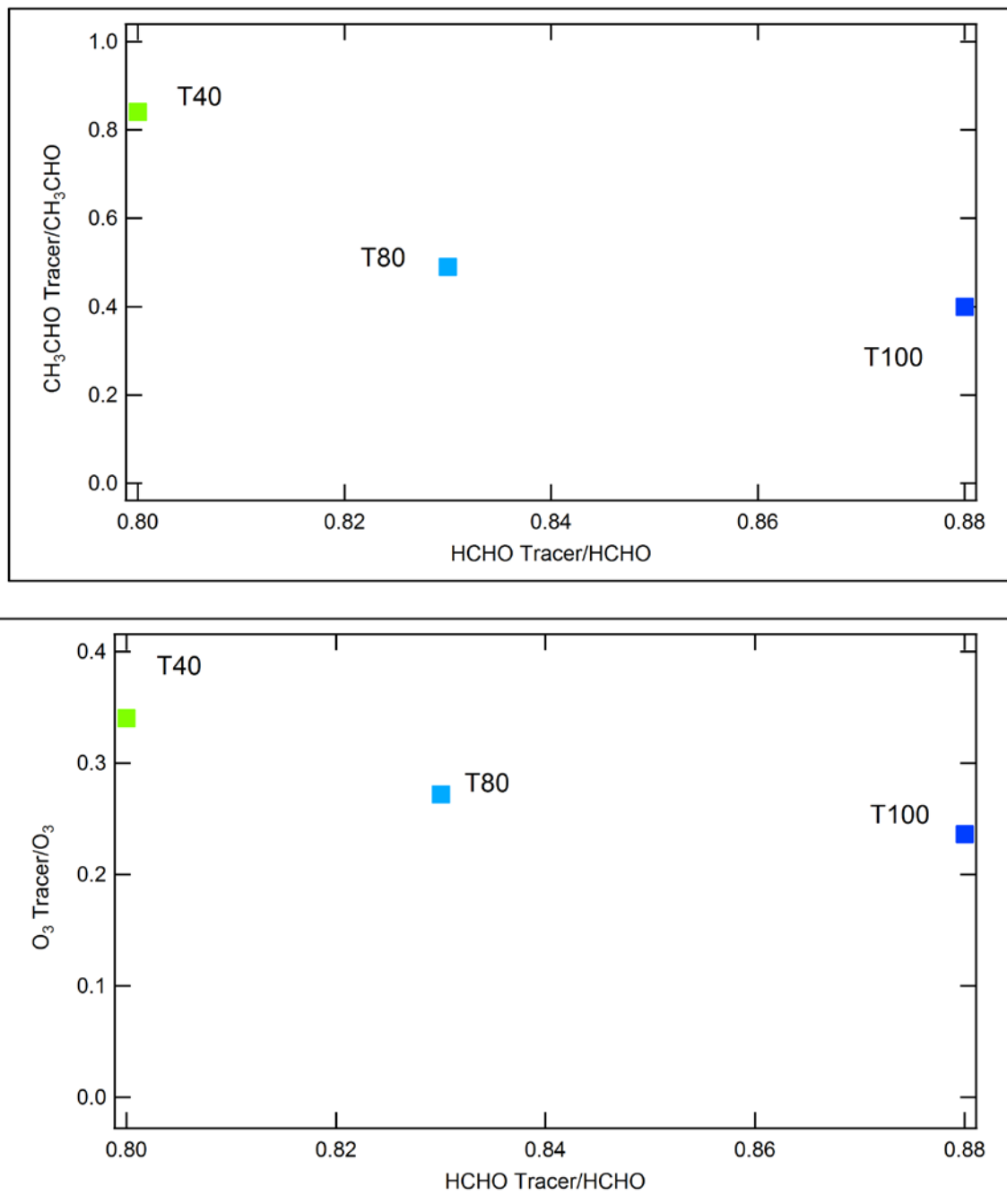
Figure 3.29. Comparison between the ratios of the secondary photochemical products (O$_3$, HCHO and CH$_3$CHO tracers) from HSC alkene emissions to total species concentrations at the three downwind transects. Model results are for the sensitivity simulation with 6 sources representing the HSC emissions.

Figure 3.30a shows the OPE as defined in Section 2.6 and Figure 2.13 (the Ox to NOz ratio) versus the photochemical aging of the plume (defined as NOx/NOy) at the three downwind transects for the base case simulation. The results show an opposite trend to the results derived from the observational analysis in Figure 2.13a. This is likely due to the under-prediction of NOz formation in the base case study. Figure 3.30b shows the OPE defined as the O_3 to NOy ratio versus the photochemical aging of the plume. The trend in Figure 3.30b is more consistent with the observed trend shown in Figure 2.13b.

The OPE results for the sensitivity study with 6 HSC sources are shown in Figure 3.31. In Figure 3.31a, the OPE is defined as the Ox to NOz ratio, and in Figure 3.31b it is defined as the O_3 to NOy ratio. From Figure 3.31a we see that the Ox/NOz ratios for the two furthest downwind transects (T80 and T100) show the same trend as the observations in Figure 2.13a, but the nearest transect (T40) still shows the opposite trend, indicating that NOz formation near the source is still under-estimated. However, the O_3/NOy ratio (Figure 3.31b) shows a trend that is consistent with the measurements (Figure 2.13b) and with the corresponding modeled ratio for the base case study with one source (Figure 3.30b).

Equation 2.7 was used to estimate the contribution of the individual alkenes to total direct O_3 formation from HRVOC based on the modeled hydroxynitrate concentrations from the base case study. Table 3-2 provides the individual contributions of HSC emissions of ethene, propene, butenes and 1,3-butadiene to the peak O_3 formed from the Channel HRVOC emissions (represented by the O_3 tracer in the alkene chemistry, also shown in the table) at the three downwind transects of the September 18, 2013 plume. The relative contributions of the more reactive alkenes (butenes and 1,3-butadiene) decrease with downwind distance while the relative contribution of ethene increases with downwind distance. The relative contribution from propene is approximately the same at all three downwind distances. The contributions are dominated by ethene, propene and butenes, due to the low 1,3-butadiene emissions (see Table 3.1).

Table 3.2. Contributions of individual alkenes to downwind O_3 from HSC HRVOC emissions

Alkene	40 km downwind O_3 tracer = 2.3 ppb	80 km downwind O_3 tracer = 2.7 ppb	100 km downwind O_3 tracer = 2.1 ppb
Ethene	24%	32%	34%
Propene	36%	36%	35%
Butenes	37%	30%	29%
1,3-Butadiene	3%	2%	2%
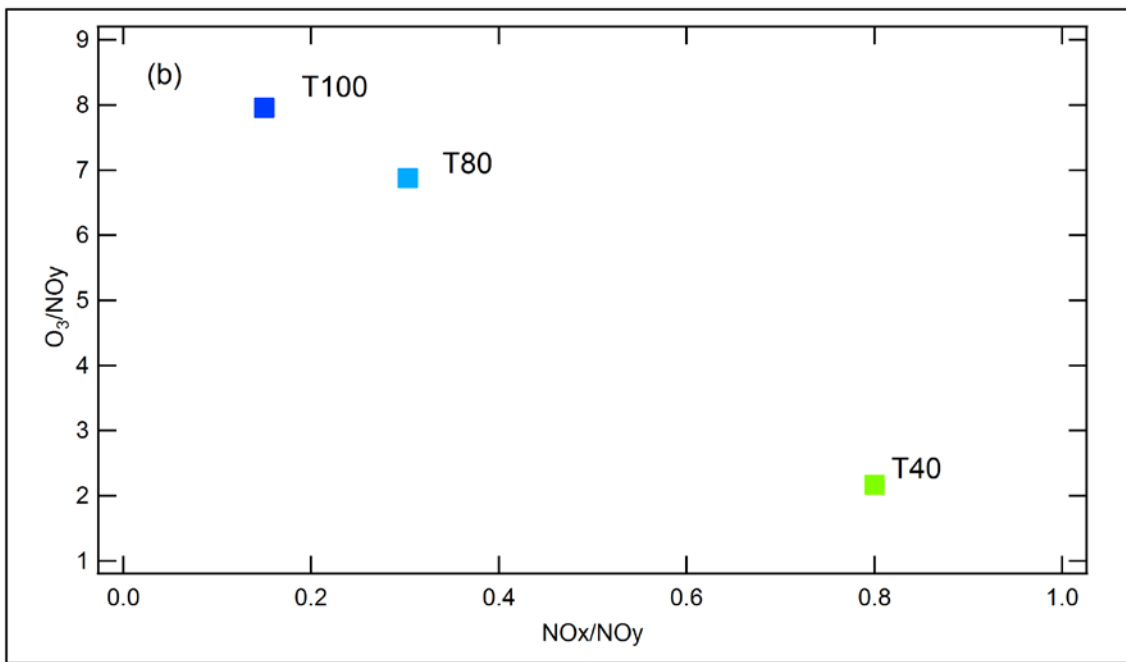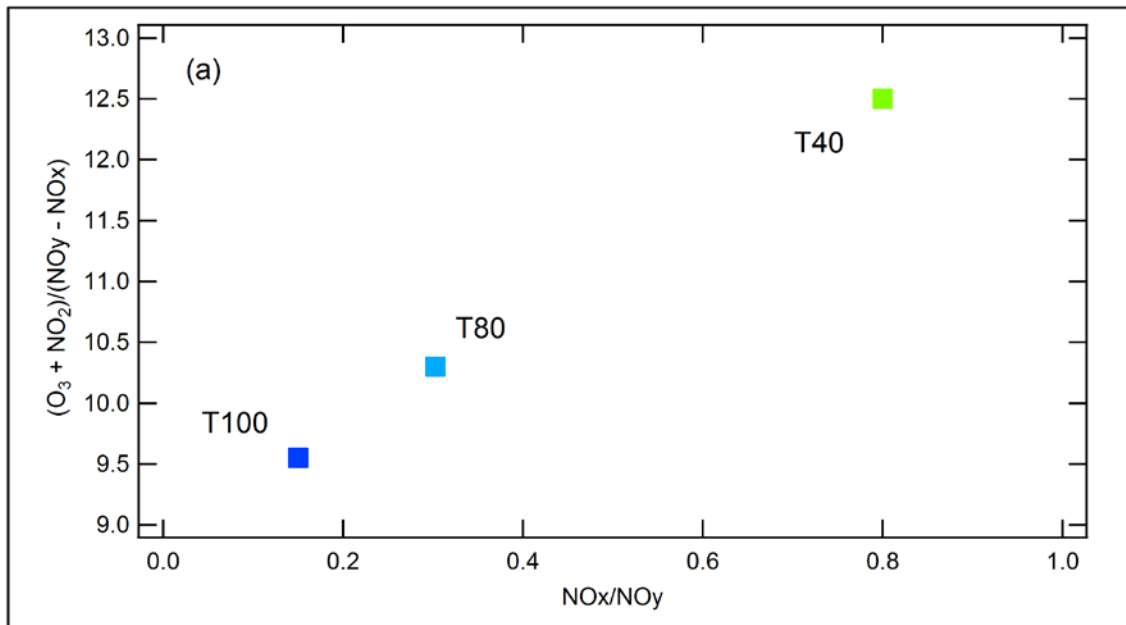
Figure 3.30. OPE versus photochemical aging of HSC plume: (a) OPE defined as Ox/NOz; (b) OPE defined as O_3/NOy. Model results are for the base case simulation with one large source representing the HSC emissions.
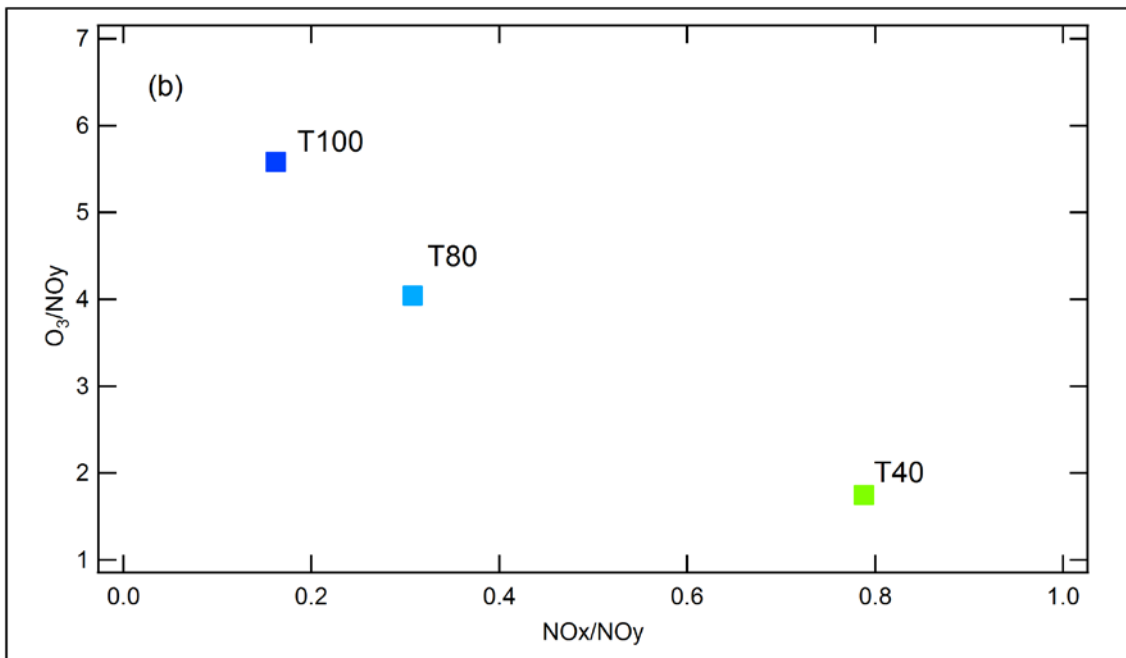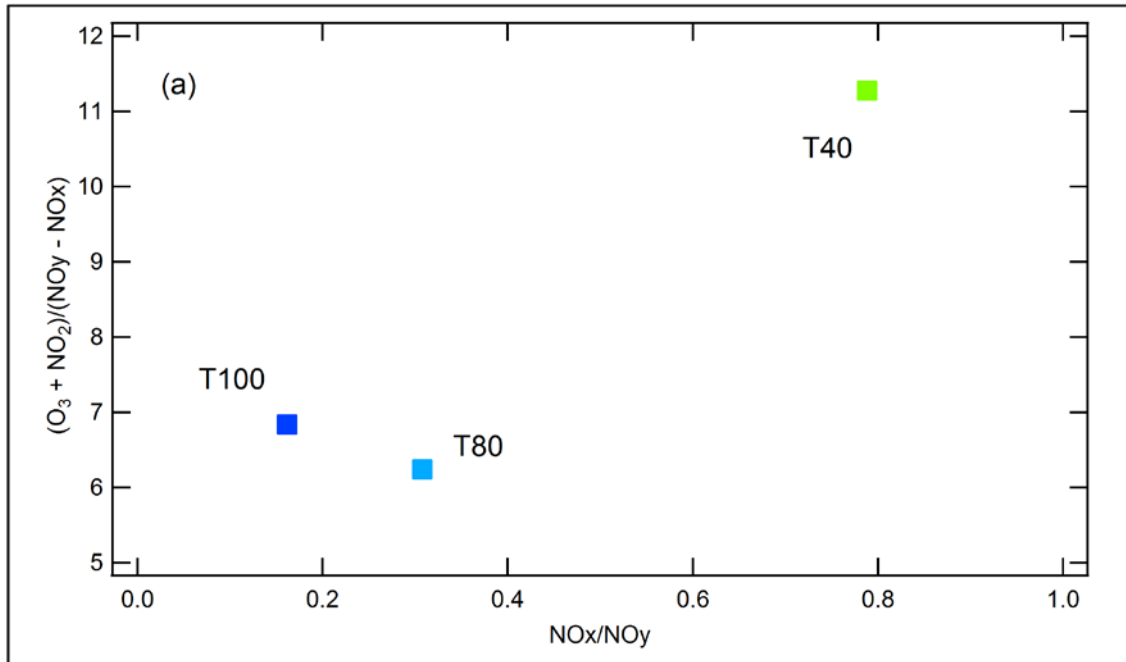
Figure 3.31. OPE versus photochemical aging of HSC plume: (a) OPE defined as Ox/NOz; (b) OPE defined as O_3/NOy. Model results are for the sensitivity simulation with 6 sources representing the HSC emissions.

.

3.3.3 Additional Sensitivity Studies

In addition to the sensitivity study with multiple sources representing the HSC emissions, a number of other sensitivity simulations were conducted with the model. These include:

- A study in which the HSC emissions were set to zero to quantify the HSC impacts and to understand the role of the alkene chemistry in forming O_3.
- Variations in the multiple source sensitivity study by segregating the NOx and VOC emissions. These studies investigate the scenario that HRVOC sources and NOx sources are separated in space, thus increasing the VOC/NOx ratio early on, and supplying NOx as the separate plumes grow and merge into the larger HSC plume.

Selected results from these studies are presented below.

Figure 3.32 shows the base case O_3 tracer (representing O_3 from the HSC alkene emissions) plotted against O_3 formed due to all the HSC emissions (determined as the difference between the base case study and the sensitivity study without HSC emissions) for the three transects. About 15 to 25% of the total O_3 produced from the HSC emissions can be attributed to O_3 produced from HRVOC oxidation. Figure 3.33 shows the corresponding figure for the sensitivity simulation with 6 HSC sources. In contrast to the base case simulation, the sensitivity study shows a larger contribution of HSC alkene oxidation (ranging from 26% at 100 km downwind to 35% at 40 km downwind) to the total O_3 formed from all HSC emissions. This confirms the previous conclusions that separating the emissions into a cluster of smaller sources results in a more reactive plume with results that are more consistent with aircraft measurements.

In the other sensitivity studies with the 6 separated sources, two configurations were used:

- Partial segregation of NOx and VOC emissions, in which the total HSC NOx and VOC emissions were split as 90:10 for 3 sources and 10:90 for the remaining 3 sources
- Total segregation of NOx and VOC emissions, in which the total HSC NOx and VOC emissions were split as 100:0 for 3 sources and 0:100 for the remaining 3 sources.

Figure 3.34 shows the effect of segregating the NOx and VOC emissions for the 6 sources on O_3 concentrations in the HSC plume at the three downwind transects. Total segregation of NOx and VOC emissions results in a plume that is less reactive for O_3 formation than the no segregation and partial segregation scenarios at all downwind distances. In contrast, partial segregation has a very small negative effect on O_3 levels in the plume at the nearest downwind distance, and small but noticeable positive effects at 80 and 100 km downwind. Additional sensitivity studies to provide more insight on these results are out of the scope of the current study but are recommended for future studies.
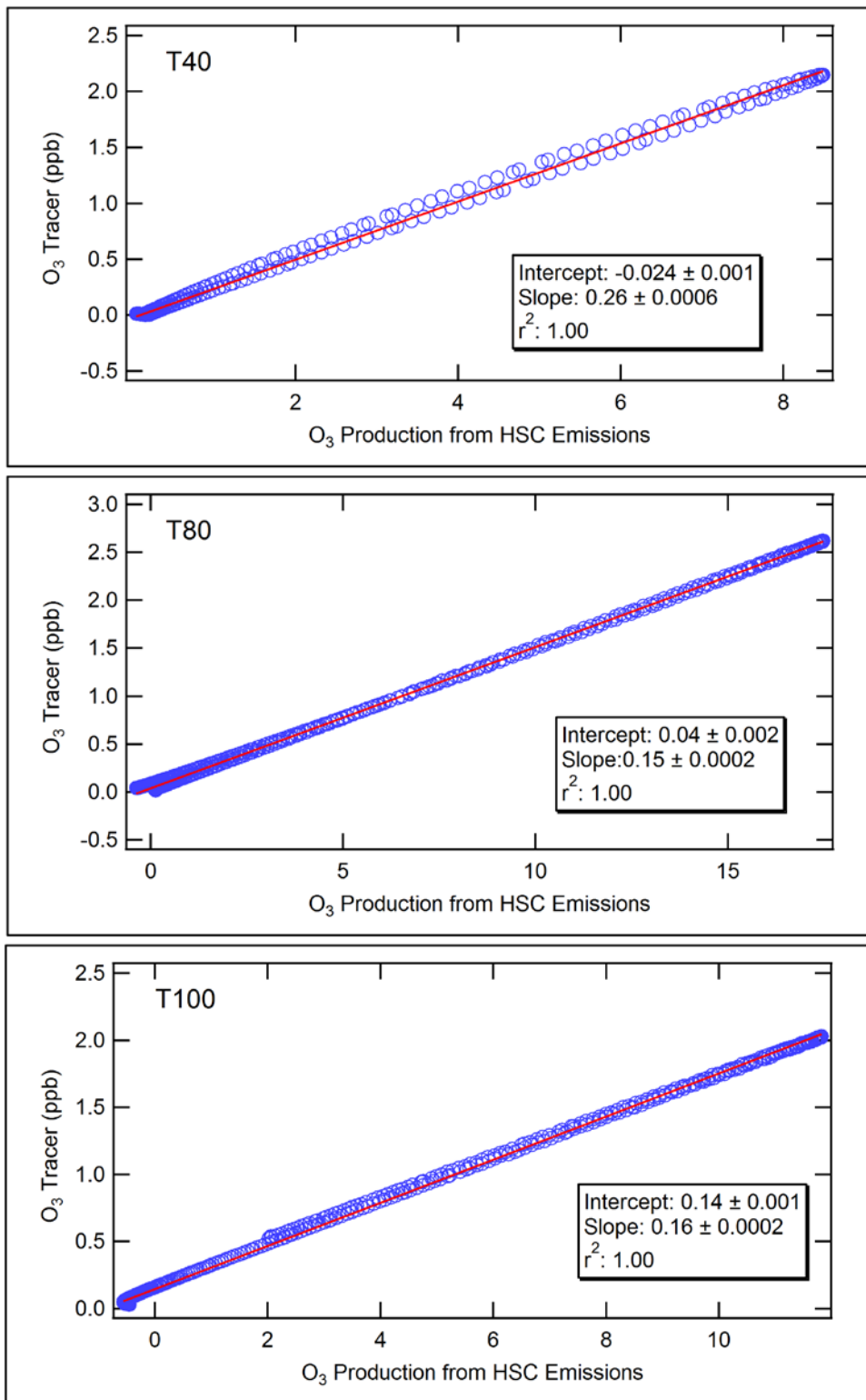
Figure 3.32. O_3 formed from oxidation of HSC alkenes versus total O_3 from HSC emissions in the September 18, 2013 HSC plume at the three downwind transects. Model results are for the base case simulation with one large source representing the HSC emissions.
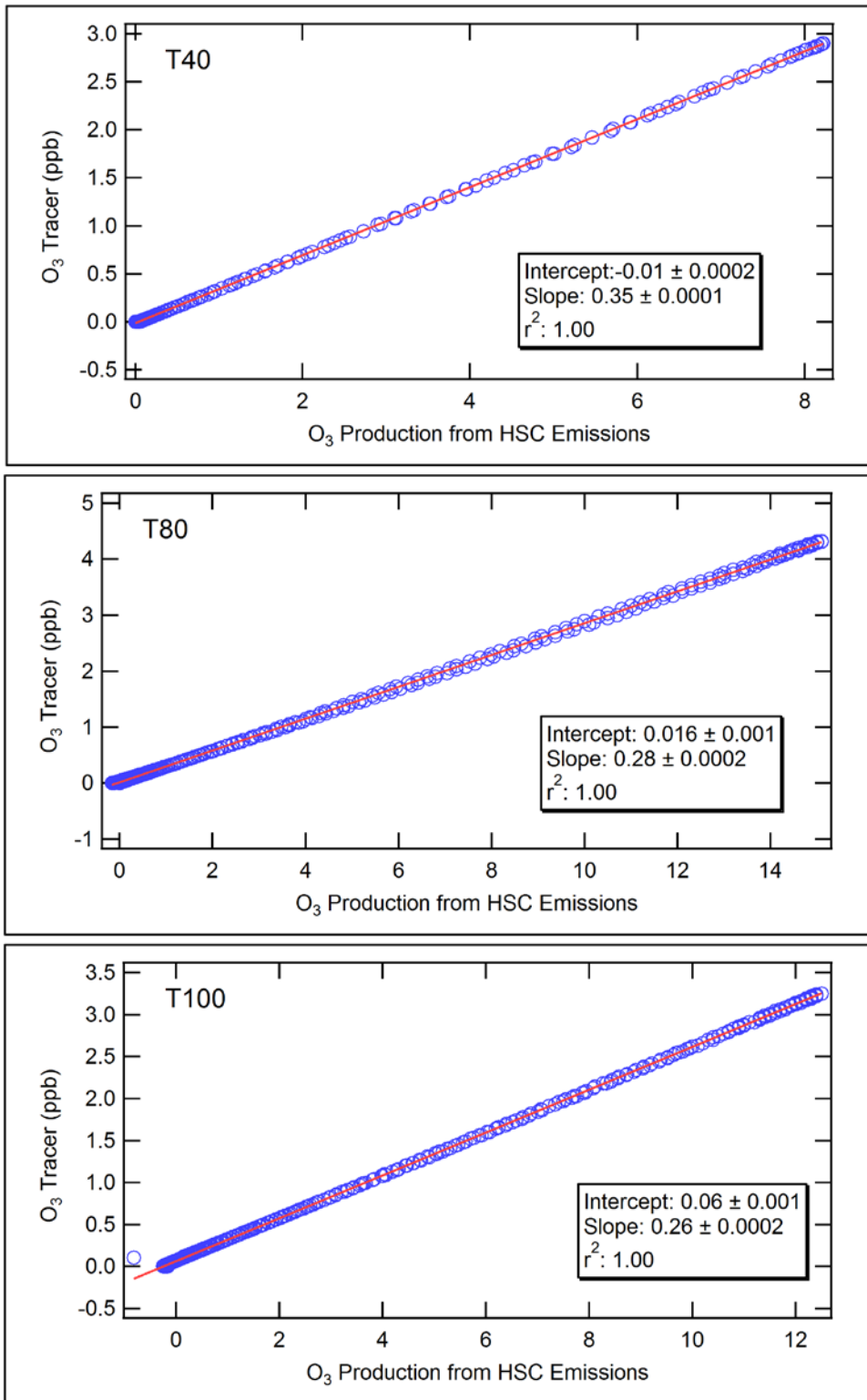
Figure 3.33. O_3 formed from oxidation of HSC alkenes versus total O_3 from HSC emissions in the September 18, 2013 HSC plume at the three downwind transects. Model results are for the sensitivity simulation with 6 sources representing the HSC emissions.
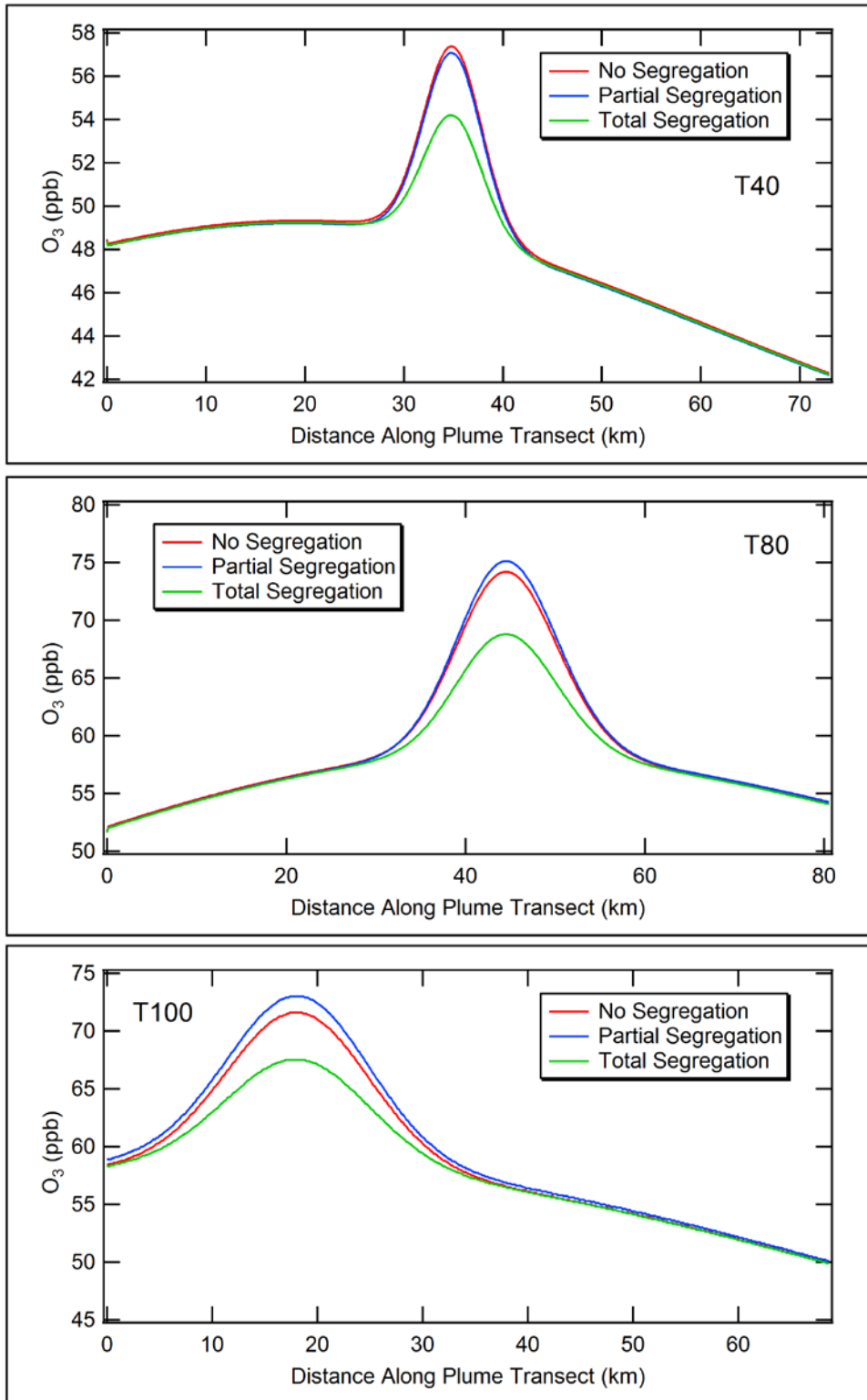
Figure 3.34. Effect of segregating NOx and VOC emissions from the 6 smaller HSC sources shown in Figure 3.11 on O$_3$ concentrations in the September 18, 2013 HSC plume at the three downwind transects.

4. SUMMARY AND CONCLUSIONS

4.1 OBSERVATIONAL ANALYSIS

Industrial emissions of highly reactive volatile organic compounds (HRVOC) contribute to localized O_3 production in Houston. The definition of HRVOC emissions includes ethene, propene, four butene isomers and 1,3-butadiene. As each individual HRVOC is oxidized through reaction with OH in the presence of NOx, a characteristic β-hydroxynitrate (βHN) is formed. The atmospheric chemistry of isoprene is similar to the HRVOC, including βHN formation, but isoprene is not defined as an HRVOC because its sources are overwhelmingly natural (biogenic). Measuring the family of βHNs in the plume downwind from the industrial emission sources provides a fingerprint of the emitted HRVOC including their relative emission rates. This fingerprint can potentially persist after the HRVOC have completely reacted; the degree of persistence depends upon the atmospheric lifetimes of the βHNs. In addition to the βHNs, oxidation of HRVOC produces O_3 and aldehydes, predominately formaldehyde and acetaldehyde. The characteristic ratios in which these photochemical products are formed from a given HRVOC are known from laboratory studies. Consequently the measured βHN fingerprint can be used to quantify the direct contributions of individual HRVOC to O_3 and aldehyde concentrations formed in the transported emission plume. Direct contribution refers to O_3 and aldehyde produced immediately following OH reacting with the HRVOC. Subsequent production, e.g., O_3 formed from the aldehydes, is referred to as an indirect contribution.

Several aircraft flights conducted during the NASA SEAC[4]RS project measured all of the above photochemical products plus other products, precursors and other tracer compounds in plumes downwind of petrochemical facilities in Houston. We have analyzed data from 20 plumes that were encountered on 11 of these flights in and around Houston from 12 August - 23 September 2013. The analysis focused on the 18 September flight when the DC-8 aircraft systematically surveyed the plume downwind from the HSC. On this day the highest 8-hour average O_3 concentration measured at ground stations in the Houston-Galveston-Brazoria region was only 47 ppb while the aircraft measured a maximum instantaneous O_3 concentration of 76 ppb. During the other flights, the maximum 8-hour average O_3 concentrations measured at ground stations in the Houston area were 46 to 78 ppb, except 16 August when 94 ppb was recorded. Instantaneous measurements by the aircraft reached 65 to 124 ppb. These O_3 levels indicate that most of these days represent typical, moderate O_3 days in Houston without unusually large HRVOC emission events. One exception is the 23 September plume, which had much larger concentrations of the βHN formed from propene, indicating larger emissions of propene on that day.

The direct contributions of HRVOC oxidation to O_3 formation in the intercepted plumes have been quantified from the measured βHN concentrations. Since background O_3 concentrations could only be poorly approximated from the aircraft data, O_3 enhancements in the plumes

were difficult to determine, but it is clear that they varied widely: from approximately 4 to 54 ppb. In these plumes from the HSC, the fraction of ozone formation directly attributable to HRVOC and isoprene emissions (as indicated by the $O_3/\beta HN$ enhancement ratios) was surprisingly small, averaging only ~13% with a range from 6% to 24%. (These percentages exclude the one unusual plume on 23 September when larger emissions of propene are indicated; in this plume, 58% of the O_3 enhancement was directly attributed to HRVOC including a small contribution from isoprene.) Isoprene contributed, on average, 35% (range of 9% to 56%) of the directly attributable O_3 enhancement, making this species' average contribution approximately equal to that of ethene, the most important HRVOC. This finding is for the identified plume downwind of HSC HRVOC sources, so such a large contribution from isoprene is surprising. The plume observed on 23 September is an exception because larger propene emissions dominated this plume.

The direct contributions of individual HRVOC to the anthropogenic O_3 enhancement (i.e., excluding the isoprene contribution) on average ranked in this order: ethene (49%), propene (32%), butenes (13%) and butadiene (6%). However there were wide variations in these relative contributions: ethene (24% to 72%), propene (14% to 66%), butenes (8% to 24%) and butadiene (2% to 13%). Some of these variations represent systematic changes in contributions with downwind distance as emissions were photochemically processed, with the more rapidly reacting HRVOC contributing a larger fraction early and the contribution from the more slowly reacting ethene gradually increasing. This trend is apparent from the relative contributions measured during the four plume transects of the 18 September flight (Table 4.1). In addition to the HRVOC contributions in Table 4.1, isoprene added ~0.7 to ~1.7 ppb to the ΔO_3 and increased the directly attributable contributions by 77% on average.

Table 4.1. Directly attributable contributions of individual HRVOC from HSC to downwind O_3 on 18 September flight.

Alkene	Over HSC $\Delta O_3 = 2.1$ ppb	40 km downwind $\Delta O_3 = 2.7$ ppb	80 km downwind $\Delta O_3 = 3.0$ ppb	100 km downwind $\Delta O_3 = 2.6$ ppb
Ethene	34%	37%	53%	53%
Propene	45%	39%	26%	27%
Butenes	16%	19%	15%	14%
1,3-Butadiene	5%	6%	6%	6%

The total O_3 formed downwind of HRVOC sources is larger than the sum of the direct contributions of the individual HRVOC and isoprene that can be explained by analysis of the DC-8 βHN data. Three potential explanations are:

- βHNs are lost from the atmosphere during plume transport, which biases low the direct O_3 contributions derived from $O_3/\beta HN$ enhancement ratios.

- As they react, HRVOC and isoprene form aldehydes, which make O_3 contributions that were not counted by the $O_3/\beta HN$ enhancement ratios.
- As they react, HRVOC and isoprene increase the OH radical concentrations, which promote O_3 formation from other VOCs present leading to indirect O_3 contributions from HRVOC emissions.

It does not appear that loss of βHNs from the atmosphere is an important factor. Importantly the $\beta HN/NOy$ enhancement ratios continually increase as the plumes age as indicated by the decreasing NOx/NOy ratio (see Figure 2.14). This continual increase would not be expected if βHNs were rapidly lost, although there is some evidence for such loss (Figures 2.4 and 2.5). The substantial contribution of isoprene confirms that other VOCs can play a major role in O_3 formation in these plumes. The nature of the indirect O_3 contributions in plumes downwind of HRVOC sources must receive careful consideration.

The observational analysis presented here has limitations that must be fully appreciated. First, it is implicitly assumed that the βHNs remain in the atmosphere, preserving the signature of the HRVOC and isoprene oxidation. However, there is some evidence for loss of βHNs, so the extent of βHN removal is uncertain. This means that the diagnosed HRVOC and isoprene contributions to O_3 are lower limits. Second, the analysis of βHNs only diagnoses the direct contribution of HRVOC to O_3, which accounts for only a fraction of the total O_3 formation. This direct contribution appears to underestimate the total O_3 impact of HRVOC emissions. Finally, the SEAC[4]RS flights analyzed were conducted on 11 days during a six-week period in 2013. It is difficult to judge the representativeness of these days, but it is clearly a small sample that cannot be taken as full characterization of the photochemical evolution of HSC plumes in 2013. Further, emissions of HRVOC and NOx from the HSC region have evolved over the years, and the situation in 2013 may not be comparable to earlier periods.

4.2   PLUME MODELING

The SCICHEM reactive plume model was used to model direct and indirect O_3 formation from the HSC HRVOC emissions. The CB6r2 chemical mechanism, which is used by TCEQ to model O_3 in Houston, was implemented in SCICHEM to model total O_3 formation from both plume and background emissions. The CB6r2 mechanism was supplemented with a HRVOC tracer mechanism that estimated direct O_3 formation from individual alkenes consistently with the relationships (O_3 to βHN ratios) that were used in the observational data analysis summarized above.

Plume modeling was conducted for 18 September 2013, a day on which several downwind traverses of the HSC plume were conducted by the aircraft during the SEAC[4]RS study. The plume was transported to the west-northwest over the Houston urban area, introducing urban emissions into the HSC plume. Background emissions, based on the CAMx grid model inputs, were used to simulate the interaction of the urban emissions with the HSC plume. The

September 18 plume was sampled by the DC-8 at three downwind distances (approximately 40, 80 and 100 km) from the HSC.

Ethene and propene emissions for the HSC were based on measurements by the Solar Occultation Flux (SOF) method for other dates, while emissions for butenes and 1,3-butadiene were estimated using their ratios to ethene in the aircraft measurements over the HSC on September 18 (see Figure 2-2). Emissions of NOx, formaldehyde and alkanes were also based on SOF measurements for other dates. In the base case study, the HSC emissions were represented as a single source with an initial width of 6 km in order to match the plume width at the closest downwind transect (at 40 km downwind).

Model results were compared with aircraft measurements of O_3, HCHO, CH_3CHO, NOy and NOz for the three downwind transects. The modeled and measured crosswind profiles of O_3 were in good agreement, particularly at the 40 and 80 km downwind transects where measurements showed peak O_3 concentrations of approximately 8 ppb and 25 ppb above the background, respectively, and the corresponding modeled increments were 8 ppb and 23 ppb. The aircraft measurements showed background O_3 of 45 to 50 ppb, while the modeled background was higher (48 to 60 ppb). Modeled NOy increments in the plume were also in good agreement with measurements at all 3 downwind distances. However, the model under-estimated NOz formation in the plume at the nearest downwind transect at 40 km by about 12%. The model under-estimated HCHO and CH_3CHO formation in the plume by 50% or more. At the 40 km transect, the peak modeled CH_3CHO plume increment was more than a factor of 2 lower than the measured increment. These results indicate that chemistry proceeded more slowly in the modeled plume than what the measurements show.

Relationships between O_3 formed directly from the HSC HRVOC emissions (obtained from the HRVOC tracer mechanism) and total Ox ($O_3 + NO_2$) were determined by regression analysis of model results for the three transects. In the base case simulation with one source representing HSC emissions, direct O_3 contributions from HRVOC emissions ranged from 22% of total Ox at the nearest downwind traverse to 12% at the 80 and 100 km downwind traverses. The direct contribution at 40 km is consistent with the observational analysis, but the model predicts higher direct contributions than the analysis at the larger downwind distances. In contrast to the observational analysis, the model results are not affected by possible loss mechanisms for the βHNs, which could explain why the modeled direct contributions are larger than those from the observational analysis at the downwind transects. Total O_3 peak increments in the modeled plume range from 8 to 25 ppb, while the O_3 increments from the HRVOC emissions range from 2 to 2.6 ppb. At 40 km downwind, butenes and propene are the largest HRVOC contributors (~36%) and the ethene contribution is 24%. Further downwind, the ethene contribution increases to greater than 30%, the propene contribution is unchanged and the contribution of butenes decreases to 30%. These contribution changes with distance occur because ethene is the slowest reacting HRVOC

whereas butenes react the fastest. The contribution of 1,3-butadiene was small (3% or less) at all downwind distances due to low emissions in the model. The modeled O_3 from butenes is larger than indicated from the observational analysis, likely due to over-stating the HSC butene emissions. The butene emissions were based on the regression of the whole air samples from the aircraft measurements (see Figure 2.2), and are likely to be biased high due to the high outlier shown in the scatter plot in Figure 2.2.

A similar approach was used to relate direct contributions to HCHO and CH_3CHO (from the HRVOC tracer mechanism) to total HCHO and CH_3CHO levels in the modeled plume at the three downwind transects. More than 50% of the formaldehyde increments in the plume are directly attributable to HRVOC emissions at all three downwind distances, with the highest contribution being about 80% at the nearest downwind distance of 40 km. For CH_3CHO, the direct contributions vary from 46% at the furthest downwind distance to 100% at the nearest downwind distance. As for O_3, the modeled direct contributions for aldehydes are generally higher than those inferred from analysis of observed βHNs, possibly because the model results are not affected by loss of βHNs.

The modeling and observational analysis results indicate that direct formation of O_3 from HRVOC emissions can explain only 12 to 22% of the O_3 increments in the HSC plume on September 18, 2013. The remaining O_3 increments in the plume are attributed to indirect O_3 formation from other precursors (including isoprene, as determined from the observational analysis) promoted by reactions of the HSC emissions. This finding could be extrapolated to other days with similar O_3 downwind of the HSC but should not be extrapolated to days with very high O_3 downwind of the HSC. We recommend additional study of the interactions that cause indirect O_3 production from HSC emissions and the non-HSC sources that participate in this indirect O_3 production.

In addition to the base case study with one source representing HSC emissions, a sensitivity study was conducted in which the emissions were represented as a line of 6 sources along the HSC separated from each other by about 2 km. The initial widths of the plumes from the 6 sources were set to 100 m and the width of the combined plume from the 6 sources at 40 km downwind was approximately the same as that from the single HSC source. The objective of the sensitivity study was to investigate how initial plume dilution and separation of sources influence modeled O_3 formation.

Much better agreement was obtained for aldehydes when the single HSC source was replaced by 6 smaller sources along the entire HSC. NOz concentrations at 40 km downwind were also in good agreement with the measurements, but NOz levels at 80 km and 100 km downwind were over-estimated with 6 sources. However, modeled O_3 concentrations were only slightly changed by using 6 sources rather than a single source. This is probably because higher direct O_3 production from HRVOC emissions was offset by lower indirect O_3 production with 6

sources – additional study is recommended because this tentative finding has implications for source attribution of O_3 observed of the HSC and similar sources. In the sensitivity study, the chemistry proceeded faster in the HSC plume and direct O_3 from HRVOC emissions ranging from 23 to 25% of total Ox as compared to 12 to 22% with a single source. Thus, the overall effect of representing the HSC emissions by multiple, narrower source plumes was that chemistry proceeded more rapidly and model performance improved at 40 km downwind.

Additional sensitivity studies were conducted with the 6-source configuration, in which the NOx and VOC emissions were segregated partially and totally. O_3 production was reduced by total segregation, i.e. with NOx and VOC released as separated plumes, because the HRVOC and NOx could only interact after the plumes had grown in width and overlapped with each other. Partial segregation of emissions had a negligible effect on O_3 production compared to no segregation.

The modeling conducted for this study represents a useful advance in understanding the role of HRVOC emissions from the HSC on downwind O_3. However, there are limitations that should be considered in future studies to develop a more quantitative assessment than the conceptual understanding gained from this study. The important limitations are listed below:

- Uncertainties in model formulation: SCICHEM uses model algorithms for dispersion, chemistry, deposition, and other processes, and these algorithms have uncertainties.
- Uncertainties in inputs. In this study, we used SOF measurements from a different date (in 2011) to estimate HRVOC emissions for modeling the September 18, 2013 plume. The actual HSC emissions for September 18, 2013 are unknown. HSC emission rates from AQRP Project 14-007 were not available in time for this work. Similarly, the emissions from the urban region to the west of the HSC (over which the September 18 plume was transported) were not specific to the date modeled.
- The source configurations used in the base case and sensitivity simulations are conceptual and likely do not represent actual conditions. The modeling showed some sensitivity to the spatial representation of the HSC emissions, which has implications for fine-scale modeling of O_3 in Houston.

4.3   RECOMMENDATIONS FOR FUTURE STUDIES

The observational analysis suggests that there may be a loss mechanism(s) for βHNs in the gas phase. If this is indeed the case, then this may have implications for the availability of NOx in the gas-phase as the plume ages, because the βHNs are formed from many VOCs and represent a substantial fraction of organic nitrates. Thus, additional studies of the fate of βHNs are warranted.

The modeling and observational analysis also indicate that a substantial fraction of the O_3 in the HSC plume is formed indirectly by the interaction of HRVOC emissions with other VOCs. For example, the observational analysis showed a large contribution of (biogenic)

isoprene to O_3 in the HSC plume. More studies are required to understand direct versus indirect O_3 formation in HSC plumes and to identify and quantify the various sources (including isoprene) of indirect contributions.

The plume modeling provided a unique opportunity to study the fine-scale photochemical interaction of plumes from nearby sources and initial segregation of NOx and VOC emissions. The current study provides a first look at these effects. Future studies can use more recent measurements of HSC emissions (e.g., from AQRP Project 14-007) and investigate further how initial plume width and emissions segregation influence O_3 production from industrial sources. Results from plume model and plume-in-grid model studies can show what resolution should be used in grid models. SCICHEM is well-suited to conducting these studies because it has full chemistry and allows overlapping plumes to interact photochemically. SCICHEM is also the underlying plume model in the recent EPA release of the plume-in-grid version of CMAQ 5.0.2 (Karamchandani et al., 2014), referred to as CMAQ-APT (where APT stands for Advanced Plume Treatment).

5. REFERENCES

Chowdhury, B., P.K. Karamchandani, R.I. Sykes, D.S. Henn, and E. Knipping, 2015. Reactive puff model SCICHEM: Model enhancements and performance studies, *Atmos. Environ*., **117**, 242-258.

ENVIRON, 2015. User's Guide Comprehensive Air Quality Model with Extensions Version 6.2. http://www.camx.com.

Gilman, J.B., et al. (2009), Measurements of volatile organic compounds during the 2006 TexAQS/GoMACCS campaign: Industrial influences, regional characteristics, and diurnal dependencies of the OH reactivity, *J. Geophys. Res*., **114**, D00F06, doi:10.1029/2008JD011525.

Johansson, J.K E., J. Mellqvist, J. Samuelsson, B. Offerle, B. Lefer, B. Rappenglück, J. Flynn, and G. Yarwood (2014a), Emission measurements of alkenes, alkanes, SO_2, and NO_2 from stationary sources in Southeast Texas over a 5 year period using SOF and mobile DOAS, *J. Geophys. Res.*, **119**, doi:10.1002/2013JD020485.

Johansson, J.K.E., J. Mellqvist, J. Samuelsson, B. Offerle, J. Moldanova, B. Rappenglück, B. Lefer, and J. Flynn, 2014b. Quantitative measurements and modeling of industrial formaldehyde emissions in the Greater Houston area during campaigns in 2009 and 2011, *J. Geophys. Res.,* **119**, 4303–4322, doi:10.1002/2013JD020159.

Karamchandani, P., L. Santos, I. Sykes, Y. Zhang, C. Tonne, and C. Seigneur, 2000. Development and evaluation of a state-of-the-science reactive plume model, *Environ. Sci. Technol*., **34**, 870-880.

Karamchandani, P., J. Johnson, G. Yarwood, and E. Knipping, 2014. Implementation and application of sub-grid-scale plume treatment in the latest version of EPA's third-generation air quality model, CMAQ 5.01, *J. Air Waste Manage. Assoc*., **64**, 453-467.

Neuman, J.A., et al., 2009. Relationship between photochemical ozone production and NOx oxidation in Houston, Texas, *J. Geophys. Res.,* **114**, D00F08, doi:10.1029/2008JD011688.

Ryerson, T.B. et al., 2003. Effect of petrochemical industrial emissions of reactive alkenes and NOx on tropospheric ozone formation in Houston, Texas, *J. Geophys. Res*., **108** (D8), 4249.

Sykes, R.I., S.F. Parker, D.S. Henn, and W.S. Lewellen, 1993. Numerical simulation of ANATEX tracer data using a turbulence closure model for long-range dispersion, *J. Appl. Met.*, **32**, 929-947.

Sykes, R.I. and D.S. Henn, 1995. Representation of velocity gradient effects in a Gaussian puff model, *J. Appl. Met.*, **34**, 2715-2723.

Teng, A.P., J.D. Crounse, L. Lee, J.M. St. Clair, R.C. Cohen, and P.O. Wennberg, 2015. Hydroxy nitrate production in the OH-initiated oxidation of alkenes, *Atmos. Chem. Phys.,* **15**, 4297–4316, doi:10.5194/acp-15-4297-2015.

APPENDIX A

SIMPLIFIED CHEMISTRY SCHEME FOR β-HYDROXYNITRATE FORMATION DURING ALKENE OXIDATION

APPENDIX A: SIMPLIFIED CHEMISTRY SCHEME FOR β-HYDROXYNITRATE FORMATION DURING ALKENE OXIDATION

The goal here is to provide a first-order scheme for both modeling and observational analysis of the hydroxy nitrate measurements made in the Houston area during SEAC⁴RS. Species of interest are hydroxy nitrates, aldehydes and O_3. Simplifying approximations made here include:

1) Using rate constants at 298K and 1 atmosphere
2) Neglecting alkene reactions with O_3 and NO_3
3) Neglecting hydroxyalkyl peroxy radical reactions with NO_2 and other organic peroxy radicals
4) Ignoring other less-important reaction channels
5) High NOx conditions have been assumed in choosing branching ratios.
6) The product yields for two aldehydes are the estimated first generation products from the unimolecular dissociation of the hydroxyalkoxy radicals from *Teng et al.,* 2015..
7) The formaldehyde yield from ethene oxidation is given for 1 atmosphere pressure.

Figure A1 illustrates the simplified reaction mechanism to describe first-generation formation of β-hydroxy nitrates, aldehydes and O_3 from alkenes. The reaction parameters defined in Figure A1 are discussed below.

Aldehyde yields: To illustrate the impact of approximation 6 listed above, Figure 3 of *Millet et al.* (2010) is reproduced at right. The yields of acetaldehyde from propene and isoprene reach their maxima during the first day of atmospheric processing for propene and isoprene. Butenes will react at a similarly rapid rate, while ethene will be somewhat delayed because ethene reacts more slowly with OH. The curves in Figure 3 of *Millet et al.* (2010) account for aldehydes formed promptly after initial reaction of OH with the VOC plus
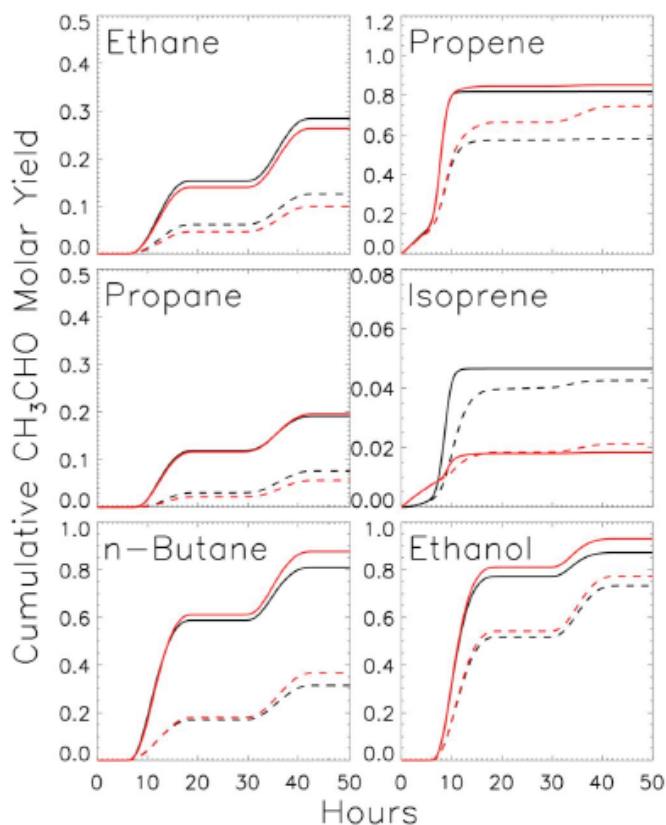

Fig. 3. Cumulative molar yield of acetaldehyde from the oxidation of VOCs. Yields are computed using the GEOS-Chem (red) and MCMv3.1 (black) chemical mechanisms, for 1 ppb NO_x (solid lines) and 0.1 ppb NO_x (dashed lines).

aldehydes formed from subsequent reactions, e.g., degradation of acetaldehyde to formaldehyde. Thus, the first generation aldehyde yields derived in Table A1 may be lower-limits.

Altitude dependence of formaldehyde from ethene: To illustrate the impact of approximation 7 above, Figure 8 of *Orlando et al.* (2003) is reproduced at right. The yield of formaldehyde from ethene has a strong pressure dependence, which implies significant altitude dependence in the lower troposphere. The value in Table A1 is for surface elevation, and thus may be an upper-limit compared to what was observed.
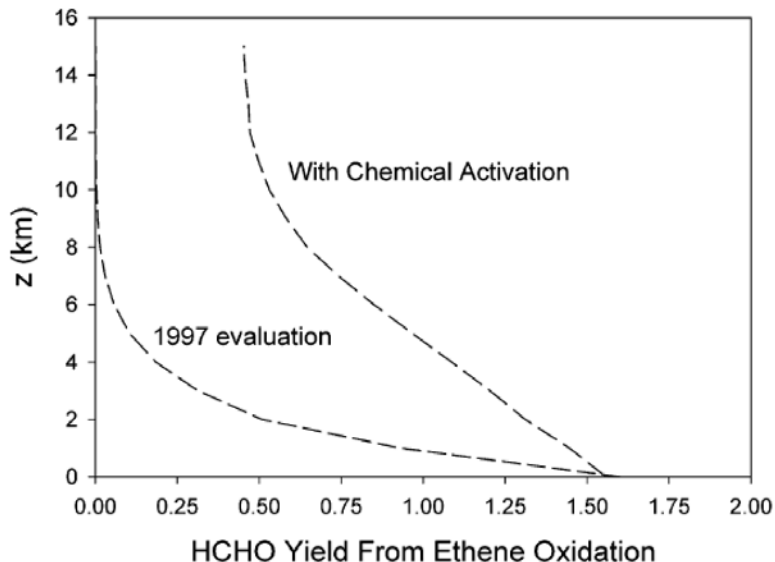
Figure 8. Molar formaldehyde yield from OH-initiated oxidation of ethene as a function of altitude. Yields were calculated with and without[14] allowance for chemical activation of the HOCH$_2$CH$_2$O$^\bullet$ radical.

Lifetime of isoprene nitrate: Isoprene nitrate has a lifetime of only ~1 hour. Caltech also measured MVKN/MACN, which are mostly second generation products produced from isoprene nitrate. Thus, the sum of the measured isoprene nitrate and MVKN/MACN is expected to provide a better estimate for the amount of isoprene oxidized, compared to isoprene nitrate alone. That sum is used here in the observational analysis.

O$_3$ **production per alkene molecule oxidized:** As each alkene molecule is oxidized, hydroxy substituted alkyl peroxy radicals are formed that oxidize NO to NO$_2$, which photodissociates to yield O$_3$. The NO$_2$ yield of this reaction is (1-α) because a small fraction (α) of the reaction forms the β-hydroxy nitrate. The yields of formaldehyde, acetaldehyde and HO$_2$ in subsequent reactions are γ, δ and ε, respectively. For the first generation chemistry outlined in Figure A1 at the high NOx limit, a single O$_3$ molecule is formed for each alkyl peroxy radical formed (corrected for the fraction forming hydroxy nitrates). Thus, the O$_3$ yield of Reaction 1 is f$_a$*(1-α). The HO$_2$ radicals formed also contribute to O$_3$ formation, which, assuming that at high NOx all HO$_2$ radicals also form O$_3$, essentially doubles the O$_3$ production. The final column in Table A1 gives this upper-limit O$_3$ yield from all peroxy radicals formed in the first generation chemistry (f$_a$*(1-α) + ε *f$_a$*(1-α)). The overall yield of formaldehyde is γ*f$_a$*(1-α) and for acetaldehyde the overall yield is δ*f$_a$*(1-α).
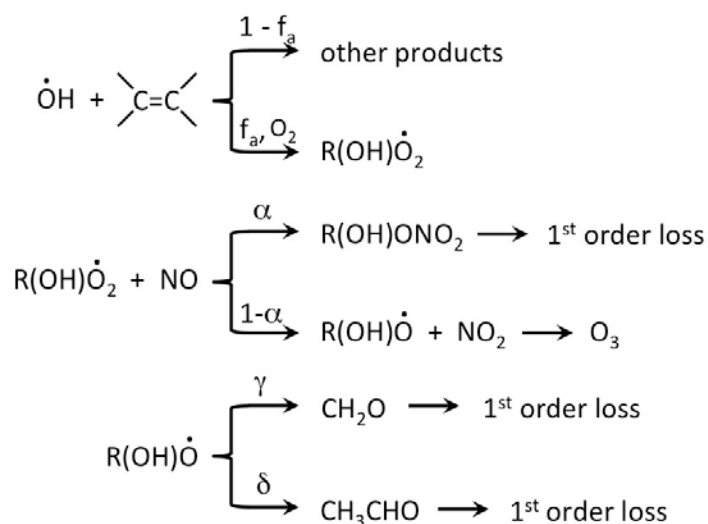
Figure A1. Simplified chemistry scheme to describe first-generation formation of β-hydroxy nitrates, aldehydes and O_3 from alkenes.

Table A1. Parameters for the simplified chemistry scheme for eight alkenes.

	kOH	fa	α	β	γ	δ	ε	γ*fa* (1-α)	δ*fa* (1-α)	ε*fa* (1-α)	O_3 yield
ethene	8.52E-12	1	0.023	1	1.6	0	1	1.563	0	0.977	1.95
propene	2.63E-11	0.97	0.053	1	1	1	1	0.919	0.919	0.919	1.87
1-butene	3.14E-11	0.92	0.117	1	1	0	1	0.812	0	0.812	1.70
2-methylpropene	5.14E-11	0.97	0.106	1	1	0	1	0.867	0	0.867	1.76
cis-2-butene	5.64E-11	0.97	0.104	1	0	2	1	0	1.738	0.869	1.77
trans-2-butene	6.40E-11	0.97	0.104	1	0	2	1	0	1.738	0.869	1.77
1,3-butadiene	6.66E-11	0.97	0.100	1	1	0	1	0.873	0	0.873	1.77
isoprene	1.00E-10	0.92	0.120	1	1	0	1	0.810	0	0.810	1.69

REFERENCES

Millet et al., 2010. Global atmospheric budget of acetaldehyde: 3-D model analysis and constraints from in-situ and satellite observations, *Atmos. Chem. Phys.,* **10**, 3405–3425, doi:10.5194/acp-10-3405-2010.

Orlando, J.J., G.S. Tyndall and T.J. Wallington, 2003. The atmospheric chemistry of alkoxy radicals, *Chem. Rev.,* **103**, 6294-6317, DOI: 10.1039/C2CS35166H.

Teng, A.P., J.D. Crounse, L. Lee, J.M. St. Clair, R.C. Cohen, and P.O. Wennberg, 2015. Hydroxy nitrate production in the OH-initiated oxidation of alkenes, *Atmos. Chem. Phys.,* **15**, 4297–4316, doi:10.5194/acp-15-4297-2015.